2016

Coming Full Circle: Epithelial Plasticity And The Natural History Of Metastasis

Nicole Aiello
University of Pennsylvania, nicolemaiello@gmail.com

Coming Full Circle: Epithelial Plasticity And The Natural History Of Metastasis

Abstract
The primary cause of cancer-related deaths is metastasis— the spread of cancer cells to distant organs— and yet the mechanisms underlying this process remain elusive due to the difficulty in detecting early metastatic events, which are rare, stochastic and microscopic. To investigate the cellular and molecular mechanisms of metastasis, I utilized an autochthonous mouse model of pancreatic cancer (KPCY) in which all tumor cells are genetically labeled with yellow fluorescent protein (YFP). The YFP lineage label allows for the detection and isolation of disseminated tumor cells as they delaminate from epithelial structures within the primary tumor, invade into the stroma and circulation, and colonize distal organs. Using this system, I characterized the development of metastatic lesions from single disseminated cells to grossly macroscopic lesions in the murine liver. I found that gross metastases closely resembled primary tumors in terms of differentiation and microenvironment— these large lesions are well differentiated, containing primarily epithelial tumor cells, and accumulate stroma consisting of myofibroblasts, leukocytes and extracellular matrix (ECM). In contrast, single disseminated cells tend to be poorly differentiated and lack any association with stromal cells, and must build up a microenvironment around them as they grow. Despite the presumably protective stroma surrounding large lesions, gross metastasis was significantly reduced with chemotherapy, while single cells were unaffected. Interestingly, residual lesions were enriched for epithelial features, suggesting that EMT confers chemosensitivity in this context. I also used the KPCY model to investigate the molecular mechanisms of epithelial-mesenchymal transition (EMT), which is widely considered to be the first step in the metastatic cascade. The YFP lineage label made it possible to identify and isolate tumor cells that have undergone EMT for transcriptional profiling. Surprisingly, I found that in a majority of pancreatic tumors, conventional transcriptional repressors were not involved in EMT. Although a mesenchymal transcriptional program was significantly enriched in cells that had undergone this "non-canonical" mechanism of EMT, the epithelial program was downregulated at the protein level by a mechanism involving protein internalization. Because cells retain both epithelial and mesenchymal properties during non-canonical EMT, this phenomenon represents an attractive explanation for the ability of tumor cells to cycle between epithelial and mesenchymal states and adapt to the changing microenvironment on their way to metastatic sites. The journey from primary tumor to metastatic site requires cancer cells to overcome many obstacles and a better understanding of how they navigate the numerous steps of the metastatic cascade could open the door to desperately needed anti-metastatic therapies.

Degree Type
Dissertation

Degree Name
Doctor of Philosophy (PhD)

Graduate Group
Cell & Molecular Biology

COMING FULL CIRCLE: EPITHELIAL PLASTICITY AND THE NATURAL HISTORY OF METASTASIS

Nicole Marie Aiello

A DISSERTATION in **Cell and Molecular Biology**

Presented to the Faculties of the University of Pennsylvania

In Partial Fulfillment of the Requirements for the

Degree of Doctor of Philosophy

2016

Supervisor of Dissertation

*Signature*_____

Ben Z. Stanger

Associate Professor of Medicine

Graduate Group Chairperson

*Signature*_____

Daniel S. Kessler

Associate Professor of Cell and Developmental Biology

Dissertation Committee

Chair: Robert H. Vonderheide, *Hanna Wise Professor in Cancer Research*

Michael A. Pack, *Professor of Medicine*

Anil K. Rustgi, *T. Grier Miller Professor of Medicine and Genetics*

COMING FULL CIRCLE: EPITHELIAL PLASTICITY AND THE NATURAL HISTORY OF METASTASIS

Dedication page

I would like to dedicate this work to my parents, Marianne and Allan Aiello, who taught me the value of an education and supported me every step of the way (even when I told them I have to do another five years of post-doctoral training).

ACKNOWLEDGMENT

As with children, it takes a village to raise a scientist. First and foremost, I would like to thank my thesis advisor, Dr. Ben Stanger, for giving me the freedom to make mistakes and learn from them, and Dr. Andy Rhim, who took me under his wing when I was just a wee baby scientist and taught me everything I needed to know to study pancreatic cancer in mice. I would also like to thank the Developmental, Stem Cell and Regenerative Biology group, especially its chair Dr. Steve Dinardo, for being endlessly supportive. My thesis committee has been extremely helpful to me by providing guidance and encouragement throughout my PhD, and I would especially like to thank Dr. Bob Vonderheide for his unwavering enthusiasm and for writing countless recommendation letters, as well as Dr. Anil Rustgi for his support through the years and for joining my committee in the eleventh hour so I could defend my thesis as planned. And finally I would like to express my sincerest gratitude to my fellow lab members, past and present, who have supported me intellectually and emotionally throughout this rollercoaster we call a PhD.

ABSTRACT

COMING FULL CIRCLE: EPITHELIAL PLASTICITY AND THE NATURAL HISTORY OF METASTASIS

Nicole Marie Aiello

Ben Z. Stanger

The primary cause of cancer-related deaths is metastasis— the spread of cancer cells to distant organs— and yet the mechanisms underlying this process remain elusive due to the difficulty in detecting early metastatic events, which are rare, stochastic and microscopic. To investigate the cellular and molecular mechanisms of metastasis, I utilized an autochthonous mouse model of pancreatic cancer (KPCY) in which all tumor cells are genetically labeled with yellow fluorescent protein (YFP). The YFP lineage label allows for the detection and isolation of disseminated tumor cells as they delaminate from epithelial structures within the primary tumor, invade into the stroma and circulation, and colonize distal organs. Using this system, I characterized the development of metastatic lesions from single disseminated cells to grossly macroscopic lesions in the murine liver. I found that gross metastases closely resembled primary tumors in terms of differentiation and microenvironment— these large lesions are well differentiated, containing primarily epithelial tumor cells, and accumulate stroma consisting of myofibroblasts, leukocytes and extracellular matrix (ECM). In contrast, single disseminated cells tend to be poorly differentiated and lack any association with stromal cells, and must build up a microenvironment around them as they grow. Despite the presumably protective stroma surrounding large lesions, gross metastasis was significantly reduced with chemotherapy, while single cells were unaffected. Interestingly, residual lesions were enriched for epithelial features, suggesting that EMT confers chemosensitivity in this context. I also used the KPCY model to investigate the molecular mechanisms of epithelial-mesenchymal transition (EMT), which is widely considered to be the first step in the metastatic cascade. The YFP lineage label made it

possible to identify and isolate tumor cells that have undergone EMT for transcriptional profiling. Surprisingly, I found that in a majority of pancreatic tumors, conventional transcriptional repressors were not involved in EMT. Although a mesenchymal transcriptional program was significantly enriched in cells that had undergone this “non-canonical” mechanism of EMT, the epithelial program was downregulated at the protein level by a mechanism involving protein internalization. Because cells retain both epithelial and mesenchymal properties during non-canonical EMT, this phenomenon represents an attractive explanation for the ability of tumor cells to cycle between epithelial and mesenchymal states and adapt to the changing microenvironment on their way to metastatic sites. The journey from primary tumor to metastatic site requires cancer cells to overcome many obstacles and a better understanding of how they navigate the numerous steps of the metastatic cascade could open the door to desperately needed anti-metastatic therapies.

TABLE OF CONTENTS

ACKNOWLEDGMENT iv

ABSTRACT v

LIST OF TABLES ix

LIST OF ILLUSTRATIONS ix

MANUSCRIPTS xi

CHAPTER 1: Introduction 1

- **Biology of pancreatic ductal adenocarcinoma** 1
- **Common themes in embryogenesis and cancer** 5
- **Fate mapping** 10
- **Mouse models of pancreatic ductal adenocarcinoma** 16
- **Chapter 1 Figures and Figure Legends** 18

CHAPTER 2: Metastatic progression is associated with dynamic changes in the local microenvironment 21

- **Abstract** 21
- **Introduction** 21
- **Results** 23
- **Discussion** 30
- **Materials and Methods** 35

Chapter 2 Figures and Figure Legends **40**

Chapter 2 Tables **58**

CHAPTER 3: A non-canonical mechanism drives epithelial plasticity *in vivo* **61**

Abstract **61**

Introduction **62**

Results and Discussion **63**

Materials and Methods **70**

Chapter 3 Figures, Figure Legends and Table **74**

CHAPTER 4: Conclusions and Future Directions **91**

Parallel evolution of a metastatic lesion and its attendant microenvironment ... **91**

EMT and response to chemotherapy **94**

Discovery of an alternative mechanism of EMT *in vivo* **94**

Concluding remarks **97**

Chapter 4 Figures and Figure Legends **99**

BIBLIOGRAPHY **101**

LIST OF TABLES

Table 2.1: Metastatic burden (raw counts) for each animal used in Figure 3b……....57

Table 2.2: Antibodies used in Chapter 2……..……58

Table 2.3: Clinicopathological characteristics of patients ……..…59

Table 3.1: Antibodies used in Chapter 3……..……..90

Table 4.1: Enriched transcription factor targets in non-canonical Ecad samples……..100

LIST OF ILLUSTRATIONS

Figure 1.1: Developmental pathways are frequently activated in cancer..…….....18

Figure 1.2: Use of lineage labeling to identify stem cells during development and tumor progression……...……..……..20

Figure 2.1: Metastatic landscape of the KPCY model…..…….……..…..40

Figure 2.2: Proliferation/apoptosis rates of metastatic lesions…….……....41

Figure 2.3: Proliferation in human PDAC tumors and metastases…….……..……42

Figure 2.4. Metastatic growth is associated with a more epithelial phenotype…...…….....43

Figure 2.5: Skewing of epithelial to mesenchymal cell ratio within primary tumor and metastatic lesions…….……..……44

Figure 2.6: Epithelial and mesenchymal features of human PDAC tumors and metastases…...45

Figure 2.7: Desmoplasia accumulates as lesions grow..……..……..…46

Figure 2.8: Myofibroblast contact with nano-metastases depends on cell size and representative images of ECM stains…..……...…48

Figure 2.9: Fibronectin deposition in human PDAC tumors and metastases…….……..……..49

Figure 2.10: Leukocytes accumulate in metastatic livers…..……..50

Figure 2.11: Metastatic growth is associated with functional hypovascularity……..……...52

Figure 2.12: Circulating tumor cells (CTCs) are decreased after long-term chemotherapy.…….54

Figure 2.13: Chemotherapy reduces metastatic burden……..55

Figure 2.14: Mesenchymal tumor cells are depleted after chemotherapy……..……..56

Figure 3.1: Two distinct EMT programs exist *in vivo*……74

Figure 3.2: Mesenchymal protein expression varies widely during EMT *in vivo*…….....76

Figure 3.3: RNAseq sorting quality controls……..77

Figure 3.4: Gene set enrichment analysis (GSEA)……..78

Figure 3.5: EMT-TF expression differs between canonical and non-canonical EMT……....79

Figure 3.6: EMT subtype correlates with histology……..80

Figure 3.7: EMT subtype correlates with PDAC subtype……..……..…..81

Figure 3.8: Cell lines segregate into canonical and non-canonical EMT…….....84

Figure 3.9: Non-canonical cell lines are competent to undergo canonical EMT……..…..86

Figure 3.10: Non-canonical EMT is characterized by Ecad internalization……..87

Figure 3.11: Prrx1 regulates Ecad trafficking……88

Figure 3.12: Non-canonical EMT confers enhanced tumor initiation potential and epithelial plasticity……89

Figure 4.1: Snail expression does not correlate with EMT in KPCY tumors……..….99

MANUSCRIPTS

The following manuscripts are discussed in this thesis:

Aiello NM & Stanger BZ. 2016. Echoes of the embryo: using the developmental biology toolkit to study cancer. *Dis Model Mech* 9(2):105-14.

Aiello NM*, Bajor DL*, Norgard RJ, Sahmoud A, Bhagwat N, Pham MN, Cornish TC, Iacobuzio-Donahue CA, Vonderheide RH and Stanger BZ. 2016. Metastatic progression is associated with dynamic changes in the local microenvironment. *Nat. Comm*. In press.

Aiello NM*, Balli D*, Maddipati R*, Norgard RJ, Li J, Sahmoud A, Yuan S, Furth EE, Bar-Sagi D and Stanger BZ. 2016. A non-canonical mechanism driving epithelial plasticity in vivo.

CHAPTER 1: Introduction

Biology of pancreatic ductal adenocarcinoma

Pancreatic ductal adenocarcinoma (PDAC) is the most common form of pancreatic cancer and also the most deadly, with a five-year survival rate of only 7.7%[1]. The poor prognosis for PDAC patients can be attributed to frequent and widespread dissemination, chemoresistance and a lack of early detection methods. The vast majority of cases present with metastasis and are thus ineligible for surgery, the only known cure for PDAC[2,3]. Even those who receive surgery have an extremely high (90%) rate of recurrence[4] and 70% of PDAC patients die from metastatic disease[5], highlighting the need for therapies that can prevent or target metastasis.

Pathology

The most common lesions preceding PDAC are pancreatic intraepithelial neoplasia (PanINs), which are microscopic and characterized by ductular architecture. As PanINs increase in grade from 1-3, they acquire nuclear atypia and cytologic abnormalities until finally progressing to frank, locally invasive malignancy[6]. Intraductal papillary mucinous neoplasia (IPMN) and mucinous cystic neoplasia (MCN) can also evolve into PDAC but at a lower frequency compared to PanINs[7]. PDAC tumors are characterized by the accumulation of desmoplasia, which consists of various stromal cell populations such as leukocytes and fibroblasts, as well as numerous extracellular matrix components[8]. Unlike most solid cancers, PDAC is typically hypovascular and poorly perfused, which, in addition to the dense stroma, is thought to contribute to the failure of drug delivery to these tumors[9-11]. However, it is not clear whether the microenvironment plays a similar role in chemoresistance at metastatic sites.

Genetics

PDAC is relatively homogenous in terms of driver mutations: over 90% of PDAC tumors harbor activating mutations in the oncogene *Kras*[12], pointing to the RAS pathway as a critical gatekeeper of pancreatic tumorigenesis. Kras is a GTPase involved in the early steps of the signal transduction cascades activated by various growth factors. Mutations in the *Kras* gene frequently occur at codon 12 but are also found at codons 13 and 61, all of which cause the protein product to be constitutively active. In addition to RAS, commonly altered signaling pathways include Hedgehog, TGF-β, WNT, apoptosis, regulation of G_1/S transition, chromatin modification, DNA damage repair and axon guidance[13,14]. Subsequent mutations of tumor suppressors involved in these pathways, such as *Tp53*, *Smad4* or *Cdkn2a*, are thought to be necessary for tumor progression[15,16]. On average, PDAC tumors possess significantly fewer somatic mutations compared to other cancer types such as breast and colorectal[13].

Subtypes

PDAC tumors can be stratified into both genetic and transcriptional subtypes. Whole genome sequencing and copy number variation have revealed four PDAC subtypes based on chromosome structural variation: stable, locally rearranged, scattered and unstable[14]. “Stable” tumors exhibit the fewest structural variation events (<50) but often exhibit aneuploidy, indicating defects in mitosis. “Locally rearranged” tumors are characterized by a single focal event, usually a large amplification or deletion or the fusion of two neighboring chromosomes. “Scattered” tumors exhibit a moderate level of chromosomal rearrangements while “unstable” tumors possess more than 200 structural variation events and exhibit the highest genomic instability of all subtypes.

Transcriptional PDAC subtypes have been identified and corroborated by three independent groups. Using microarray data from patient samples and established human and murine PDAC cell lines, Collisson *et al.* were the first to stratify tumors into three subtypes: classical, exocrine and quasi-mesenchymal[17]. Classical tumors are moderate to well differentiated (i.e. exhibit epithelial histology) and tend to be sensitive to erlotinib, an EGFR inhibitor. The exocrine subtype is characterized by high expression of pancreatic enzyme genes and, like classical tumors, tends to be more differentiated in terms of histology. Quasi-mesenchymal tumors are often poorly differentiated, express high levels of mesenchyme-related genes and are sensitive to gemcitabine, the standard of care for PDAC. Using RNA-sequencing, Bailey *et al.* uncovered essentially the same PDAC subtypes plus an additional one in a panel of 96 human PDAC tumors: pancreatic progenitor (Collisson's classical), aberrantly differentiated endocrine exocrine (ADEX; Collisson's exocrine), squamous (Collisson's quasi-mesenchymal) and immunogenic[18]. Most recently, Moffitt *et al.* utilized virtual microdissection to bioinformatically separate tumor and stromal gene expression in PDAC microarray data and identified two tumor subtypes, classical and basal-like, which closely resemble Collisson's classical and quasi-mesenchymal subtypes, respectively[19]. Thus, there is clear consensus on the existence of at least two distinct PDAC subtypes that differ in histology, drug sensitivity and gene expression.

Treatment

There are limited options for PDAC treatment, with only a handful of FDA-approved chemotherapeutic regimens. The standard of care for the last fifteen years has been gemcitabine, a nucleoside analog that causes apoptosis by inhibiting DNA replication[20]. More recently, clinical trials have attempted to combine gemcitabine with

other drugs, but few have represented improvements[21]. One successful combination, gemcitabine plus the microtubule inhibitor nab-paclitaxel, increased median overall survival by 1.8 months and is considered the new standard of care[22]. Another more aggressive four-drug regimen consisting of fluorouracil, irinotecan, oxaliplatin, and leucovorin (FOLFIRINOX) also increases median overall survival compared to gemcitabine alone (11.1 months vs. 6.8 months, respectively) but is used less frequently because of its side effects[23]. For patients with resectable disease, one of these drug combinations is usually given as adjuvant therapy after surgery, however most develop distant recurrence[24-26], suggesting that nearly all PDAC patients have occult micrometastatic disease. There are ongoing clinical trials testing the efficacy of neoadjuvant therapy to reduce primary tumor size and involvement and target micrometastatic disease early on. For most patients, surgery is not an option so they must rely on aggressive chemotherapy, sometimes combined with radiation, to control the disease[2]. Despite recent advances, the five-year survival rate for those eligible for surgery, have locally advanced disease and metastatic disease are 29.3%, 11.1% and 2.6% respectively[1]. Thus there is a critical need to understand and target chemoresistance at primary as well as metastatic sites.

Metastasis

During the metastatic cascade, tumor cells break off from epithelial structures as either single cells or clusters, intravasate into the circulation, lodge in the capillary beds of distant organs and extravasate into the parenchyma where they grow into larger lesions[27]. Eighty percent of PDAC patients present with locally advanced or metastatic disease[1], with dissemination primarily to the lymph nodes, liver, peritoneum, diaphragm and lung[28]. It was once thought that a tumor's pattern of metastatic colonization reflected

blood flow and biomechanics, however in 1889 Paget's "seed and soil" hypothesis completely upended this idea[29]. Paget postulated that tumors "seed" organs that are conducive to growth (i.e. fertile soil). It is now clear that not only do tumor cells selectively seed organs, but they also "fertilize" the soil to generate a receptive pre-metastatic niche[30-34].

Gross metastatic lesions typically resemble the primary tumor they arose from histologically, which in the case of PDAC tend to be epithelial in nature[35-37]. However epithelial cells are not particularly motile or invasive, so it has been postulated that metastasizing cells must go through epithelial-mesenchymal transition (EMT) to escape from the primary tumor and then the reverse process, mesenchymal-epithelial transition (MET) during colonization. There is precedent for this paradigm in embryogenesis, during which multiple rounds of EMT/MET are necessary for the formation of the three germ layers and various organs[38]. Numerous studies have demonstrated that EMT increases tumor cell dissemination but not metastatic colonization, while epithelial tumor cells have high colonization potential[39-41].

Common themes in embryogenesis and cancer

The process of embryogenesis requires precise spatial and temporal activation of developmental signaling pathways. Re-activation of these embryonic signals in adult cells, a consequence of mutations and epigenetic remodeling, is a characteristic feature of cancer. Key developmental signaling pathways – including the Wnt, Hedgehog, and Notch pathways – are frequently dysregulated in cancer and participate in all stages of tumor progression, from initiation and maintenance to metastatic spread and growth at distant sites (Figure 1.1).

During development, Wnt signaling is involved in cell fate specification, proliferation and migration, and in the adult this pathway is involved in maintaining homeostasis in tissues such as the intestine, where Wnt signaling is critical for stem cell function[42,43]. There are three known Wnt pathways: canonical, which regulates gene expression, and two non-canonical pathways that regulate planar cell polarity and calcium flux[44]. In this review we have focused on canonical Wnt signaling because this is the most frequently implicated Wnt pathway in cancer. As depicted in Figure 1.1A, in the absence of a Wnt signal, the canonical Wnt effector beta-catenin (CTNNB) is continuously phosphorylated and targeted for degradation by glycogen synthase kinase-3 (GSK3), which is stabilized when complexed with adenomatous polyposis coli (APC) and Axin. In response to Wnt glycoproteins, which signal through Frizzled receptors (FRZ) and their coactivators low-density lipoprotein receptor-related proteins 5 and 6 (LRP), Axin binds FRZ and is unable to stabilize the APC/GSK3/CTNNB complex, freeing CTNNB to enter the nucleus and facilitate the transcriptional activity of the T-cell specific transcription factor (TCF) and lymphoid enhancer binding factor (LEF) family[44]. Canonical Wnt signaling is active in nearly all developing tissues and plays a critical role in body axis patterning[45], stem cell maintenance and lineage specification[46,47]. In the adult, hyper-activation of the Wnt pathway – typically due to loss of the tumor suppressor protein APC – represents the first step in colorectal tumorigenesis[48]. Ligand-independent activation of CTNNB is a more common alteration in cancers outside the gut, especially in endometrioid ovarian cancer, hepatoblastoma and Wilms' tumors[49,50].

The Hedgehog (HH) pathway, like the Wnt pathway, plays a critical role in the development of many organs including but not limited to the patterning of the central nervous system (CNS), tooth development and limb formation[51-53]. HH ligands, of which there are three including Sonic hedgehog (SHH), Indian hedgehog (IHH) and Desert

hedgehog (DHH), act as morphogens to direct left-right asymmetry and cell fate decisions and pattern developing tissues[54]. In the absence of HH ligands, the transmembrane protein Patched (PTC) indirectly facilitates the degradation of GLI-family zinc finger proteins (GLI) by blocking Smoothened (SMO) activity. In the presence of HH ligands, PTC is unable to inhibit SMO, which stabilizes GLI and allows it to translocate into the nucleus where it acts as a transcription factor (Figure 1.1B)[55]. In the pathogenic context, activation of the HH pathway can lead to basal cell carcinoma (BCC) (a type of skin cancer)[56] or to the recruitment of a fibroblast-rich stroma in pancreatic cancer[57,58].

The Notch pathway is similarly involved in embryonic cell fate decisions; specifically, it is critical for the development of organs including but not limited to the CNS, pancreas, bone, and heart[59]. This pathway is activated by juxtacrine signaling between the Notch receptor on the receiving cell and Notch ligands including Delta-like (DLL) and Jagged (JAG) on the signaling cell. Upon binding of Notch ligands to the receptor, gamma-secretase (γ-SEC) cleaves the intracellular Notch domain (NICD), allowing it to enter the nucleus and facilitate the transcriptional activity of Recombination signaling binding protein for kappa J region (RBPJ) (Figure 1.1C)[60]. Notch's role in tumor progression seems to be context-dependent, as the pathway can act as an oncogene in some settings (e.g. breast cancer and T-cell leukemia) or as a tumor suppressor gene in others (e.g. skin cancer)[61-63], although the latter may be through a non-cell autonomous mechanism[64]. Other cellular signaling pathways in addition to Wnt, HH and Notch play critical roles in cell fate specification and migration during embryogenesis and have also been implicated in cancer invasion and metastasis. These include the fibroblast growth factor (FGF) and transforming growth factor beta (TGFβ)/bone morphogenic protein (BMP) signaling pathways which will be discussed later in this section for their ability to promote cell migration and invasion in both the developmental and cancer contexts[65-68].

Thus, the molecular cues used to pattern an embryo are harnessed by tumor cells to enhance growth, recruit stromal cells and coordinate spread from the primary tumor.

A recurring motif in development is reciprocal signaling between neighboring cell populations; crosstalk that facilitates morphogenesis of the emerging tissue. Reciprocal signaling between developing epithelium and mesenchyme occurs repeatedly during embryogenesis and is critical for the formation of limbs, epidermal appendages, pancreas, lungs, kidney and other organs[69-75]. Carcinomas also contain a mixture of epithelium - cancer cells - and mesenchyme, which in the cancer context is known as stroma. The latter consists of leukocytes, fibroblasts, endothelium and lymphatic vessels, and collectively form what is known as the “tumor microenvironment” (TME). These cell populations engage in molecular crosstalk with cancer cells, which can effect cancer cell survival, proliferation and migration. An example is provided by pancreatic cancer. As touched upon above, pancreatic tumor cells secrete SHH, a HH ligand, which recruits fibroblasts to form the dense “desmoplastic” or fibrotic stroma of that cancer type[57,76,77]. The fibroblast-rich stroma of pancreatic cancer has been demonstrated to exert both pro- and anti-tumor effects. Although desmoplasia is known to impair drug delivery[9-11], depletion of myofibroblasts using genetic and pharmacological methods results in increased tumor growth and metastasis[58,78]. Nonetheless, signaling between cancer cells and the stromal cells they recruit is a common theme in carcinoma progression. Through reciprocal interactions such as these, tumors build a non-cancerous stroma that in turn influences cancer cell behavior.

Embryogenesis entails dramatic morphological changes and cellular movements that are recapitulated within tumors. One of the most notable of these is epithelial to mesenchymal transition (EMT), a process in which epithelial cells lose their epithelial characteristics, including apical-basal polarity and cell-cell adhesion, and take on the

motile features of fibroblasts. The primary role of EMT is during embryonic development, where it is critical for gastrulation, and other developmental events; however, cancer cells exploit this property of increased motility to facilitate spread. During gastrulation, WNT, TGF-β and FGF orchestrate primitive streak formation by promoting EMT via the activation of transcription factors Snail and Twist[65,79,80]. These developmental EMT transcription factors (EMT-TFs) are also drivers of EMT and consequent metastasis in breast, pancreatic and colorectal cancers, among others[81,82]. EMT is again required later in development, for neural crest cell migration, and is facilitated by Snail, Slug (also known as Snail2), and the Zeb family of transcription factors; these too have been implicated in cancer cell invasion and dissemination[83-85].

The primary function of EMT-TFs is to transcriptionally repress epithelial genes and activate mesenchymal genes[86]. One classic EMT-TF target is E-cadherin (*Cdh1*), a critical regulator of epithelial identity and a component of adherens junctions where it interacts with catenins. E-cadherin is a calcium-dependent cell adhesion molecule that tethers epithelial cells closely together[87]. Loss of E-cadherin allows an epithelial cell to disengage from its neighbors and is considered a hallmark of EMT[88]. In addition to E-cadherin, other epithelial proteins such as those within tight junctions (claudins and occludins) and the cytoskeleton (keratins) are also downregulated[89-91]. Concurrently, mesenchymal genes involved in cell motility and extracellular matrix interactions are switched on to facilitate invasion[92]. MicroRNAs (miRNA), including the miR-34[93,94] and miR-200 families[95-99], negatively regulate EMT-TFs to keep the EMT program in check. Alternative splicing, epigenetic modifications and post-translational regulation are layered on top of miRNA negative feedback loops, resulting in complex regulatory circuitry that controls the balance of EMT-promoting and -inhibiting factors[86].

Fate mapping

Once a cancer cell undergoes EMT it becomes indistinguishable from the surrounding non-cancerous stroma. Likewise, studying metastasis *in vivo* has been challenging, particularly in the context of a spontaneously-growing tumor because each of the events that occur during metastasis – from invasion through basement membranes to growth at distant sites – involve rare stochastic phenomena that are difficult to capture experimentally. Fate mapping, also known as lineage-labeling or lineage-tracing, was originally developed to visualize the fate of individual cells and their progeny, referred to as clones, during embryogenesis, but it has also proven useful for the study of tumor-initiating populations and dynamic cellular movements in the context of cancer. Early fate mapping experiments employed vital dyes, fluorescent dyes, or radio-labeling to mark a specific region, lineage, or even a single cell of an embryo and follow it throughout development as cells divide and migrate away from their original positions. These studies allowed embryologists to generate detailed fate maps for a number of model organisms, including frog, zebrafish and chick[100-102].

With the advent of site-specific recombinase technology such as the Cre-lox system it became possible to genetically label and track a cell lineage, facilitating fate mapping in mammals, which, unlike lower model organisms are not transparent and contain many more cells and lineages. Cre recombinase (Cre) recognizes specific DNA sequences (loxP sites) and targets these for recombination, which, depending on the orientation of the sites can result in deletion, inversion or translocation of intervening sequences[103,104]. Typically, loxP sites are used to delete regions of DNA, such as, for example, a gene of interest or a stop codon located upstream of a fluorescent reporter gene[105]. Cre expression can be restricted to specific cell types by altering upstream promoter elements, which permits spatial control of gene expression[106]. Thus the Cre-lox

system can be utilized to specifically and indelibly label tumor cells, allowing for the detection and isolation of cancer cells that have undergone EMT, intravasated into the circulation and colonized distant organs.

Cell-of-origin

A pressing issue in cancer biology is the elucidation of tumor-initiating cells or "cell-of-origin" in cancer: which cells in a normal tissue give rise to cancer? Given the robust self-renewal capacity of cancer cells, it is often assumed that cancers arise from resident, adult stem cells within tissues, and hence the concepts of "cell-of-origin" and "cancer stem cells" are often conflated. (The cancer stem cell hypothesis posits that a subset of cells within the tumor harbor most of the tumor's long-term self-renewal capacity, a concept quite distinct from the cell-of-origin, which merely points to the cell type within a tissue most likely to be transformed by the initiating mutation). Importantly, because cancer cells can, in principle, *acquire* stem cell properties as a consequence of mutation or epigenetic remodeling, they need not arise from stem cells. The ability of tumors to emerge in tissues where it is questionable whether stem cells exist (e.g. the kidney) is further evidence that cancers can arise from fully differentiated cells.

Lineage tracing has been a powerful tool to identify stem cell populations in embryonic and adult tissues, and the same approach has now been used to identify tumor-initiating cells in cancer (Figure 1.2). Several years ago, Lgr5 – a Wnt-target gene – was identified as a marker of intestinal stem cells, as Lgr5+ cells labeled with Cre-based technology durably gave rise to all the differentiated cell types of the intestinal villi as well as more Lgr5+ cells[107,108]. Building on this approach, Barker and colleagues (2009) used additional Cre-based tools to delete the tumor suppressor gene *Apc* in either the stem cell compartment (using Lgr5-Cre) or the non-stem cell "transient

amplifying" compartment--capable of short-term self-renewal only-- using Ah-Cre. While *Apc* deletion in the stem cells resulted in adenomas (premalignant lesions) that exhibited unimpeded growth, *Apc* deletion in the transient amplifying cells resulted in microadenomas (tumors less than 10mm in diameter) whose growth rapidly stalled[109109109]. This result suggested that intestinal stem cells are more competent than their transient-amplifying cell progeny – in the context of an APC mutation – to form tumors.

At present, lineage tracing offers the most robust method of addressing the cancer stem cell hypothesis *in vivo*. By using inducible Cre systems such as CreER and titrating the dose of tamoxifen, one can limit recombination to rare, sparse cells within a tissue, providing the resolution to identify clonal populations. Utilizing this concept, Driessens and colleagues (2012) were able to identify cancer stem cells and their progeny in a chemical-induced carcinogenic model of squamous cell carcinoma (SCC). Using a lineage labeling system driven by Keratin 14 (K14)-CreER which marks basal epithelial cells within the epidermis, the authors found that only 20% of these cells were capable of generating a large clonal population of pre-malignant papilloma cells. However, when the authors allowed these papillomas to progress to malignant SCC, the tumors were became poorly differentiated and exhibited a much higher frequency of long-term replicative cells, suggesting that in the transition from benign to malignant the cancer stem cell/differentiated progeny hierarchy starts to fall apart[110].

Such lineage tracing experiments support the general notion that cancer is the result of having the "right" mutations in the "right" cell at the "right" time. In other words, certain cell populations (stem cells or non-stem cells) might be susceptible to the oncogenic effects of certain gene mutations that have no effect in other cell populations. Additional factors, such as the local environment (e.g. inflammation), could contribute to

the susceptibility or resistance of various cell types to the cancer-causing effects of a given mutation. Similar lineage tracing experiments have identified cells-of-origin in a number of contexts[111-115]. From these studies, it appears that in some cases tumors arise from resident tissue stem cells (e.g. intestinal tumors and basal cell carcinomas), whereas in other cases it appears that tumors can arise from fully differentiated cells (e.g. pancreatic tumors, cholangiocarcinomas, gliomas).

Clonal heterogeneity and tumor evolution

Genomic analyses have confirmed that tumors are composed of numerous "sub-clones," or clones with distinct mutations in addition to the original tumor-driving mutation(s)[116,117]. Such tumor heterogeneity is a consequence of "clonal evolution," a process whereby cells within a cancer can acquire different mutations that lead them to be genetically and phenotypically distinct. A recent study has suggested that interactions between different sub-clones might drive tumor growth[118], suggesting that heterogeneity might not be merely a byproduct of clonal evolution but could also underlie key features of tumor biology.

Lineage tracing lends itself to the study of clonal evolution and the complex relationships between clonal populations. One useful tool has been the "Confetti" mouse, a strain in which cells are labeled with one of four fluorescent colors upon activation of Cre activity[119]. The system relies on the fact that Cre mediates different recombination events depending upon the orientation of LoxP sites: if LoxP sites are oriented in the same direction, the DNA sequence between them will be excised, if they are oriented in opposite directions, the gene between them will be inverted, and if they are located on separate chromosomes, Cre will mediate a translocation[120]. Within the Confetti allele, four fluorescent protein genes are flanked by LoxP sites and oriented in such a way that

excision or inversion results in the (somewhat) random expression of one of the four lineage labels. Using this system, it has been possible to identify “bottlenecks” during the clonal evolution of a tumor *in vivo*. For example, premalignant progression in pancreatic cancer is associated with a shift from acinar-to-ductal metaplasia (ADM), which are polyclonal, to more advanced pancreatic intraepithelial neoplasia (PanIN), which are monoclonal. This model has also revealed differences in metastatic potential between different tumor sub-clones, providing evidence for inter-clonal cooperation during tumor dissemination[121].

Lineage tracing has also provided insight into clonal evolution following chemotherapeutic selective pressures. Using a Cre-inducible mouse model of glioblastoma, for example, Chen *et al*. found that Nestin^{+} adult neural stem cells genetically labeled with green fluorescent protein (GFP) made up only a small fraction of naïve tumor, but upon treatment with temozolomide, an alkylating agent that is used to treat some brain cancers, these cells and their progeny expanded to become the most abundant tumor clone[122]. Similarly, in a mouse model of SHH-driven medulloblastoma, rare quiescent Sox2^{+} adult neural stem cells were found to be resistant to anti-mitotic and SHH-targeted therapy and responsible for recurrence after treatment[123]. These studies offer an explanation for why single therapies typically fail-- there is almost inevitably a resistant tumor subclone that will repopulate the tumor. The best strategy likely involves using multiple therapies targeting different pathways to reduce the chance of a single resistant subclone growing out.

EMT and invasion

It is comparatively easy to identify cells undergoing EMT during embryogenesis, as whole cell populations (e.g. the epiblast) can be observed to undergo a

transformation from an epithelial sheet to highly migratory fibroblast-like cells. However, it has proven to be exceptionally difficult to study cancer-associated EMT *in vivo*, because once a cancer cell undergoes EMT it becomes indistinguishable from the surrounding non-cancerous stroma. Likewise, studying metastasis *in vivo* has been challenging, particularly in the context of a spontaneously-growing tumor because each of the events that occur during metastasis – from invasion through basement membranes to growth at distant sites – involve rare stochastic phenomena that are difficult to capture experimentally.

Again, lineage tracing has proven to be a useful technique in studying these processes. For example, by introducing a yellow fluorescent protein (YFP) lineage label into a well-established genetically engineered mouse model (GEMM) of pancreatic cancer, it became possible to unambiguously identify cells that had undergone EMT, as such cells still bore the lineage marker confirming their epithelial origins, despite acquiring a mesenchymal phenotype[124]. Lineage tracing has also been used to elucidate the dynamics of metastasis. For example, Aytes and colleagues (2013) used a YFP reporter in the context of a mouse model of prostate cancer to determine the temporal occurrence of lung metastasis: at one month post-induction, rare single YFP^+ cells could be observed in the lung; at two months, YFP^+ micrometastases were evident; and by three months, gross metastases were found in 100% of animals[125]. Similar observations have been made in pancreatic cancer, where lineage tracing has enabled the examination of the rare events involved in metastatic growth, down to single cell resolution.

Mouse models of pancreatic ductal adenocarcinoma

Numerous mouse models of PDAC exist, and they all share the common theme of *Kras* deregulation and closely recapitulate the human disease in terms of progression from PanIN to PDAC, frequency and location of metastasis and poor response to chemotherapy. In each of these models, Cre-mediated recombination of loxP-stop-loxP (LSL) $Kras^{G12D}$ (a constitutively active mutant) is driven by one of three pancreas-specific promoters: *Pdx1*, *Ptf1a* (also called *p48*) or *Ela1*[126]. *Pdx1* and *Ptf1a* are both expressed by pancreatic progenitor cells during development, however *Pdx1* becomes restricted to endocrine cells in the adult pancreas while *Ptf1a* expression is limited to acinar cells of the exocrine compartment[127]. On the other hand, *Ela1* is expressed only in mature acinar cells[128]. Mutant Kras alone drives pancreatic tumorigenesis in only a fraction of mice and with a long latency (>1 year)[129], so many models also employ floxed or dominant negative (DN) tumor suppressor alleles such as *Tp53*, *Smad4 or Cdkn2a* (lost in 50-95% of human PDAC tumors)[126]. Loss of one of these tumor suppressors in addition to the expression of a constitutively active mutant Kras dramatically shortens tumor latency to 2-5 months and increases penetrance[126]. Addition of a genetic lineage label such as LSL-$Rosa26^{YFP/YFP}$ allows for the visualization of rare, stochastic events such as EMT and early metastatic colonization. Using the KPCY model (Pdx1-Cre, LSL-$Kras^{G12D}$, $Tp53^{fl/+}$, LSL-$Rosa26^{YFP/YFP}$), our lab previously demonstrated that EMT does indeed occur in living tumors and that there is evidence of dissemination to the liver even at pre-neoplastic stages[124].

At present, a diagnosis of metastatic pancreas cancer is essentially a death sentence; thus there is a dire need for effective anti-metastatic treatments. However, to develop new therapies a basic understanding of the mechanisms driving metastasis is necessary. The molecular mechanisms underlying cancer cell EMT *in vivo* are still poorly

understood; much of what we know about EMT has been revealed by forcing cancer cell lines to undergo EMT through Tgf-β treatment or overexpression of known EMT-TFs, which may not accurately reflect spontaneous EMT in living tumors. Another poorly understood aspect of metastasis is that of colonization: it is unclear how single disseminated cells develop into large metastatic lesions that closely resemble the original primary tumor. A stronger grasp of the mechanisms of spontaneous EMT and the natural history of metastatic colonization would open up new avenues for the prevention and treatment of metastasis. My thesis work sheds light on these processes using a lineage labeled mouse model of PDAC, which allowed me to isolate and transcriptionally profile of tumor cells that have undergone EMT *in vivo* and to detect occult micro-metastases and follow their development.

Chapter 1 Figures and Figure Legends

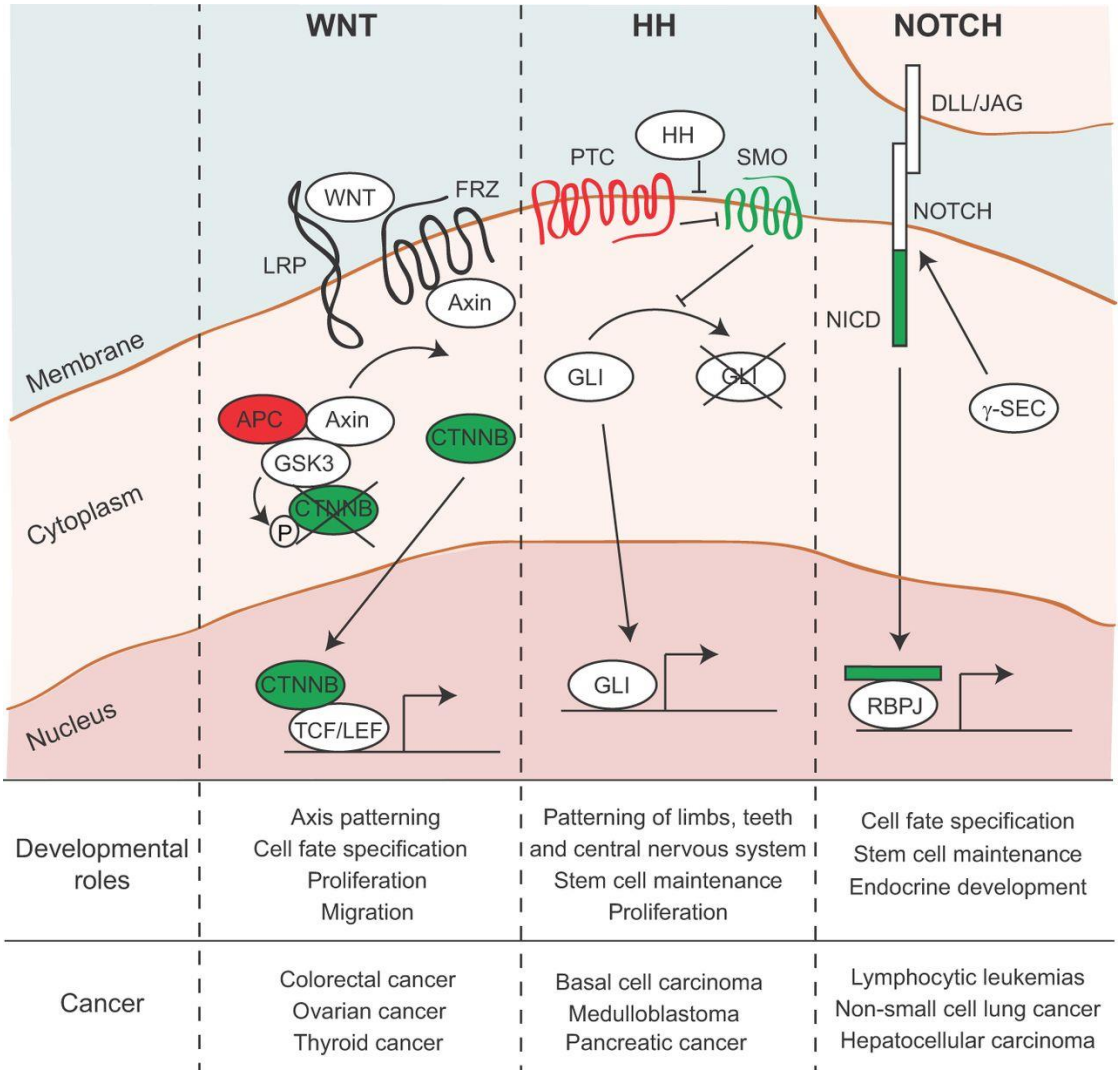

Figure 1.1: Developmental pathways are frequently activated in cancer. WNT, HH and NOTCH pathways are involved in many aspects of embryogenesis, including, but not limited to, patterning, cell fate specification, proliferation and stem cell maintenance. Dysregulation of each of these signal transduction pathways has been implicated in tumor initiation. In each case, the pathway is activated upon binding of a ligand to a receptor on the plasma membrane. This sets off a cascade of events allowing an

effector to translocate to the nucleus and affect gene transcription. Pathway genes that are typically inactivated in cancer are highlighted in red; genes that are frequently hyperactivated in cancer are shown in green. WNT, wingless-type MMTV integration site; FRZ, Frizzled; LRP, low-density lipoprotein receptor-related protein; APC, adenomatous polyposis coli; GSK3, glycogen synthase kinase-3; CTNNB, β-catenin; P, phosphorylation; TCF, T-cell-specific transcription factor; LEF, lymphoid enhancer binding factor; HH, hedgehog; PTC, patched; SMO, smoothened; GLI, GLI-family zinc finger; DLL, delta-like; JAG, jagged; NICD, notch intracellular domain; γ-sec, γ-secretase; RBPJ, recombination signaling binding protein for kappa J region.

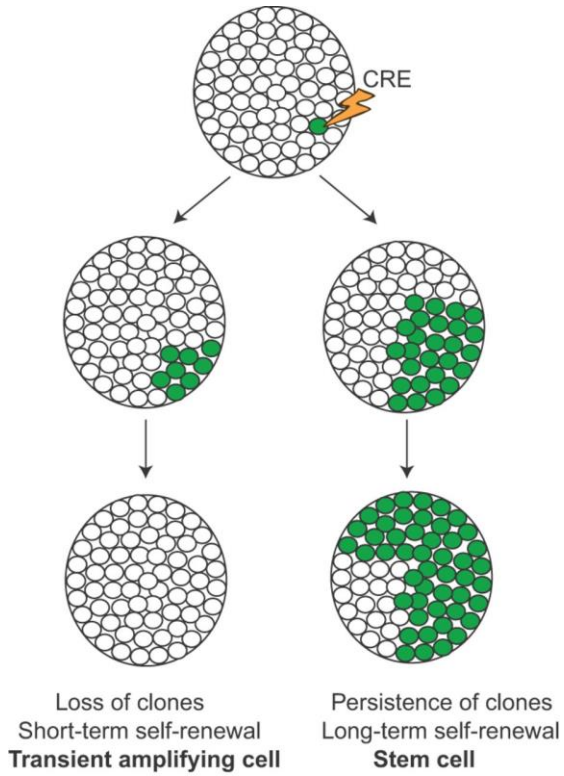

Figure 1.2: Use of lineage labeling to identify stem cells during development and tumor progression. Using inducible Cre-recombinase technology, cells within a lineage are sparsely labeled to provide the resolution necessary to identify clonal populations. After a short period of time, labeled progeny (shown in green) become apparent. If the original labeled cell is a genuine stem cell, the labeled clones will persist over the lifetime of the tissue (or tumor) because the stem cell is continuously self-renewing and producing differentiated daughter cells. If, on the other hand, the labeled clones are lost over time, the original labeled cell was most likely a transient amplifying cell, which is capable of short-term self-renewal but eventually becomes terminally differentiated, no longer contributing to the pool of cells. This test is not only useful for identifying stem cells and cancer stem cells but also for detecting drug-resistant clones. After sparse labeling and chemotherapy, drug-resistant clones will persist and begin to take up a much larger fraction of the tumor cell population, much like a stem cell.

CHAPTER 2: Metastatic progression is associated with dynamic changes in the local microenvironment

Abstract

Most cancer-associated deaths result from metastasis. However, it remains unknown whether the size, microenvironment, or other features of a metastatic lesion dictate its behavior or determine the efficacy of chemotherapy in the adjuvant (micrometastatic) setting. Here, we delineate the natural history of metastasis in an autochthonous model of pancreatic ductal adenocarcinoma (PDAC), using lineage tracing to examine the evolution of disseminated cancer cells and their associated microenvironment. With increasing size, lesions shift from mesenchymal to epithelial histology, become hypovascular, and accumulate a desmoplastic stroma, ultimately recapitulating the primary tumors from which they arose. Moreover, treatment with gemcitabine and nab-paclitaxel significantly reduces the overall number of metastases by inducing cell death in lesions of all sizes, challenging the paradigm that PDAC stroma imposes a critical barrier to drug delivery. These results illuminate the cellular dynamics of metastatic progression and suggest that adjuvant chemotherapy affords a survival benefit by directly targeting micrometastases.

Introduction

Pancreatic ductal adenocarcinoma (PDAC) has a 5-year survival rate of less than 6%, a dismal outcome related to late detection and a high rate of spread at the time of diagnosis[1,130]. Hence, metastatic disease accounts for a majority of PDAC-related deaths, even for patients with resectable tumors and no evidence of metastasis at the

time of diagnosis[2,5]. However, the mechanisms by which tumor cells navigate the "metastatic cascade" – a gauntlet that requires cellular escape from the primary tumor, survival in the circulation, invasion into distal tissues and colonization (growth) in a foreign, potentially hostile microenvironment – remain poorly understood[131].

One process thought to facilitate metastasis is epithelial-mesenchymal transition (EMT), whereby epithelial cells lose their adhesive contacts with neighbors and take on the migratory phenotype of mesenchymal cells[92]. Although EMT is believed to play a role in the dissemination of carcinoma cells, it has also been observed that metastases tend to exhibit the epithelial histology of their parent primary tumors[35,36,132]. This has led to the idea that the reverse process – mesenchymal-epithelial transition (MET) – drives the formation of a more epithelial phenotype at metastatic sites[133]. Although several studies support the view that MET is critical for metastatic colonization[39-41], evidence for this phenomenon is lacking from spontaneous tumor models.

Like primary tumors, metastases are a conglomerate of cancer cells, stromal cells, and extracellular matrix (ECM). In primary pancreatic cancer, a particularly dense (desmoplastic) stroma containing leukocytes, fibroblasts, and ECM makes up a large portion of the tumor mass, while the density of blood vessels tends to be low[8]. Although macro-metastatic lesions of various cancers – including PDAC, ovarian and breast – also exhibit a dense stromal infiltrate, it remains unclear when during metastatic progression this re-establishment of the tumor microenvironment occurs.

Here, we have taken advantage of a lineage-labeled autochthonous model of pancreatic cancer to carefully catalog the changes that occur within metastatic cells and their immediate microenvironment during metastatic colonization and growth. We report that the process is highly dynamic, as both tumor cells and the stroma undergo marked changes during progression from singly seeded cells to micro- and macro-metastases.

Furthermore, we show that treatment with gemcitabine and nab-paclitaxel results in killing of metastatic tumor cells despite the presence of an ostensibly protective microenvironment. These results provide insight into the process of metastatic colonization and challenge the hypothesis that stroma acts as a physical barrier to drug delivery.

Results

Lineage tracing permits detection of micro-metastases

We began by characterizing metastatic PDAC lesions in KPCY mice – in which **C**re-mediated recombination triggers mis-expression of mutant **K**ras^{G12D}, deletion of one copy of **p**53, and activation of a **Y**FP lineage label in pancreatic epithelial cells – allowing us to track tumor cells at the single cell level[124]. KPCY mice, like related mouse models[134,135], exhibit a pattern of gross metastasis similar to the human disease, consisting of spread to liver (40.5% of mice), diaphragm (32.4%), lung (10.8%), peritoneum (5.4%) and kidney (2.7%) (n= 40). We confined our subsequent analysis to the liver as it is the most frequent site of metastasis. Lesions were binned into five size categories according to the number of YFP$^+$ cells: single, nano (2-10 cells), micro (11-100 cells), milli (101-1000 cells) and macro (greater than 1000 cells) (Fig. 2.1a). When examined microscopically, nearly all tumor-bearing KPCY mice exhibited single cells (95.6%) or nano-metastases (91.3%) in the liver, while a lower frequency of animals had micro-metastases (65.2%) or milli- and/or macro-metastases (39.1%) (n=23). Most metastatic lesions contained 100 or fewer cells, with nano- and micro-metastases being the most abundant (Fig. 2.1b). Detailed metastatic burden quantification for each animal is listed in Table 2.1.

We next sought to determine baseline levels of proliferation and apoptosis within metastatic lesions. Surprisingly, proliferation rates (as measured by the percentage of $Ki67^+$ cells within each lesion) were not significantly different across lesions of all five metastatic categories (11-19%) and were comparable to the primary tumor (Fig. 2.1c, Fig. 2.2a). These results were corroborated by staining for phospho-histone H3 (pH3), a marker of mitosis (Fig. 2.2b,e) and proliferating cell nuclear antigen (PCNA) (Fig. 2.2c,f). Apoptosis, as measured by the percentage of cleaved caspase-3 (CC3) positive cells within each lesion, was absent from single cells and rarely seen in nano-metastases (0.2% of cells within nano-metastases were $CC3^+$). Primary tumors and larger lesions also exhibited low (~1%), albeit significantly higher levels of apoptosis compared to single cells (Fig. 2.1c; Fig. 2.2d). To determine if proliferation is also constant across lesions in human PDAC we stained matched primary tumors, gross metastases and micro-metastatic lesions from patients for Ki67 (Fig. 2.3a-d). We found that the rate of Ki67 positivity (mean ± SD) was not significantly different between primary tumors (2.1 ± 1.9), gross metastases (5.4 ± 5.6) and micro-metastases (3.1 ± 5.9), similar to what we observed in mouse PDAC. These data suggest that metastatic cancer cells exhibit similar rates of proliferation regardless of lesion size.

Metastatic lesions become more epithelial as they grow

We next determined the epithelial-mesenchymal status of cells at various stages of metastatic growth by co-staining with a panel of epithelial and mesenchymal markers and the YFP lineage label. To identify tumor cells with epithelial characteristics, we used antibodies that recognize E-cadherin (ECAD) and Claudin-7 (CLDN7)[82,89,136] and measured the percentage of YFP^+ cells that exhibited positive staining as a function of lesion size. Compared to single cells and nano-metastases, in which fewer than half of

the cells were positive for these markers, metastases having 100 cells or more (milli- and macro-) exhibited rates of epithelial staining in the range of 60-80%, resembling primary tumors (Fig. 2.4a, b, e). A complementary pattern of staining was observed when antibodies against fibroblast-specific protein-1 (FSP1) or zinc finger E-box binding homeobox 1 (ZEB1) were used[90,137], as milli- and macro-metastases exhibited reduced staining with these markers relative to nano-metastases (Fig. 2.4c, d, e). Comparing the frequency of epithelial (ECAD/CLDN7) cells to mesenchymal (FSP1/ZEB1) staining within each size group revealed that single cells and nano-metastases exhibited comparable frequencies of cells positive for these epithelial and mesenchymal markers; by contrast, larger lesions had a significantly greater fraction of epithelial cells (Fig. 2.5). These results are consistent with the notion that small metastatic lesions contain a higher percentage of cells that have undergone EMT, and that such cells revert to a more epithelial state, via MET, during colonization and growth. To determine whether this trend is also observed in human PDAC, we performed IHC on primary human PDAC tumors, gross liver metastases and microscopic liver metastases for CLDN7 and FSP1. Consistent with the murine data, CLDN7 staining was greater in primary tumors than micro-metastases while FSP1 staining was greater in micro-metastases compared to gross metastases and primary tumors (Fig. 2.6). Thus, in both mouse and human PDAC, metastatic cells appear to re-acquire an epithelial phenotype with increasing lesion size.

Desmoplasia gradually accumulates at metastatic lesions

Desmoplasia – a dense infiltrate of non-cancerous stromal cells and extracellular matrix (ECM) components – is a hallmark of PDAC, where it is thought to promote tumor growth and act as a barrier to the effective delivery of chemotherapy[138]. Myofibroblasts, a subset of fibroblasts involved in wound healing and fibrosis, are among the most

prevalent stromal cell types in PDAC. To determine if and when myofibroblasts accumulate during metastatic growth, we stained metastatic livers for YFP and α-smooth muscle actin (αSMA). Importantly, and in contrast to a recent publication[139], αSMA is specific to myofibroblasts and is never expressed in cancer cells that have undergone EMT (under review). Nearly all metastatic lesions consisting of 10 or more cells were in direct contact with myofibroblasts, while smaller lesions were less frequently associated, especially single cells (Fig. 2.7a, b). In particular, myofibroblast recruitment seemed to occur at the nano-metastasis stage, as there was a direct correlation between the number of cells present in a lesion (from 2 to 10) and their association with myofibroblasts (Fig. 2.8a). Additionally, the number of associated myofibroblasts significantly increased with lesion size, as demonstrated by an increase in αSMA^{+} area at larger lesions (Fig. 2.7c).

ECM components can be deposited by myofibroblasts or by tumor cells themselves (following EMT), and contribute to the desmoplastic reaction in PDAC[8,140]. Collagen I (COL1), hyaluronic acid (HA), fibronectin (FN) and secreted protein acidic and rich in cysteine (SPARC) represent the most abundant constituents in PDAC[140,141]. With the exception of FN density, which peaked at intermediate-sized micro-metastases, all other ECM components exhibited an increase as lesions grew (Fig. 2.7d-g, Fig. 2.8b-e) with the most dramatic change being the levels of SPARC present in all lesions as compared to single cells (Fig. 2.7f). These results demonstrate that the desmoplastic response begins at the nano-metastasis stage and that most stromal components increase in density as a function of lesion size. We also sought to determine whether ECM accumulation occurs during metastatic growth in human PDAC. We performed IHC for FN on primary human PDAC tumors, gross liver metastases and microscopic liver metastases and found that FN expression is higher in micro-metastases compared to

primary tumors (Fig. 2.9), consistent with the pattern of FN deposition observed in KPCY metastases.

In addition to myofibroblasts and ECM, pancreatic neoplasia is accompanied by a robust infiltration of leukocytes, particularly myeloid cells, which can comprise more than half of the cells within a tumor[142,143]. We thus determined how leukocyte populations change during metastatic progression by staining livers for CD45 (pan-leukocyte), F4/80 (macrophages), Gr-1 (myeloid-derived suppressor cells [MDSCs]), CD3 (T lymphocytes) and YFP (Fig. 2.10). Although the number of macrophages, MDSCs and leukocytes in general was increased in uninvolved areas of metastatic livers compared to control (Pdx1-Cre; $Rosa^{YFP}$) livers (Fig. 2.10a-e), only MDSCs showed a significant association with metastatic lesions, specifically nano-, micro- and milli-metastases (Fig. 2.10h,m). In contrast, T lymphocyte density, which was lower overall compared to the other leukocyte subsets, was unchanged between metastatic and control livers and across metastatic lesions (Fig. 2.10j,n). These results suggest that the presence of a primary pancreatic tumor causes a marked increase in certain leukocyte subsets in the liver, only MDSCs exhibit dynamic changes during metastatic progression.

Metastatic growth is associated with hypovascularity

PDAC tumors are commonly hypovascular, leading to increased hypoxia as well as impaired drug delivery[9,10]. To characterize the vascular properties of metastatic lesions, we stained metastatic livers for VE-cadherin (VECAD) and calculated vessel density ($VECAD^+$ lumen-containing blood vessels per 40x field). As expected given the high prevalence of vascular sinusoids in the normal liver, vessel density in the vicinity of small lesions (single cells and nano-metastases) was high, ranging between 25-30 vessels per field (Fig. 2.11a,b). In bigger lesions, however, vessel density decreased,

approaching the mean of five vessels per field found in primary tumors (Fig. 2.11a,b). Quantification of the average distance from metastatic cells to the closest $VECAD^+$ vessel produced a similar trend: single cells and nano-metastases were in close proximity to blood vessels (mean distance 5.4 ± 7.7 and 11.1 ± 9.2 microns, respectively) while cells within milli- and macro-metastases were far removed from the nearest blood vessel (mean distance 38.5 ± 30.1 and 36.2 ± 35.3 microns, respectively) similar to primary tumors (mean distance 19.2 ± 16.7 microns) (Fig. 2.11c).

To assess whether these observations result in functional differences in perfusion, we injected tumor-bearing KPCY mice with Texas-red dextran, a high molecular weight fluorescent polysaccharide. Consistent with the observation that metastatic lesions become more hypovascular as they grow, we observed a “halo” of dextran-poor areas that became more prominent with increased size (Fig. 2.11d). These data demonstrate that metastatic PDAC liver lesions are initially well-vascularized and perfused but become progressively hypovascular with growth. To determine if this trend of decreasing vascularity with increasing lesion size holds true in human disease, we stained human PDAC tumors and matched small and large liver metastases for CD31 and calculated vascular density as $CD31^+$ vessels per micron. Consistent with our findings in the KPCY model, small but not large metastases had a higher vessel density compared to primary tumors (Fig. 2.11e,f). Thus, in both the KPCY model and human PDAC, metastatic growth is associated with decreasing vascular density.

The impact of chemotherapy on metastasis

The studies described so far reveal that large metastatic lesions are hypovascular and surrounded by dense, desmoplastic stroma while small lesions and single cells, although well-perfused by nearby liver sinusoids, have not yet established a

local tumor microenvironment. As PDAC stroma has been proposed to act as a physical barrier to drug delivery in primary tumors[9,10], we hypothesized that large metastases would be more resistant to chemotherapy compared to small lesions and single cells. To test the this “stromal barrier” hypothesis, we treated tumor-bearing KPCY mice with standard of care chemotherapy – the nucleoside analog gemcitabine (GEM) and the albumin-bound microtubule inhibitor nab-paclitaxel (PTX) – to examine the effects of chemotherapy on metastasis. Animals received intraperitoneal (IP) injections of GEM and PTX (each at 120 mg kg^{-1}) every four days for 2-4 weeks, for a total of 4-8 doses of chemotherapy, and were sacrificed when moribund. Compared to untreated historical controls (matched for age and tumor weight; Fig. 2.12a,b), this treatment regimen led to a dramatic reduction in metastatic tumor burden with a decrease in the mean (± SD) number of lesions from 50.7 ± 64.9 (untreated) to 13.3 ± 13.0 (treated) (Fig. 2.13a). In addition, the metastases that did form were significantly smaller (Fig. 2.13b), with no macro-metastases and only a single milli-metastasis evident in chemotherapy-treated animals. Interestingly, chemotherapy also led to a reduction in the frequency of circulating tumor cells (CTCs) in tumor-bearing KPCY mice, with a log decrease in the mean number of CTCs from 141.6 ± 390.0 per ml (untreated) to 14.6 ± 14.6 per ml (treated) (Fig. 2.12c).

We reasoned that GEM/PTX could shift the numerical and size distribution of metastases by either preventing the progression of small lesions or by reducing the burden of multicellular metastatic lesions at every stage. To distinguish between these possibilities, we treated tumor-bearing KPCY mice with a single dose of chemotherapy and assessed cell death in primary tumors and metastases 10-12 hours later by CC3 staining. With the exception of single cells, metastases in all size categories exhibited a significant increase in CC3 staining after treatment (Fig. 2.13c, Fig. 2.12d). Surprisingly,

almost no cell death was observed in single YFP^+ cells following GEM/PTX treatment (Fig. 2.13c), consistent with the observation that the number of single cell lesions did not change after chemotherapy (Fig. 2.13b). These data suggest that chemotherapy induces comparable degrees of cell death in lesions of all sizes greater than one cell.

We considered the possibility that EMT is responsible for the apparent chemoresistance of single cells. EMT has been implicated in resistance to GEM in PDAC[144-146], and since small metastases have high rates of EMT (Figure 2.4), we hypothesized that lesions treated with GEM/PTX for 2-4 weeks would be enriched for mesenchymal features. We assessed the expression of ECAD and FSP1 in untreated and treated primary tumors and small metastatic lesions, focusing only on single cells and nano-metastases since nearly all treated lesions fell into these two size categories (representative images in Fig. 2.14a,c). Surprisingly, treated primary tumors and metastatic lesions were significantly depleted of $ECAD^-$ and $FSP1^+$ mesenchymal tumor cells (Fig. 2.14b,d). We then assessed the rate of apoptosis in $ECAD^+$ and $ECAD^-$ tumor cells from mice treated with one dose of GEM/PTX and harvested 10-12 hours later. Consistent with the loss of mesenchymal tumor cells with long-term treatment, $ECAD^-$ tumor cells in the primary tumor and metastases had significantly higher rates of CC3 positivity compared to $ECAD^+$ cells (Fig. 2.14e,f). These data suggest that EMT promotes chemosensitivity in the context of GEM/PTX treatment.

Discussion

The highly inefficient nature of metastasis has made it difficult to observe the cellular and molecular events underlying tumor cell spread and growth at distant sites. As a result, most animal studies of metastasis have relied on transplantation of tumor

cell lines into recipient animals. In this study, we used a genetically engineered mouse model to characterize the key events that accompany metastatic growth, from single cells to large grossly detectable metastases. Importantly, the stochastic nature of tumor development and metastatic progression in the KPCY model allowed us to assess the natural history, and treatment response, of metastasis in the setting of naturally evolving and genetically heterogeneous tumors, an approach that has not been taken previously with any cancer type.

The vast majority of animals with advanced pancreatic tumors had either overt or occult metastases, mirroring the human disease in which relapse is the norm despite surgery, with most lesions being smaller than 100 cells in size. Although small metastatic lesions exhibited features that distinguished them from primary tumors, they progressively acquired cell-intrinsic and –extrinsic features of the primary tumor. One of the biggest surprises of our study was that the rate of cell proliferation did not fluctuate with lesion size despite the dramatic changes in the microenvironment with progression. Large lesions were predominantly comprised of tumor cells with an epithelial phenotype, an observation consistent with the notion that epithelial properties are advantageous at metastatic sites[39-41]. Because proliferation rates did not vary across lesions and death rates were negligible, the tendency for large metastatic lesions to have an epithelial phenotype is most likely the result of MET rather than selective outgrowth of the epithelial population. Although the factors that drive EMT and MET *in vivo* remain to be determined, the observation that lesions acquire stroma as they grow represents one potential source of signals.

Myofibroblasts appear early during metastatic growth, with most lesions having direct contact with myofibroblasts by the time they are 6-7 cells in size. This rapid recruitment suggests that factor(s) produced by the cancer cells either attract pre-

existing myofibroblasts to the lesion or activate local stellate cells to differentiate into myofibroblasts. ECM deposition became more evident in advanced lesions, with macro-metastases exhibiting levels of collagen I, fibronectin, hyaluronic acid and SPARC comparable to levels present in primary tumors, consistent with a recent study reporting similar levels of myofibroblasts, collagen, and hyaluronic acid in human primary pancreatic cancers and large metastases[147].

The vasculature also underwent dynamic changes during metastatic progression, with small lesions surrounded by blood vessels and larger lesions exhibiting hypovascularity, mirroring the hypovascular nature of primary PDACs in this model and in the majority of patients. Importantly, we found that human pancreatic tumors exhibit the same phenomenon, with small metastatic lesions having a higher vessel density than large lesions and primary tumors. Although the mechanism leading to vessel paucity in primary tumors and large metastases remains unknown, we recently showed that depletion of stromal fibroblasts (by interfering with Shh signaling) results in increased vessel density, suggesting that fibroblasts and/or ECM components exert an anti-angiogenic effect[58]. Hence, it is possible that hypovascularity is a consequence of increased myofibroblast activity. Regardless of the mechanism, it appears that the so-called “angiogenic switch” – whereby tumor cells activate an angiogenic signal to increase their vascularity – is dispensable for the transition from micro-to macro-metastasis in PDAC.

For patients with metastatic PDAC, treatment with chemotherapy provides minimal improvement of survival[22,23], whereas adjuvant chemotherapy for patients in clinical remission after initial resection offers a more substantial benefit, doubling overall survival. In the KPCY model, we observed killing in a wide spectrum of metastases, providing direct evidence that adjuvant chemotherapy targets lesions that are too small

to detect by standard imaging. We had initially hypothesized that small lesions, with their close proximity to endothelium and lack of stroma, would be particularly susceptible to chemotherapy, while large lesions, which are hypovascular and protected by stroma, would be resistant[9-11]. Thus, it was surprising that chemotherapy resulted in comparable levels of cell death in small lesions, large lesions, and primary tumors, while having only minimal impact on single cells. These results suggest that the stromal barrier hypothesis – which postulates that blood vessel paucity and desmoplastic stroma impedes the delivery of chemotherapy – is incomplete, at least with respect to metastatic lesions.

There are several possible explanations for the apparent resistance of single cells to both long-term and short-term chemotherapy. The simplest possibility is that single disseminated cells are replenished by the primary tumor faster than they are being removed by chemotherapy. However, the observation that treated mice have significantly fewer CTCs would argue against this hypothesis. Mesenchymal tumor cells were acutely sensitive to chemotherapy, consistent with the observation by Collisson *et al*. that human and murine mesenchymal PDAC cell lines are more susceptible to gemcitabine compared to epithelial lines[17]. Single cells were enriched for epithelial features after long-term treatment, and since the average number of single cells did not differ between untreated and treated mice this likely reflects a mesenchymal-epithelial transition. Therefore, another possibility is that the epithelial plasticity of single disseminated cells plays a role in resistance to the combined treatment of gemcitabine and nab-paclitaxel. Finally, as nab-paclitaxel is thought to act by binding SPARC in the tumor microenvironment, increasing its local concentration, it is possible that the absence of SPARC near single cells spares them from cytotoxicity. This is an especially attractive mechanism in light of the fact that EMT induces SPARC expression[148], and

there is significantly less EMT within treated lesions. While SPARC's role in primary tumor chemosensitivity is disputed[149-152], its role in metastasis is yet to be explored. Our data also have implications for the treatment of patients with resectable PDAC. KPCY animals treated for only 2-4 weeks with gemcitabine/nab-paclitaxel exhibited a marked improvement in metastatic burden, yet no animals had complete absence of metastatic disease. Indeed, this failure of combination chemotherapy to demonstrate "curative potential" in KPCY mice mirrors a critical failing of adjuvant chemotherapy for patients with PDAC; namely, improvement in median survival compared to observation, yet only rare long-term remissions or cures. Thus, even as gemcitabine/nab-paclitaxel and other combinations are beginning to be tested in the adjuvant clinical setting, our findings provide additional motivation to evaluate novel, non-chemotherapeutic approaches that target residual micrometastatic disease.

Materials and Methods

Mouse Strains

Pdx1-cre, $Kras^{LSL\text{-}G12D}$, $p53^{L/+}$, $Rosa^{YFP/YFP}$ mice have been described previously[124]. KPCY mice were palpated and examined for evidence of morbidity twice per week. Tumor-bearing animals were sacrificed when moribund. Both male and female mice were used for analysis with a mean age of 22.6 ± 8.1 weeks. Pdx1-cre, $Rosa^{YFP/YFP}$ mice were used as controls. All vertebrate animal experiments were conducted in compliance with the National Institutes of Health guidelines for animal research and approved by the University of Pennsylvania Institutional Animal Care and Use Committee.

Immunofluorescence (IF)

Tissues were fixed in Zn-formalin, paraffin embedded and stained as previously described [124]. In brief, after sections were deparaffinized, rehydrated and subjected to antigen retrieval, sections were blocked in 5% donkey serum for 1 hour at room temperature (RT), incubated with primary antibodies for 1 hour at RT, washed, incubated with secondary antibodies for 1 hour at RT, washed and mounted. Rabbit anti-Zeb1 (Santa Cruz Biotechnology, Santa Cruz, CA) required additional tyramide signaling amplification (PerkinElmer, Waltham, MA). See Table 2.3 for a list of antibodies used. Slides were visualized using an Olympus IX71 inverted multicolor fluorescent microscope.

Metastasis Quantification

Gross metastases were confirmed by fluorescent microscopy using a Leica MZ16FA multi-color fluorescent stereomicroscope. To determine metastatic burden, YFP^+ lesions

were quantified for 5 liver sections spaced 100 µm apart. Large metastatic lesions that were captured on multiple sections were only counted once.

Percent Area Quantification (IF)

Percent area was determined for a subset of stains (αSMA, COL1, HA, SPARC, FN, CD45, F4/80, GR-1, CD3 & VECAD) by first cropping the image within one cell diameter of each metastatic lesion. Using ImageJ, fluorescent channels were split and the channel of interest was thresholded to highlight positive staining while excluding background. The 'analyze particles' tool was then used to calculate percent area.

Fluorescent Dextran Administration

Tumor-bearing mice were injected with 25 ug kg^{-1} Texas red-conjugated dextran (70,000 MW; Thermofisher Scientific, Waltham, MA) 30 minutes prior to euthanasia. Tissues were embedded in OCT (Electron Microscopy Sciences, Hatfield, PA), cut into 5 um sections and imaged on an Olympus IX71 inverted multicolor fluorescent microscope.

Human Specimens

Tissue samples were obtained from patients who consented to a research autopsy in association with the IRB approved Johns Hopkins Rapid Medical Donation Program (PMID: 19273710). Clinicopathological characteristics are listed in Table 2.3. Formalin-fixed and paraffin-embedded samples of the primary carcinoma, two independent gross liver metastasis sections from these patients were used for image analysis and immunohistochemistry. Micrometastases were detected within the normal liver parenchyma adjacent to gross liver metastases and were identified by nuclear atypia and larger cell size.

Immunohistochemistry

Sections were deparaffinized in xylene, rehydrated and subjected to antigen retrieval. Endogenous peroxidases were blocked with 1.5% H_2O_2. Endogenous avidin and biotin were also blocked using an Avidin/Biotin Blocking Kit (Vector Labs, Burlingame, CA) according to the manufacturer's instructions. Sections were then blocked with 5% donkey serum in 0.3% Triton-X100 (MP Biomedicals, Santa Ana, CA) in PBS for 1 hour at RT, then incubated with primary antibodies at 4^{o}C overnight. The next day, slides were washed in 0.1% Tween-20 (Fisher Scientific, Pittsburgh, PA) in PBS (PBST) and incubated with a biotin-conjugated secondary antibody for 1 hour at RT. Slides were washed in PBST and staining was revealed using ABC-HRP and DAB kits (Vector Labs) according to the manufacturer's instructions.

Human CD31 quantification

Immunolabeled slides were scanned at 200x total magnification at a resolution of 0.49 µm/pixel using an Aperio Scanscope CS digital slide scanner (Aperio Technologies, Inc., Vista, CA). Aperio ImageScope was used to extract 735 μm^2 (1500 x 1500 pixel) fields as TIFF images for further analysis. The fields were randomly selected in the area of interest using a low magnification view of the slide. To compare vessel density in primary and metastatic tumor, up to five fields were extracted from each slide. The extracted fields were then analyzed with image analysis software written using ImageJ (Wayne Rasband, NIH, http://rsbweb.nih.gov/ij/). Total tissue area was measured by manually thresholding a grayscale version of the original field. The CD31-positive area was then measured by first masking out any areas with background staining using manual drawing tools and then performing color deconvolution to separate the DAB and

hematoxylin staining [153]. The DAB image was then manually thresholded to select the CD31 positive pixels. Particles (groups of connected pixels) less than 150 pixels (73.5 μm^2) in size were excluded to reduce the degree of large vessel fragmentation and the presence of single immunoreactive cells. CD31+ vessel density was calculated as the number of CD31 positive particles/total tissue area.

Chemotherapy Administration

Tumor-bearing animals in healthy condition were enrolled once the tumor had reached an estimated 1 cm in diameter based on palpation. With the knowledge that the average number of metastases per mouse in our historical, untreated controls is 50.7 (± 64.9), we concluded that a large effect size of at least a 75% decrease in metastasis with a relatively small (≤10) standard deviation would be necessary to detect significant changes after treatment. Using these values, with an alpha error level of ≤5%, we determined that a sample size of 8 mice would be sufficient. Gemcitabine-HCl (Sun Pharmaceuticals, Mumbai, India) and nab-paclitaxel (Abraxane; Celgene, Summit, NJ) were both dissolved in PBS and administered via intraperitoneal injection at 120 mg kg^{-1}. The drugs were administered simultaneously once every four days until the mouse became moribund, between 2-4 weeks from enrollment. Each mouse received at least 4 (and a maximum of 8) doses.

Flow Cytometry

Blood was collected by cardiac puncture as previously described [124]. Erythrocytes were removed using RBC lysis buffer (G-biosciences, St. Louis, MO) according to the manufacturer's instructions. The remaining cellular fraction was stained with APC anti-

mouse CD45 (Biolegend, San Diego, CA) and analyzed on a BD FACSVerse flow cytometer. $DAPI^-$/ $CD45^-$/YFP^+ events were counted as circulating tumor cells.

Statistical Analysis

Differences between two groups were analyzed by two-tailed Student's t-test with Welch's correction to account for unequal SDs, or by Mann-Whitney test for non-normally distributed data. Differences between three or more groups were analyzed by one-way ANOVA with Tukey's multiple comparisons test used as a post hoc test to assess differences between 'single cells' and all other groups. For experiments in which 'single cell' means were binary (0 or 100%), differences between 'single cells' and all other groups were analyzed by one-sample t-test. All statistical analyses were performed using GraphPad Prism 6 (GraphPad, La Jolla, CA). $P \leq 0.05$ denotes differences that are statistically significant.

Chapter 2 Figures and Figure Legends

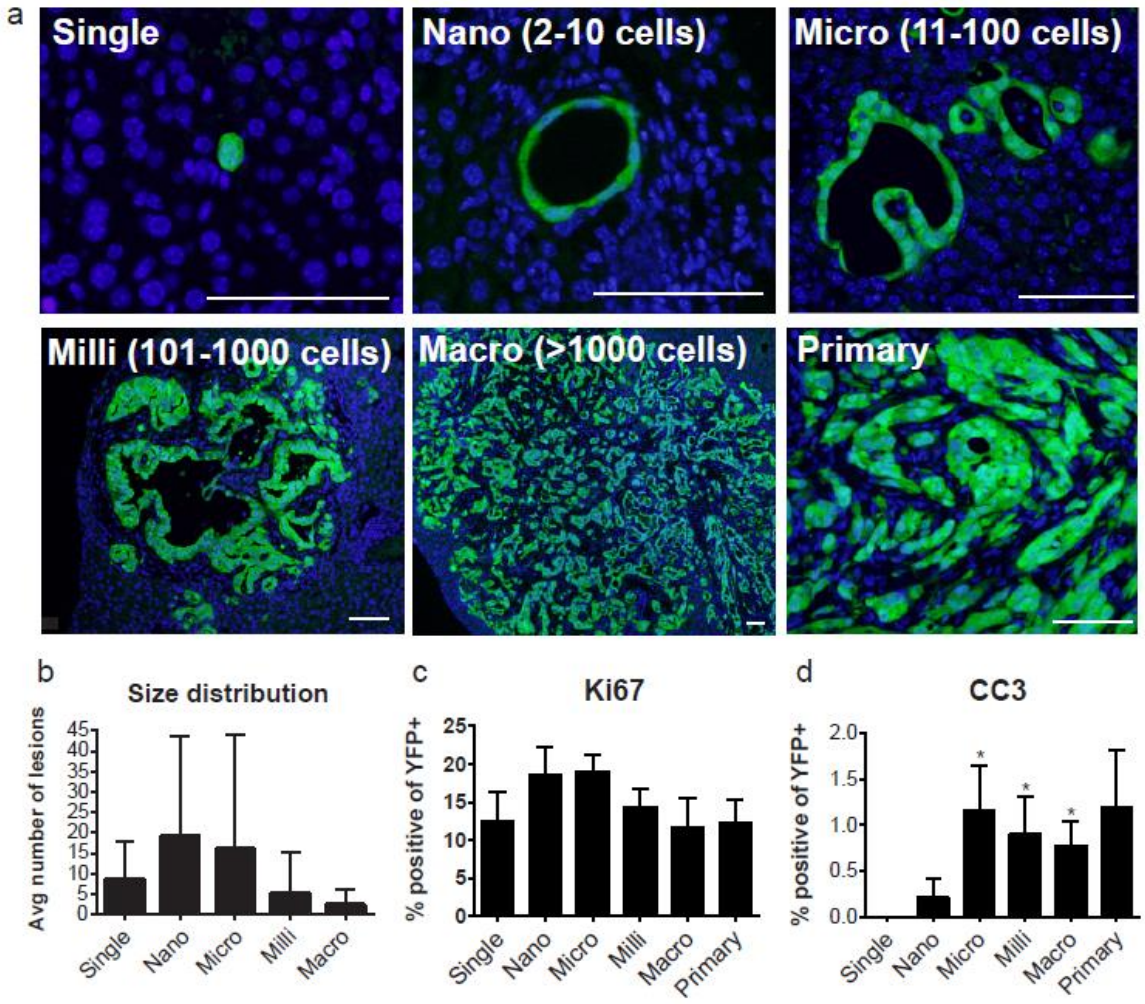

Figure 2.1: Metastatic landscape of the KPCY model. (a) Representative images of YFP$^+$ liver metastases and primary tumor. Scale bars, 50μm. (b) Size distribution of metastatic lesions in the liver grouped according to size (n=23 mice). (c) Quantification of KI67$^+$ (p=0.9439) tumor cells in liver metastases (n= 6 mice, 159 lesions). (d) Quantification of CC3$^+$ (p= 0.1621) tumor cells in liver metastases (n= 4 mice, 46 lesions). P-values were calculated by one-sample t-test against 'single cell' means. Data are presented as mean ± SD.

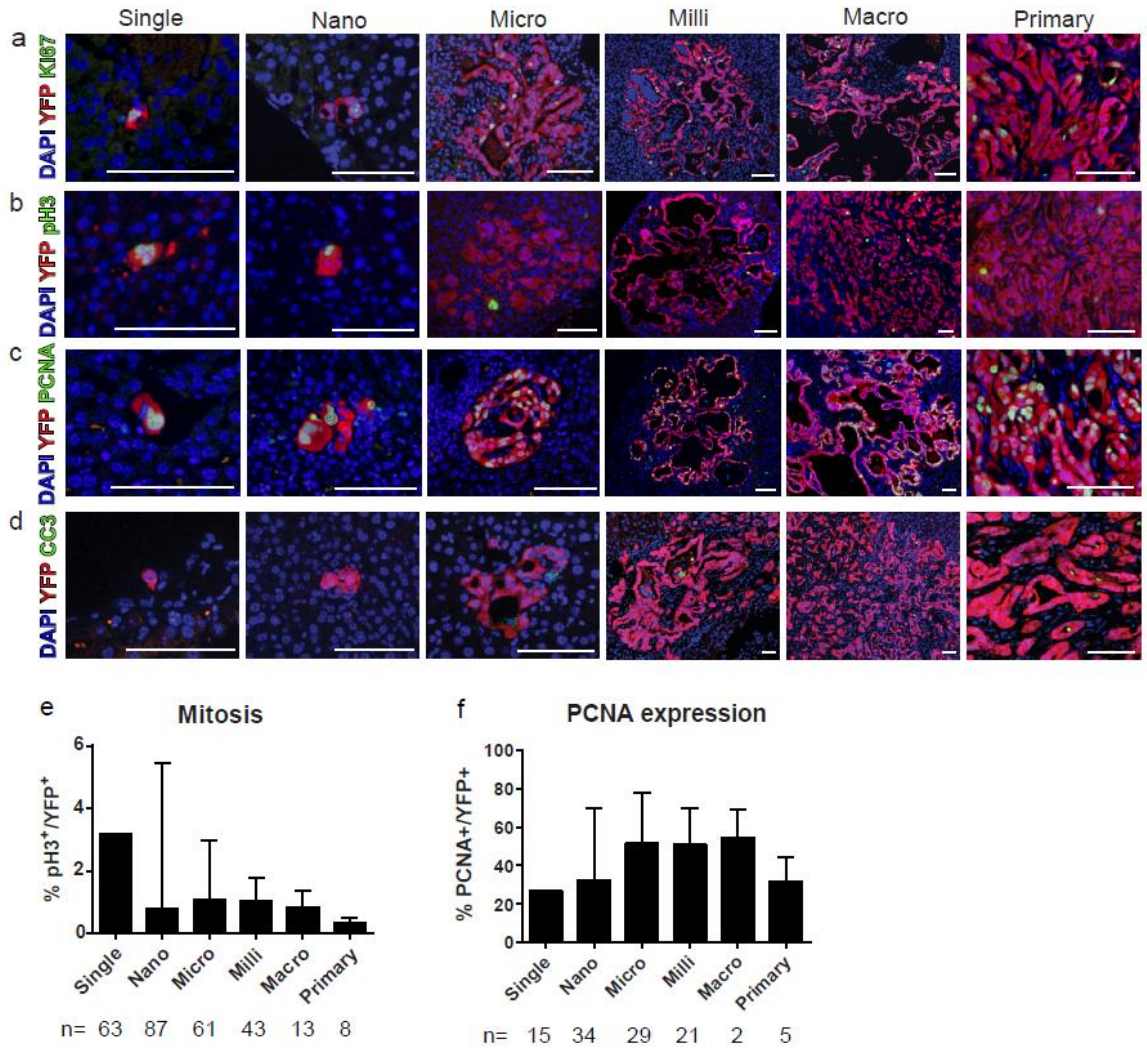

Figure 2.2: Proliferation/apoptosis rates of metastatic lesions. (a) Proliferation. Primary tumor and metastases were stained for YFP (red), DAPI (blue) and Ki67 (green). (b) Mitosis. Primary tumor and metastases were stained for YFP (red), DAPI (blue) and pH3 (green). (c) PCNA expression. Primary tumor and metastases were stained for YFP (red), DAPI (blue) and PCNA (green). (d) Apoptosis. Primary tumor and metastases were stained for YFP (red), DAPI (blue) and CC3 (green). (e) Quantification of pH3 staining; p= 0.9633. (f) Quantification of PCNA staining; p=0.0642. Bars represent means ± SD. Scale bars, 50 μm.

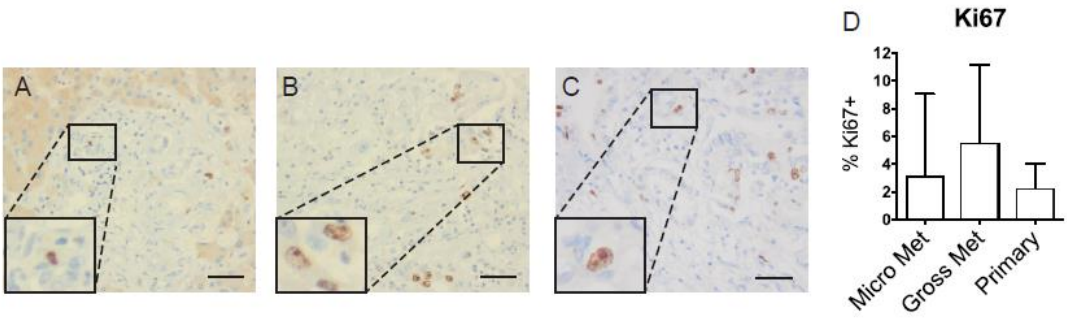

Figure 2.3: Proliferation in human PDAC tumors and metastases. (a-c) Representative images of a micrometastatic lesion (a), gross metastasis (b) and primary tumor (c) stained for Ki67 by IHC. (d) Quantification of Ki67 staining. The percentage of $Ki67^{+}$ cells was determined for micro-metastases (n=126), gross metastases (n=11) and primary tumors (n=7); p=0.3890. For large lesions (gross metastases and primary tumors), five fields were averaged together. Bars represent means ± SD.

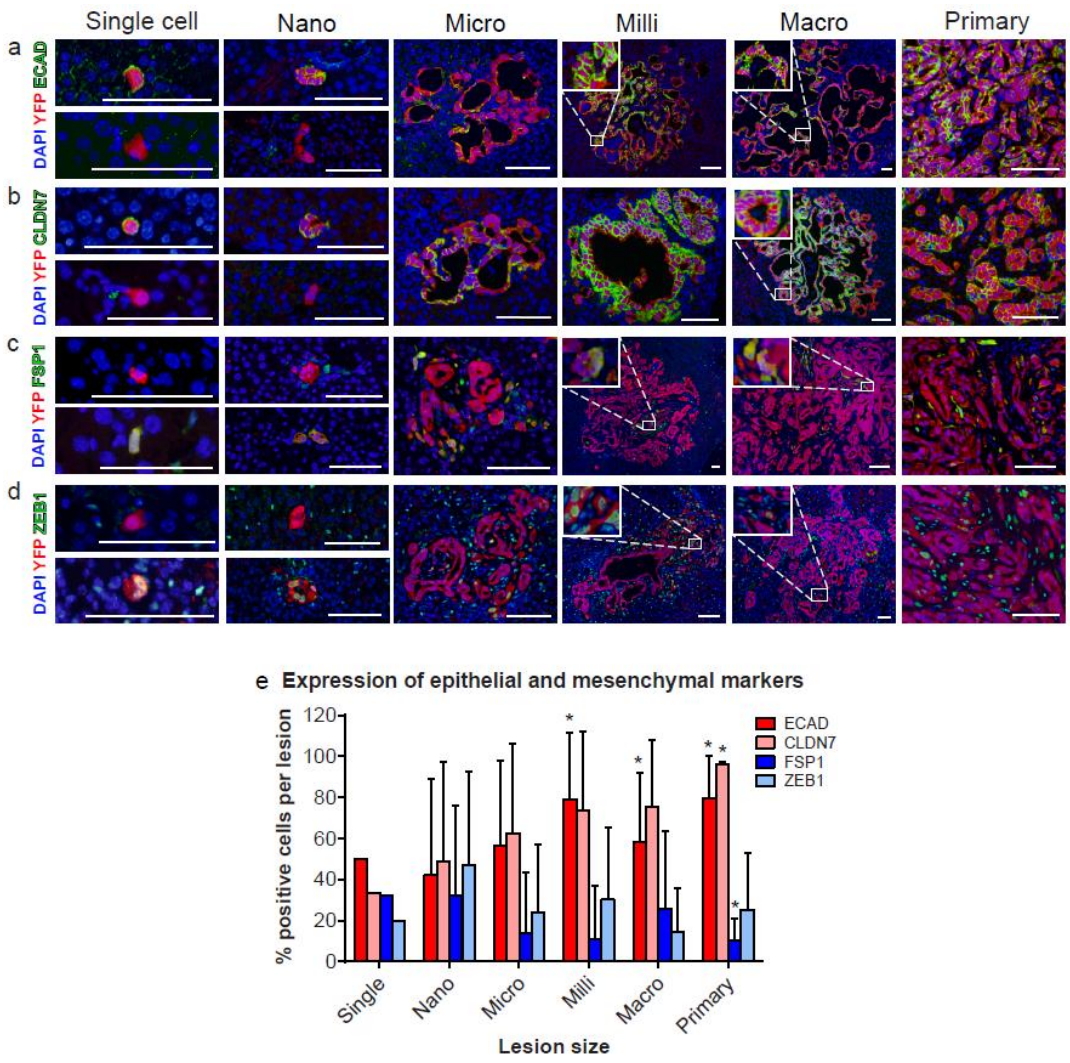

Figure 2.4: Metastatic growth is associated with a more epithelial phenotype. (a-d) Representative images of metastases and primary tumor stained for DAPI (blue), YFP (red) and ECAD (a), CLDN7 (b), FSP1 (c) and ZEB1 (d) (green). Scale bars, 50 μm. (e) Quantification of EMT in metastases. The percent of positive cells for each lesion was determined and the percentages were averaged across lesions of the same size (ECAD, $p<0.05$; CLDN7, ns; FSP1, $p<0.05$; ZEB1, ns). $n \geq 8$ mice, ≥100 lesions for each stain. Data are presented as mean ± SD. P values were calculated by one-way ANOVA and one sample t-tests against 'single cell' means; *, $p<0.05$.

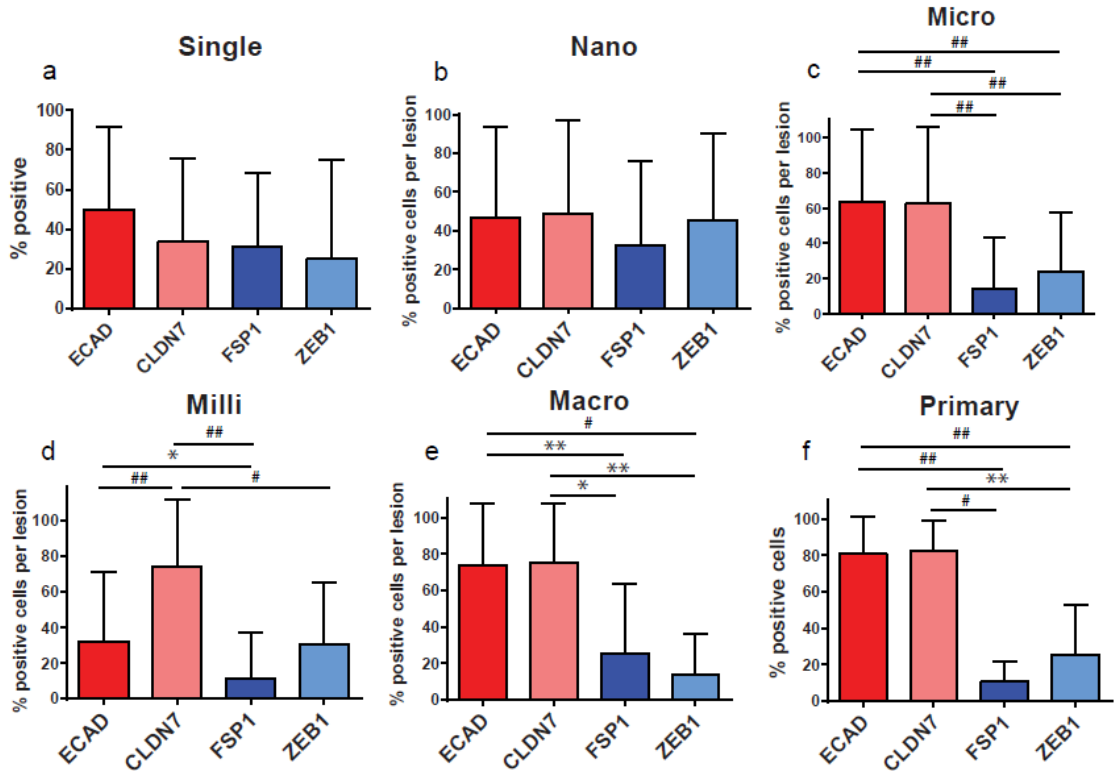

Figure 2.5: Skewing of epithelial to mesenchymal cell ratio within primary tumor and metastatic lesions. (a-f) Comparison of epithelial (ECAD+, CLDN7+) and mesenchymal (FSP1+, ZEB1+) cell frequency within each size category. Bars represent means ± SD; *, p<0.05; **, p<0.01; #, p<0.001; ##, p<0.0001.

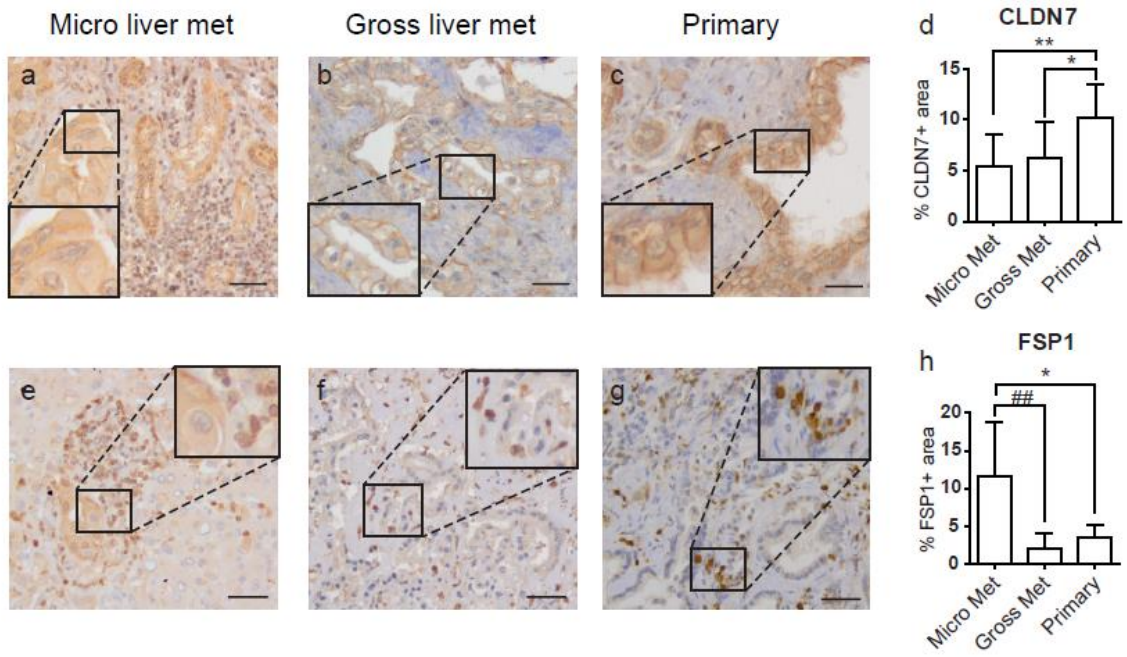

Figure 2.6: Epithelial and mesenchymal features of human PDAC tumors and metastases. (a-c) Representative images of human microscopic liver metastasis (n=114), gross liver metastasis (n=24) and primary PDAC tumors (n=6) stained for CLDN7 by IHC. (d) Quantification of CLDN7+ area per 20X field for gross metastases and primary tumors or within one cell diameter for micro-metastases. (e-g) Representative images of human microscopic liver metastasis (e), gross liver metastasis (f) and primary PDAC tumors (g) stained for FSP1 by IHC. (h) Quantification of FSP1+ area per 20X field for gross metastases (n=18) and primary tumors (n=6) or within one cell diameter for micro-metastases (n=57). For large lesions (gross metastases and primary tumors), five fields were averaged together. Bars represent means ± SD; *, $p<0.05$; **, $p<0.01$; #, $p<0.001$; ##, $p<0.0001$.

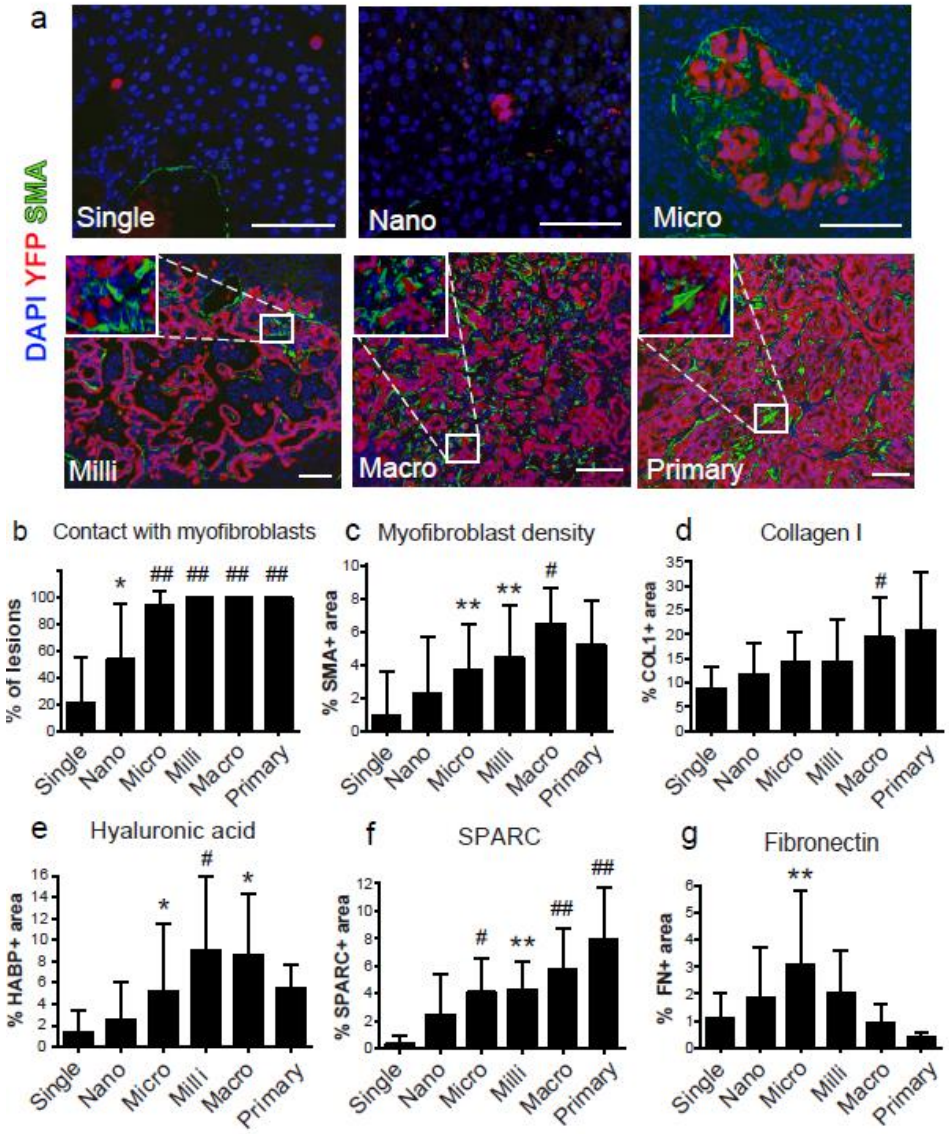

Figure 2.7: Desmoplasia accumulates as lesions grow. (a) Representative images of metastases and primary tumor stained for DAPI (blue), YFP (red) and α-SMA (green). Scale bars, 50μm. (b) Contact between metastases and α-SMA$^+$ fibroblasts. Each lesion was binned by size and scored for direct contact with an α-SMA$^+$ cell (n= 9 mice, 167 lesions). (c) α-SMA$^+$ fibroblast density at metastatic lesions. Percent α-SMA$^+$ area was quantified within one cell diameter of metastatic lesions (n= 9 mice, 167 lesions). (d-g) Extracellular matrix (ECM) density at metastatic lesions. Metastatic livers were stained

for ECM components COL1 (d), HABP (e), SPARC (f) and FN (g). Percent positive area was quantified within one cell diameter of each lesion. n ≥ 5 mice, ≥ 50 lesions for each stain. Data are presented as mean ± SD. P values were calculated by one-way ANOVA and one sample t-tests against ‘single cell’ means; *, $p<0.05$; **, $p<0.01$; #, $p<0.001$; ##, $p<0.0001$.

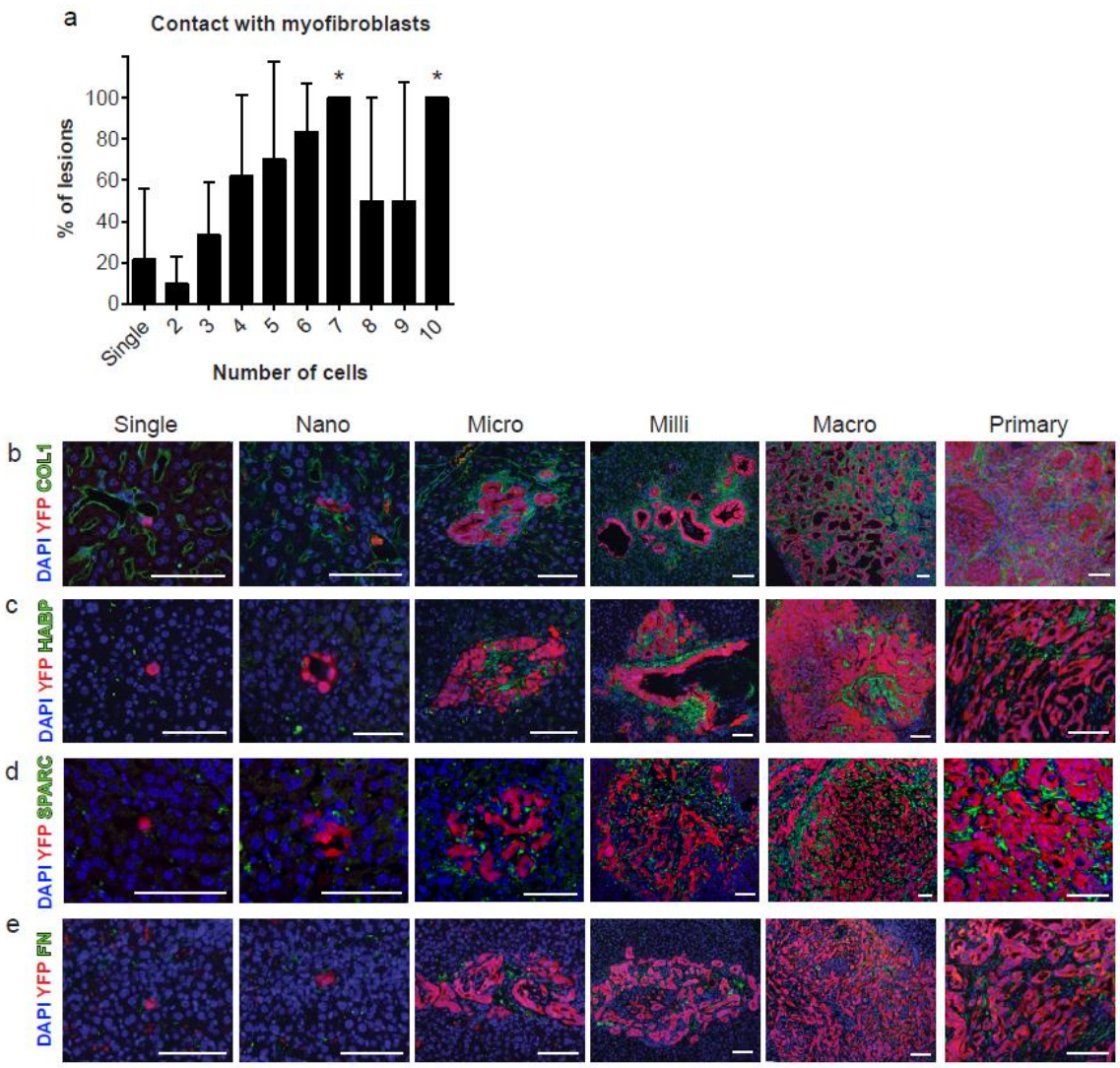

Figure 2.8: Myofibroblast contact with nano-metastases depends on cell size and representative images of ECM stains. (a) Contact between nano-metastases and myofibroblasts by cell number. Data are shown as mean ± SD. P values were calculated by one sample t-tests against 'single cell' mean; *, $p<0.05$. (b-e) Representative images of primary tumor and metastases stained for YFP (red), DAPI (blue) and (b) Collagen 1 (COL1); (c) Hyaluronic acid binding protein (HABP); (d) Secreted protein acidic and rich in cysteine (SPARC); and (e) Fibronectin (FN) in green. Scale bars, 50μm.

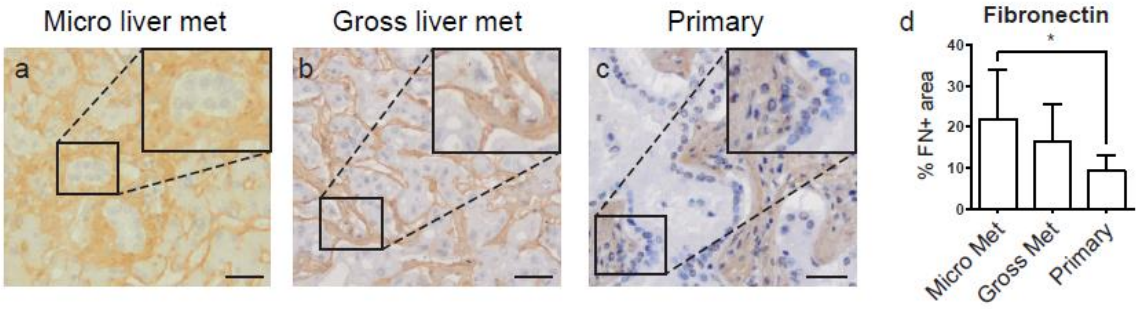

Figure 2.9: Fibronectin deposition in human PDAC tumors and metastases. (a-c) Representative images of human microscopic liver metastasis (n=52), gross liver metastasis (n=18) and primary PDAC tumors (n=6) stained for FN by IHC. (d) Quantification of FN+ area per 20X field for gross metastases and primary tumors or within one cell diameter for micro-metastases. For large lesions (gross metastases and primary tumors), five fields were averaged together. Bars represent means ± SD; *, $p<0.05$.

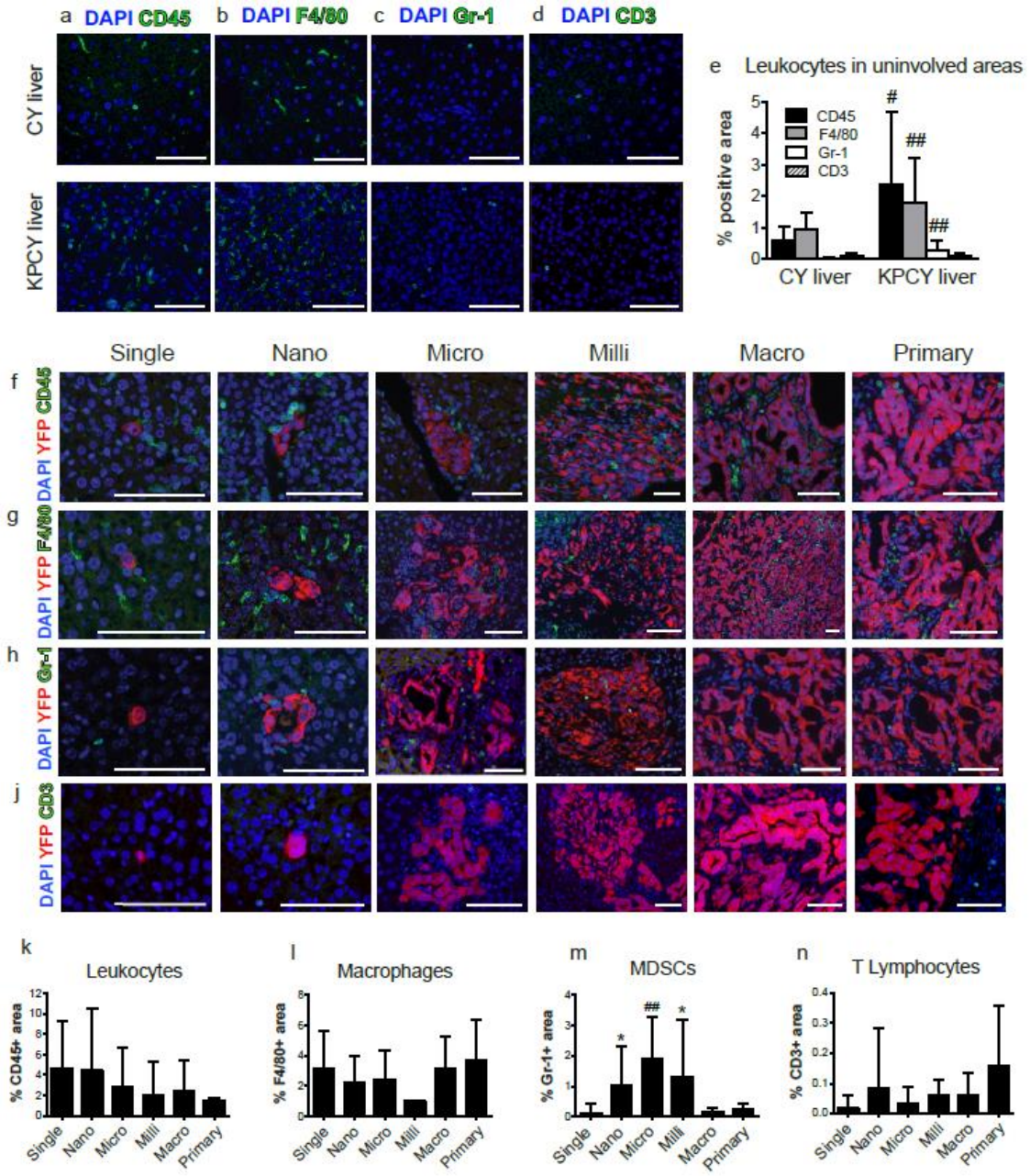

Figure 2.10: Leukocytes accumulate in metastatic livers. (a-d) Representative images of CD45 (a), F4/80 (b), Gr-1 (c) and CD3 (d) staining (green) and DAPI (blue) in uninvolved areas of control (Pdx1-cre, $Rosa^{Y/Y}$) and metastatic (KPCY) livers. Scale bars, 50μm. (e) Quantification of leukocyte density in uninvolved areas of liver (CD45, p=0.0002; F4/80, p<0.0001; Gr-1, p<0.0001; CD3, p=0.3243). (f-j) Representative

images of leukocyte density at metastatic lesions. Metastases and primary tumor were stained for YFP (red), DAPI (blue) and (f), CD45 (leukocytes); (g), F4/80 (macrophages); (h), Gr-1 (MDSCs); and (j), CD3 (T cells) in green. Scale bars, 50μm. (k-n) Quantification of leukocyte density at metastatic lesions. The percent positive area for each leukocyte stain was quantified within one cell diameter of metastatic lesions. Data are presented as mean ± SD. Data are presented as mean of the percent positive area within a 40X field ± SD. n ≥ 5 mice, ≥ 50 lesions for each stain. P values were calculated by one-way ANOVA and unpaired Student's t-test with Welch's correction; *, $p<0.05$; **, $p<0.01$; #, $p<0.001$; ##, $p<0.0001$.

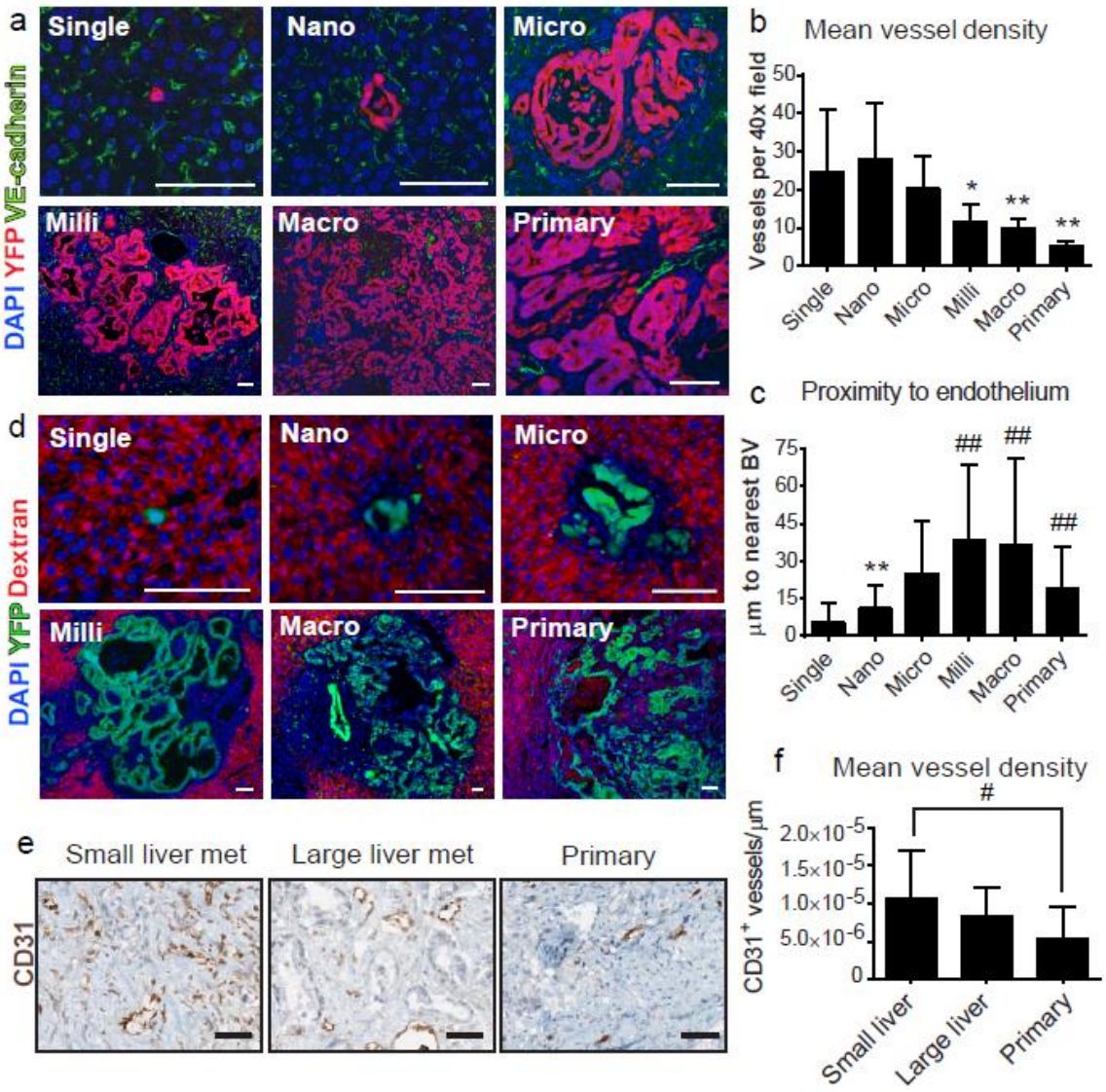

Figure 2.11: Metastatic growth is associated with functional hypovascularity. (a) Representative images of metastases and primary tumor stained for VECAD (green), YFP (red) and DAPI (blue). Scale bars, 50µm. (b) Metastatic vessel density. VECAD$^+$ blood vessels were quantified at metastases within 40x fields. Data are presented as mean ± SD; n = 7 mice, 100 lesions. (c) Proximity to blood vessels. For each lesion, the distance between five random tumor cells and the nearest VECAD$^+$ blood vessel was determined. Data are presented as mean ± SD. n = 7 mice, 100 lesions. P values were

calculated by one-way ANOVA and one sample t-tests against ‘single cell’ means. (d) Functional hypovascularity at large metastases. Representative images of fluorescent dextran accumulation (red) at metastatic lesions (YFP, green; DAPI, blue). (e) Representative images of human primary PDAC and matched liver metastases stained for CD31 (brown). Scale bars, 50μm. (f) Mean vessel density quantification of human primary PDAC and matched liver metastases (n=25 cases). Data are presented as mean ± SD; *, $p<0.05$; **, $p<0.01$; #, $p<0.001$; ##, $p<0.0001$.

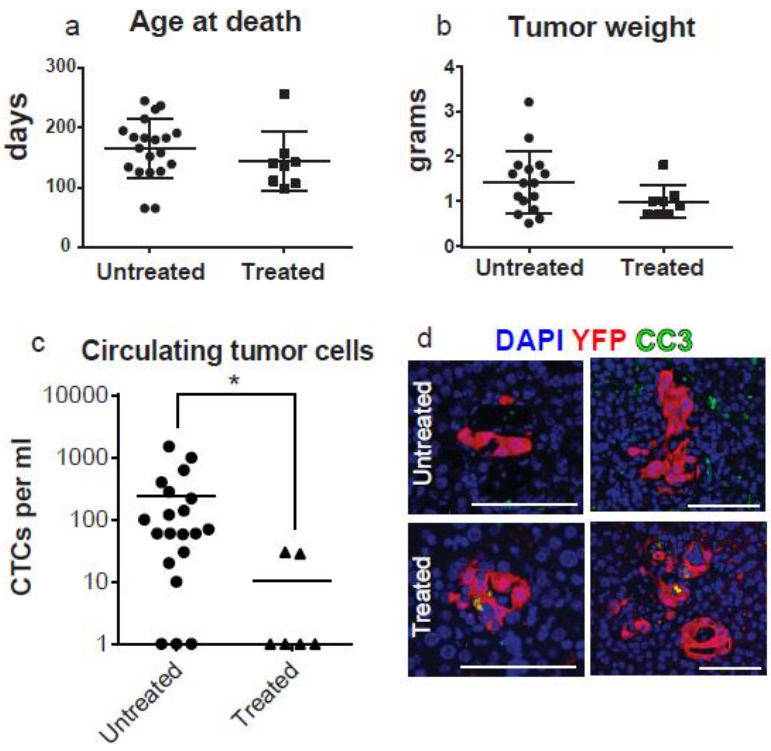

Figure 2.12: Circulating tumor cells (CTCs) are decreased after long-term chemotherapy. (a-b) Age at death (a) and tumor weight (b) for untreated historical controls and treated animals. Lines represent mean ± SD. P value by Student's t-test. (c) CTCs in untreated (n=23) and treated (n=8) mice; *, $p < 0.05$. Lines represent the mean. P value by Student's t-test. (d) Representative images of untreated and treated metastatic lesions stained for CC3 (green), YFP (red) and DAPI (blue). Scale bars, 50μm.

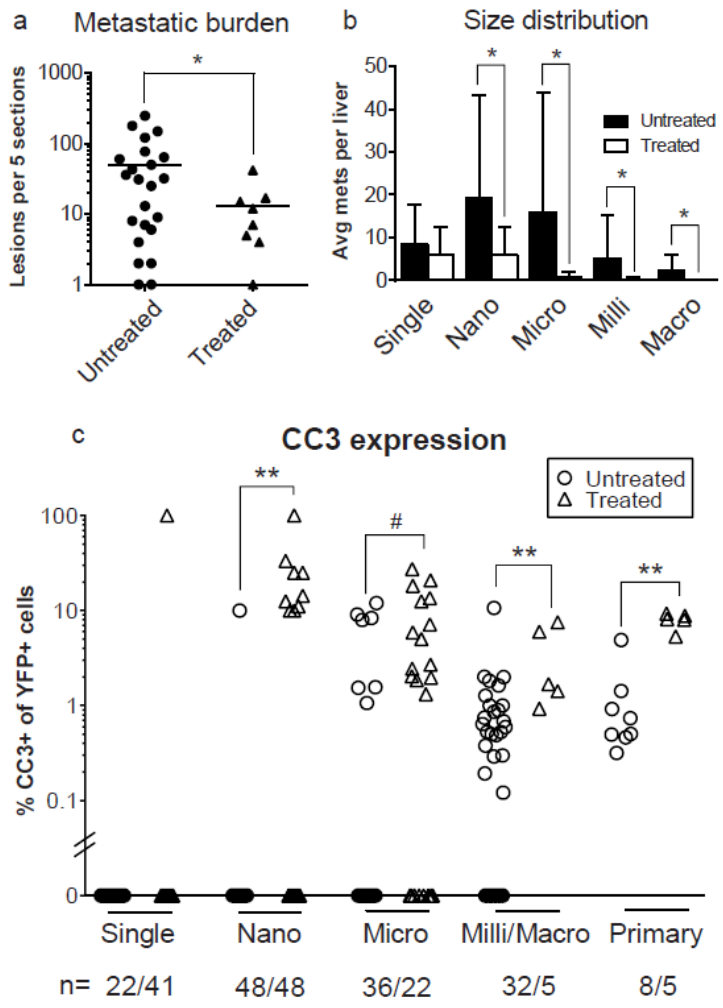

Figure 2.13: Chemotherapy reduces metastatic burden. (a) Liver metastatic burden after long-term chemotherapy. Each dot represents one mouse. Untreated group consists of historical controls from Figure 1B (untreated, n= 23; treated, n=8). Bars represent means ± SD; *, $p<0.05$, Student's t-test with Welch's correction. (b) Size distribution of metastatic lesions after long-term chemotherapy. Data are presented as mean ± SD, *, $p<0.05$, Student's t-test with Welch's correction. (c) Apoptosis rates in metastases after single dose chemotherapy. CC3 positivity in metastases was assessed 10-12 hours after treatment. Each dot represents a lesion; line represents the mean. *, $p<0.05$; **, $p<0.01$; #, $p<0.001$ by Mann-Whitney test.

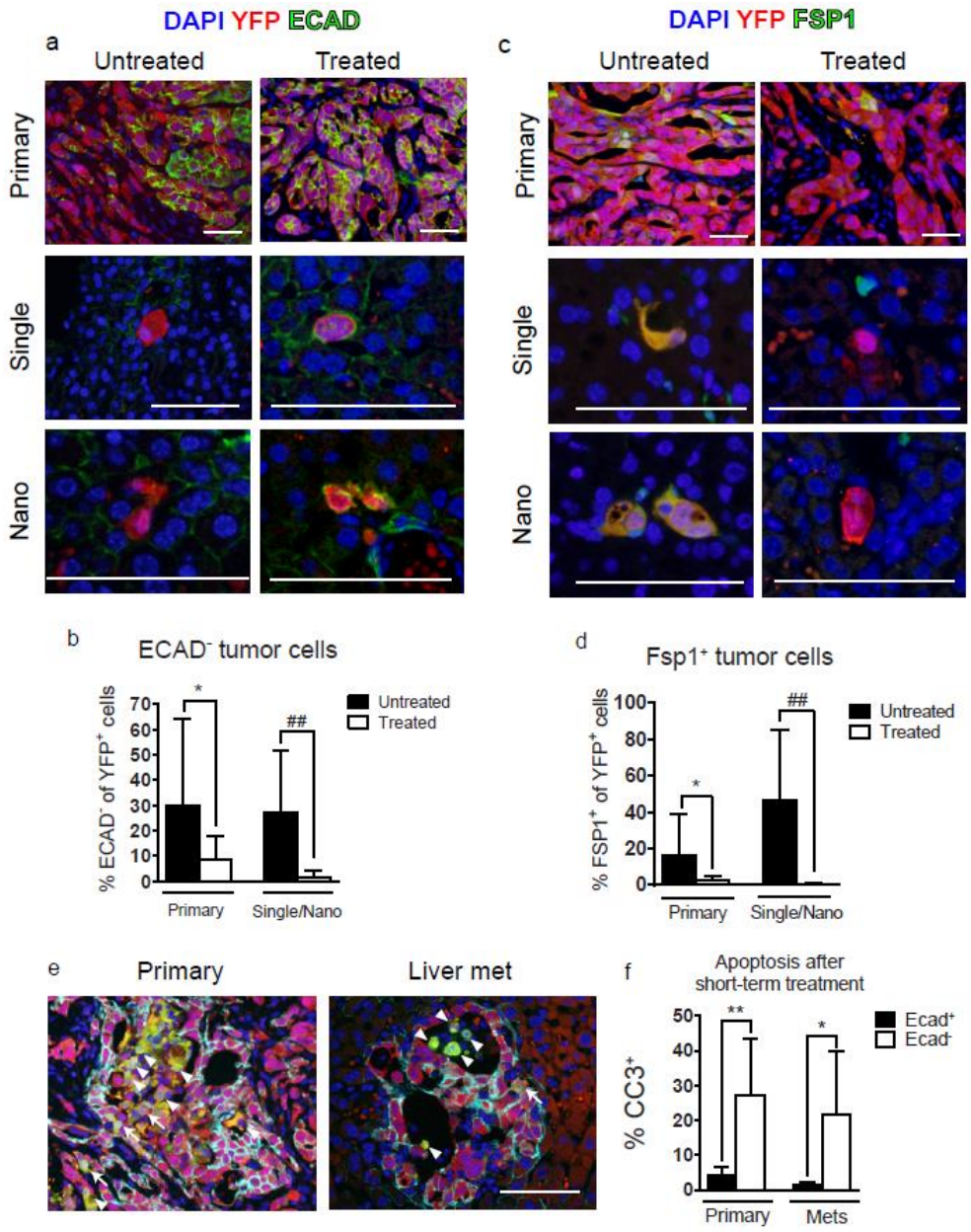

Figure 2.14 Mesenchymal tumor cells are depleted after chemotherapy. (a) Representative images of untreated and treated (GEM/PTX for 2-4 weeks) primary tumors and small metastatic lesions stained for ECAD (green), YFP (red) and DAPI (blue). (b) Quantification of ECAD$^-$ tumor cells in untreated and treated primary tumors and small metastatic lesions. (c) Representative images of untreated and treated primary tumors and small metastatic lesions for FSP1 (green), YFP (red) and DAPI

(blue). (d) Quantification of $FSP1^+$ tumor cells in untreated and treated primary tumors and small metastatic lesions. n ≥ 7 mice for each condition. Bars represent means ± SD. Statistical significance was determined by Student's t-test with Welch's correction. (e) Representative images of treated (1 dose GEM/PTX) primary tumor and liver metastasis stained for CC3 (green), ECAD (cyan), YFP (red) and DAPI (blue). Arrows denote $YFP^+/ECAD^+/CC3^+$ cells, arrowheads denote $YFP^+/ECAD^-/CC3^+$ cells. (f) Quantification of CC3 staining in $ECAD^+$ and $ECAD^-$ tumor cells (n ≥ 4 mice). Bars represent means ± SD. Statistical significance was determined by Mann-Whitney test. Scale bars, 50 um. *, $p<0.05$; **, $p<0.01$; #, $p< 0.001$; ##, $p < 0.0001$.

Chapter 2 Tables

Mouse ID	Single	Nano	Micro	Milli	Macro	Total
PD012	1	1	0	0	0	2
PD122	1	1	0	0	0	2
PD1806	7	13	19	11	10	60
PD1821	9	33	21	1	0	64
PD1849	1	9	22	11	7	50
PD2039	11	15	5	0	0	31
PD2204	14	16	12	0	1	43
PD2329	1	0	0	0	0	1
PD2420	0	1	6	1	0	8
PD2523	13	16	6	0	1	36
PD333	1	0	0	0	0	1
PD350	24	48	5	0	0	77
PD422	6	69	120	41	11	247
PD431	12	31	69	27	10	149
PD463	5	4	0	0	0	9
PD483	1	8	10	5	1	25
PD487	5	2	0	0	0	7
PD635	25	44	34	10	8	121
PD661	10	20	2	0	0	32
PD796	3	3	0	0	0	6
PD798	4	8	1	0	0	13
PD8482	1	3	0	0	0	4
PD883	37	94	35	9	3	178

Table 2.1: Metastatic burden (raw counts) for each animal used in Figure 3b.

Antibody	Concentration	Company
Goat and Chicken α GFP	1:500	Abcam
Rabbit α CK19	1:1000	In house
Rabbit α Phospho-Histone H3	1:400	Cell Signaling
Rat α Ki67	1:100	DAKO
Rabbit α PCNA	1:1000	Cell Signaling
Rabbit α Cleaved Caspase-3	1:200	Cell Signaling
Rat α E-cadherin	1:1000	Invitrogen
Rabbit α Claudin-7	1:100	Abcam
Rabbit α Fsp1	1:500	DAKO
Rabbit α Zeb1	1:100	Santa Cruz
Rabbit α αSMA	1:100	Abcam
Rabbit α Collagen I	1:200	Abcam
Biotinylated bovine hyaluronic acid binding protein	1:200	Calbiochem
Goat α SPARC	1:100	R&D Systems
Rabbit α Fibronectin	1:300	Abcam
Rat α CD45	1:50	BD Biosciences
Rat α F4/80	1:50	Ebioscience
Rat α Gr-1	1:50	Ebioscience
Goat α VE-cadherin	1:100	R&D Systems

Table 2.2: Antibodies used in Chapter 2.

Average age ± SD	61.6 ± 11.3	**Chemotherapy, n (%)**	23 (76.7)
Average OS, mo ± SD	10.5 ± 9.2	**Radiation, n (%)**	10 (33.3)
Average tumor size, cm ± SD	5.6 ± 3.0	**Metastatic burden, n (%)**	
Sex, n (%)		≤10	2 (6.7)
Male	18 (60)	11-100	10 (33.3)
Female	12 (40)	>100	18 (60)
Location, n (%)		**Differentation, n (%)**	
Head	18 (60)	Well/Moderate	1 (3.3)
Body	7 (23.3)	Moderate	10 (33.3)
Tail	4 (13.3)	Moderate/Poor	12 (40)
Unknown, n (%)	1 (3.4)	Poor	6 (20)
Stage at diagnosis, n (%)		**KRAS status, n (%)**	
IIB	2 (6.7)	Mutant	29 (96.7)
III	7 (23.3)	WT	1 (3.3)
IV	21 (70)	**TP53 status, n (%)**	
Surgery, n (%)	4 (13.3)	Mutant	26 (86.7)
		WT	4 (13.3)

Table 2.3: Clinicopathological characteristics of patients. Abbreviations: standard deviation (SD); overall survival (OS); month (mo); number of patients (n); wildtype (WT).

CHAPTER 3: A non-canonical mechanism drives epithelial plasticity *in vivo*

Abstract

Metastasis is responsible for the majority of cancer-related deaths, and yet the molecular mechanisms underlying tumor cell spread remain elusive. It is widely believed that epithelial-to-mesenchymal transition (EMT) – during which epithelial cells lose their adhesive behavior and acquire a fibroblast-like morphology and migratory behavior – is an important step in cancer progression[154]. EMT is reawakened during tumorigenesis in mouse models[124,155,156], where it contributes to invasion and hematogenous dissemination[81,82,157]. EMT is thought to be regulated primarily at the transcriptional level through the repressive activity of EMT transcription factors (EMT-TFs) on epithelial genes including *E-cadherin (Cdh1)*[158,159]. However, these canonical EMT mechanisms have been parsed out almost exclusively *in vitro* under defined experimental conditions, and the molecular programs that drive EMT in physiological context remain to be delineated. Here, we describe a post-translational mechanism that accounts for EMT in the majority of tumors in a murine model of pancreatic ductal adenocarcinoma (PDAC). This “non-canonical” program employs epithelial protein internalization, rather than transcriptional repression, to suppress the epithelial program. At a global transcriptional level, tumors utilizing this alternative EMT program are associated with the recently identified classical/progenitor/exocrine transcriptional subtypes of PDA, while those tumors utilizing canonical EMT programs correspond to the squamous/basal/quasi-mesenchymal subtype of PDAC. Most strikingly, tumor cells utilizing non-canonical EMT mechanisms exhibit greater epithelial-mesenchymal plasticity and tumor initiation capacity compared to tumor cells utilizing canonical mechanisms. Taken together our

data demonstrate that the programs driving tumor-associated EMT *in vivo* differ dramatically from the classically described Tgfβ-Snail-Twist axis.

Introduction

Metastasis is responsible for the majority of cancer-related deaths, and yet the molecular mechanisms underlying tumor cell spread remain elusive. During a tumor cell's journey to the metastatic site it must adapt to ever-changing obstacles, from local desmoplasia to the circulatory system to foreign and potentially hostile microenvironments. Thus a key feature of any successful metastasizing cell is plasticity. It is widely believed that epithelial-mesenchymal transition (EMT) and the reverse process mesenchymal-epithelial transition (MET) are responsible for ushering cancer cells through the gauntlet of the metastatic cascade[154]. During EMT, an epithelial cell loses its apicobasal polarity and adhesion to neighboring cells to take on a more fibroblast-like morphology and migratory behavior[86]. EMT is an evolutionarily conserved program critical for aspects of embryogenesis that require dynamic cellular movements, such as gastrulation and neural crest cell migration[38,160]. We and others have demonstrated that EMT is reawakened during spontaneous tumorigenesis in mouse models[156,161,162], in some cases even before frank malignancy[124,163]. EMT appears to be vital for early steps of metastasis (hematogenous dissemination)[39-41], however metastatic lesions tend to have an epithelial histology[35,132,156] and numerous studies have demonstrated that reversion back to an epithelial state is essential for later steps of metastasis (colonization)[39,40].

Canonical mechanisms of EMT hinge on the transcriptional repression of epithelial genes, most notably E-cadherin, by various EMT transcription factors such as Snail, Slug, Twist and Zeb1/2[86]. These transcription factors are induced by many

different extracellular signals, including but not limited to TGFβ[164], HGF[165], WNT[166] and EGF[167], and are negatively regulated by microRNAs such as mir-34[93,94] and the miR-200 family[97,99,168]. To date, the mechanisms driving EMT have been parsed out almost exclusively *in vitro* under pre-defined conditions (ie, by using recombinant TGFβ or overexpressing Snail), but it remains to be seen whether the machinery that regulates *in vitro* EMT is physiologically relevant. Here we show that *in vivo*, and in contrast to canonical mechanisms, EMT is driven primarily by post-translational regulation of the epithelial program which we have termed non-canonical EMT. This alternative mechanism has functional consequences for tumor cells, as it promotes greater epithelial-mesenchymal plasticity and enhances tumor initiation and metastasis compared to canonical EMT.

Results and Discussion

EMT is accompanied by dramatic morphological and molecular changes during which epithelial markers are lost while mesenchymal markers, including transcription factors and cytoskeletal components, are gained. The loss of E-cadherin (Ecad) is considered a hallmark of EMT, and we found that in the pancreatic tumors of *Pdx1-cre; LSL-Kras^{G12D}; P53$^{loxP/+}$; LSL-Rosa$^{YFP/YFP}$* (KPCY) mice, 89% ± 11.9 (mean ± SD) of YFP^{+} tumor cells that had delaminated from epithelial structures were negative for membranous Ecad (Fig. 3.1a). By contrast, only a fraction of tumor cells that had lost Ecad staining also exhibited higher expression of mesenchymal markers or EMT-TFs such as zinc-finger E-box homeobox 1 (*Zeb1*), slug (*Snai2*), vimentin (*Vim*), or fibroblast-specific protein 1 (*Fsp1*) (Fig. 3.2a-e). Moreover, expression of these mesenchymal markers was rarely observed in tumor cells that were positive for membranous Ecad.

Thus, Ecad loss, rather than the gain of a single mesenchymal marker, is the most reliable indicator of cells that have undergone EMT in this model.

To better understand the transcriptional changes associated with EMT *in vivo*, we used fluorescence-activated cell sorting (FACS) to isolate $Ecad^+$ (epithelial; E) and $Ecad^-$ (mesenchymal; M) YFP^+ cancer cells from 11 primary KPCY tumors for RNA sequencing (Fig. 3.1a-b; Fig. 3.3a). We confirmed accurate sorting by visual inspection of sorted cells and ruled out contamination of non-tumor cells by performing qPCR for *Cd45* and *YFP* (Fig. 3.3b-d). Although we expected $Ecad^+$ samples to be closely related to each other and distinct from the $Ecad^-$ samples, principal component analysis and unsupervised hierarchical clustering arranged samples into two subgroups organized independently of epithelial-mesenchymal status but instead according to tumor identity (Fig. 3.1c,d). In the first tumor subgroup (3/11), EMT was associated with robust downregulation of *Ecad* mRNA (Fig. 3.1e,f), as expected. In the second subgroup (8/11), by contrast, EMT was associated with stable levels of mRNA for *Ecad* and other epithelial genes (Fig. 3.1e,f). Thus, loss of the epithelial program occurs in the absence of transcriptional repression in the majority of KPCY tumors undergoing EMT.

To distinguish between these mechanisms, we applied the term canonical EMT (C-EMT) to refer to those tumors in which the epithelial program was eliminated by transcriptional repression and the term non-canonical EMT (NC-EMT) to refer to those tumors in which the epithelial program was suppressed by other means. Tumors in both subgroups exhibited a robust upregulation of mesenchymal-related transcripts within the $Ecad^-$ population, including periostin (*Postn*), fibroblast-activated protein (*Fap*), platelet derived growth factor receptor beta (*Pdgfrβ*), GLI-Kruppel family member 1 (*Gli1*), tenascin C (*Tnc*), secreted protein acidic and cysteine rich (*Sparc*), podoplanin (*Pdpn*), palladin (*Palld*) and numerous collagens (Fig. 3.1f). Gene set enrichment analysis

(GSEA) of both C- and NC-EMT samples confirmed that Ecad$^-$ transcriptomes strongly correlated with published EMT datasets (Fig. 3.4). Importantly, transcripts for several known EMT-TFs – *Snai2, Twist1, Zeb1* and ETS variant 1 (*Etv1*) – were significantly more abundant in C-EMT tumors (Fig. 3.5), possibly accounting for the marked reduction in epithelial transcripts in Ecad$^-$ samples from these tumors. Thus, tumors characterized as either C-EMT or NC-EMT exhibit overlapping EMT-associated mesenchymal programs despite having distinct mechanisms for repressing their epithelial programs during EMT.

We noticed that tumors categorized as C-EMT tended to be poorly differentiated while tumors characterized as NC-EMT tended to be moderately-to-well differentiated (Fig. 3.6). Consequently, we hypothesized that these two modes of EMT may be related to known PDAC subtypes, which also exhibit histological heterogeneity. To test this, we compared our KPCY tumor transcriptomes to three reported PDAC subtype signatures (Fig. 3.7). In all cases, C-EMT tumors were strongly associated with poorly-differentiated subtypes (quasi-mesenchymal, squamous, and basal-like) while NC-EMT tumors were strongly associated with well-differentiated subtypes (classical/exocrine-like, pancreatic progenitor/ADEX, and classical)[17-19]. Hence, the mode by which the epithelial phenotype is lost in murine models of PDAC correlates with transcriptional subtypes in human PDAC, suggesting that tumor class dictates EMT mechanism *in vivo*.

To further understand these distinct mechanisms, we developed a quantitative PCR (qPCR) signature that could distinguish between C- and NC-EMT and applied it to a panel of mouse and human PDAC cell lines (Fig. 3.8a,b). As predicted, cell lines expressing the C-EMT signature exhibited robust down-regulation of *Ecad* mRNA when FACS sorted into Ecad$^+$ and Ecad$^-$ populations. By contrast, cell lines expressing the NC-EMT signature exhibited no change in *Ecad* mRNA levels when Ecad$^+$ and Ecad$^-$

cells were compared (Fig. 3.8c,d). This suggests that canonical and non-canonical mechanisms of Ecad repression are retained in cell lines derived from mouse and human PDAC. Using principal component analysis, we also found a significant correlation between the C-EMT and quasi-mesenchymal PDAC subtypes, and the NC-EMT and classical PDAC subtypes in human PDAC cell lines, consistent with our findings in murine PDAC tumors and cell lines (Fig. 3.8e). The relationship between tumor subtypes and mode of EMT also applies to breast cancer. Luminal A/B and normal-like breast cancer cell lines, which tend to be well differentiated, are strongly associated with a non-canonical EMT transcriptional profile, while poorly differentiated basal cell lines tend to have a canonical EMT expression pattern (Fig. 3.8f).

EMT is often induced *in vitro* by treating cells with specific growth factors, most commonly Tgfβ. As expected, our PDAC cell lines exhibited morphological features of EMT (Fig. 3.9a) with loss of Ecad protein (Fig. 3.9b) upon Tgfβ treatment. Exposure to Tgfβ resulted in robust transcriptional down-regulation of *Ecad* and up-regulation of *Snail*, *Slug* and *Zeb1*, regardless of whether the cell line was categorized as C-EMT or NC-EMT (Fig. 3.9c). This suggests that cell lines that utilize non-canonical EMT mechanisms under standard culture conditions remain competent to employ a canonical mechanism when confronted with an exogenous (and overriding) growth factor signal.

We next sought to understand the NC-EMT phenotype using our stratified murine PDAC cell lines. Since *Ecad* mRNA abundance remained unchanged during NC-EMT, we examined the fate of Ecad protein during this process. First, to determine whether residual *Ecad* mRNA was being translated, we sorted cells from our cell line panel into $Ecad^{+}$ (E) and $Ecad^{-}$ (M) fractions and compared Ecad protein levels in whole cell lysates (Fig. 3.10a). While the M fraction from C-EMT cell lines lacked any Ecad protein, as expected, the M fraction from NC-EMT cell lines retained Ecad protein (Fig. 3.10b).

Other epithelial proteins, including claudin-7 (Cldn7) and epithelial cell adhesion molecule (Epcam) were also maintained upon NC-EMT at the transcript and protein levels (Fig. 3.10b). In contrast, C-EMT cell lines did not express appreciable levels of these proteins in either the E or M fraction. Levels of p120-catenin, an important direct Ecad regulator, did not vary between E and M in either C- or NC-EMT cell lines. However, NC-EMT cell lines expressed both 1A (mesenchymal) and 3A (epithelial) isoforms[169] while C-EMT cell lines only expressed the 1A isoform (Fig. 3.10b). These data demonstrate that epithelial proteins continue to be translated in cells that have undergone NC-EMT.

We reasoned that Ecad internalization might account for the lack of membrane staining in NC-EMT. To test this, we performed dual antibody live cell immunofluorescence by first staining live cells for Ecad using the fluorophore BV421 (to detect membrane-associated Ecad; M-Ecad) followed by fixation, permeabilization and a second staining of Ecad using the fluorophore APC (to detect intracellular Ecad; I-Ecad) (Fig. 3.10c). As expected, C-EMT cells lacking membranous Ecad (M-Ecad$^-$) were negative for I-Ecad, consistent with the loss of *Ecad* mRNA (Fig. 3.10d). In NC-EMT cell lines, by contrast, the majority of M-Ecad$^-$ cells were positive for I-Ecad (Fig. 3.10d). Consistent with this finding, we detected I-Ecad in sections from tumors expressing a NC-EMT signature (Fig. 3.10e) but not those expressing a C-EMT signature (Fig. 3.10f). These results suggest that Ecad protein is internalized by cells undergoing NC-EMT both *in vitro* and *in vivo*.

We next investigated the molecular mechanisms responsible for changes in Ecad localization and abundance. The only known EMT-related transcription factor significantly upregulated in mesenchymal NC tumor samples compared to epithelial NC tumor samples was *pair-related homeobox 1* (*Prrx1*) (Fig. 3.11a). Prrx1 acts as a

transcriptional activator and has been described as “a more potent mesenchymal inducer than epithelial repressor”[86], fitting the profile of a potential NC-EMT regulator. *Prrx1* produces two isoforms, *Prrx1a* and *Prrx1b,* which are associated with epithelial and mesenchymal phenotypes, respectively[170,171]. Surprisingly, we did not observe isoform switching from Prrx1a to Prrx1b between NC-E and –M tumor samples; rather both isoforms were significantly increased in NC-EMT. Hence we sought to determine whether overexpression of one or both Prrx1 isoforms was sufficient to drive the NC-EMT phenotype, specifically Ecad internalization. Using the PiggyBAC transposon system, we overexpressed Prrx1a, Prrx1b, both isoforms simultaneously or the control vector in C- and NC-EMT KPCY cell lines and assessed their effects on Ecad surface expression and internalization. Overexpression of the mesenchymal isoform, *Prrx1b*, resulted in a subtle but significant increase in M-ECAD$^-$ NC-EMT cells compared to the control while *Prrx1a* alone and *Prrx1a/b* dual expression had no effect on the frequency of M-ECAD$^-$ cells (Fig. 3.11b). Interestingly, the frequency of M-ECAD$^-$/I-ECAD$^+$ cells was significantly increased in an NC-EMT cell line with overexpression of any combination of *Prrx1* isoforms compared to control, suggesting that both Prrx1 isoforms promote the retention of Ecad in the cytoplasm (Fig. 3.11c). These data suggest that while Prrx1 may not be a master regulator of the NC-EMT program, it does play a role in the post-translational regulation of Ecad, which is a prominent feature of the NC-EMT phenotype.

Finally, we explored the functional impact of C- and NC-EMT with respect to tumor initiation and epithelial plasticity. We used flow cytometry to sort cell lines into Ecad$^+$ (E) and Ecad$^-$ (M) populations and then assessed subcutaneous tumor initiation potential by *in vivo* limiting dilution. While the tumor-initiating cell (TIC) frequency was the same for canonical Ecad$^+$ (C-E), canonical Ecad$^-$ (C-M) and non-canonical Ecad$^+$

(NC-E) cells, non-canonical Ecad$^-$ (NC-M) cells exhibited a significantly higher rate of tumor outgrowth (Fig. 3.12a,b). Hence, non-canonical EMT is associated with a higher capacity to initiate tumors. We harvested the resulting tumors from the limiting dilution assay to assess epithelial plasticity. NC-E and –M tumors had high Ecad expression similar to unsorted NC tumors, and C-E and –M tumors had low Ecad expression resembling unsorted C tumors (Fig. 3.12c). These data suggest that NC-M cells and C-E cells are highly plastic, since they exhibit the largest shift in Ecad positivity. In both EMT subtypes, sorted tumors skewed in the same direction as unsorted tumors (NC toward epithelial, C toward mesenchymal), suggesting that the cells exhibit memory of the original epithelial:mesenchymal ratio, or reach an equilibrium determined by as yet unknown factors.

In summary, we have shown that pancreatic cancer cells employ two distinct mechanisms for shedding their epithelial programs during EMT *in vivo* – one utilizing transcriptional repression of epithelial genes and another involving post-translational regulation of protein localization and stability. Given prior work showing that Ecad is subject to dramatic trafficking and turnover in normal epithelial cells[172-175], it is not difficult to envision how cancer cells might utilize such post-translational mechanisms to lose their epithelial properties. Moreover, cytoplasmic Ecad staining has previously been observed in surgical PDAC specimens, suggesting the process is conserved in human PDAC[176]. Protein relocalization could also help explain the phenomenon of circulating tumor cell clusters[177-179], as the greater plasticity afforded by NC-EMT might permit tumor cells to become invasive while still retaining their adhesive properties. Although EMT has customarily been viewed as a transcriptionally regulated process, our identification of an alternate mechanism for suppressing the epithelial program – one

that underlies EMT in the majority of PDAC tumors *in vivo* – underscores the importance of examining the process under physiological conditions.

Materials and Methods

Mouse Strains

Pdx1-cre, $Kras^{LSL\text{-}G12D}$, $p53^{L/+}$, $Rosa^{YFP/YFP}$ mice have been described previously[124]. KPCY mice were palpated and examined for evidence of morbidity twice per week. Tumor-bearing animals were sacrificed when moribund. Both male and female mice were used for analysis with a mean (±SD) age of 16.3 (± 8.5) weeks. All vertebrate animal experiments were conducted in compliance with the National Institutes of Health guidelines for animal research and approved by the University of Pennsylvania Institutional Animal Care and Use Committee.

Immunofluorescence (IF)

Tissues were fixed in Zn-formalin, paraffin embedded and stained as previously described[124]. In brief, after sections were deparaffinized, rehydrated and subjected to antigen retrieval, sections were blocked in 5% donkey serum for 1 hour at room temperature (RT), incubated with primary antibodies for 1 hour at RT, washed, incubated with secondary antibodies for 1 hour at RT, washed and mounted. Rabbit anti-Zeb1 (Santa Cruz Biotechnology, Santa Cruz, CA) required additional tyramide signaling amplification (PerkinElmer, Waltham, MA). See Table 3.1 for a list of antibodies used in Chapter 3. Slides were visualized using an Olympus IX71 inverted multicolor fluorescent microscope or a Zeiss LSM 710 confocal microscope. Confocal images were taken with Zen 2011 software and spectral imaging coupled with image analysis using linear unmixing was performed when necessary.

Fluorescence activated cell sorting (FACS) and flow cytometry

FACS was used to sort KPCY cell lines as well as primary KPCY pancreatic tumors. To prepare cell lines, cells were incubated in cell dissociation buffer (Thermofisher) at 37^{o}C for 15-60 minutes. To prepare tumors and create a single cell suspension, pancreatic tissue was rinsed vigorously in cold DMEM/F12 three times before mincing with scissors (approximately 100 chops). The minced pieces were then incubated in preheated collagenase with protease inhibitors (2 mg/ml; Sigma) for 20 min at 37°C. Vigorous vortexing was performed every 5 min during this incubation. The dissolved pieces were then poured over a 40 μM cell strainer and the large remaining pieces of tissue were mechanically dissociated using the plunger of a 3mL syringe. The flow through was resuspended in cold 2% FCS/DMEM/F12, centrifuged, washed once, and kept on ice in the dark. Samples were incubated with the primary antibody (1:200) and then secondary antibody (1:100) in 10% FCS /DMEM/F12 for 15 min at 4°C. Dissociated cells were stained for E-cadherin (ECCD-2 clone, Thermofisher) prior to sorting on either the FACSVantage or Influx (BD) and flow cytometry on the LSRII (BD). Sorting and flow cytometry were performed at the Penn PathBioResource Flow Cytometry Core.

RNA isolation, library construction, and next-generation sequencing

RNASeq libraries were prepared using the Clontech Ultra low RNA kit – HV, with 12 cycles of PCR for cDNA amplification, and the Clontech Low Input Kit for library prep, with 9 cycles of PCR amplification, following the manufacturer's protocol. The amplified library was purified using AMPure beads, quantified by Qubit and QPCR, and visualized in an Agilent Bioanalyzer. The libraries were pooled equimolarly, and loaded on either

one rapid run HiSeq 2500 flow cell, onboard clustering protocol, or on HiSeq 25000 high output flow cell lanes, as paired 50 nucleotide reads.

Sequencing alignment, differential gene expression and clustering analysis

The quality of raw reads was assessed using Fastqc (v0.11). Reads passing quality control were aligned to the mouse genome version NCBI GRCm38/mm10 with STAR (v2.3.1) using default parameters. Total reads, with alignment quality of at least 10, mapping to each gene were counted using HTseq-count and GRCm38/mm10 gene annotation files. Differential gene expression analysis was performed using the R/Bioconductor package DESeq2. Genes with Benjamini-Hochberg adjusted P values ≤ 0.1 and absolute log2 fold change ≥ 1.0 were considered differentially expressed. As an alternate approach for normalization of gene and transcript level abundances, transcripts per million (TPM) were calculated using RSEM (v1.2.18) with default parameters.

Gene expression heat maps

For unsupervised hierarchical clustering and heat map generation, variance-stabilized expression values were clustered using average linkage with distance metric equal to 1 minus the Pearson correlation coefficient using the 2000 genes with the most variable expression levels. To visualize expression of specific genes involved in EMT, the log2 ratio of normalized TPM values between paired mesenchymal (YFP+/Ecad-) and epithelial (YFP+/Ecad+) fractions from each individual tumor sample were plotted with ggplot2 in R. Markers specific for epithelial cells, mesenchymal cells and EMT transcription factors were selected from published literature[86,92,159,180].

Comparison of human PDA cell lines

Microarray expression data for human pancreatic cancer cell lines were obtained from the Cancer Cell Line Encyclopedia[181].

RNA extraction, cDNA synthesis and qPCR

RNA was extracted using the RNeasy Micro kit (Qiagen) and cDNA was synthesized using the High Capacity cDNA Reverse Transcription kit (Thermofisher) according to the manufacturers' instructions. qPCR was performed using SsoAdvanced Universal SYBR Green Supermix (Biorad) on a CFX384 Touch Real-Time PCR Detection System (Biorad) as previously described[124]. Relative expression was determined after adjusting for GAPDH.

Chapter 3 Figures, Figure Legends and Table

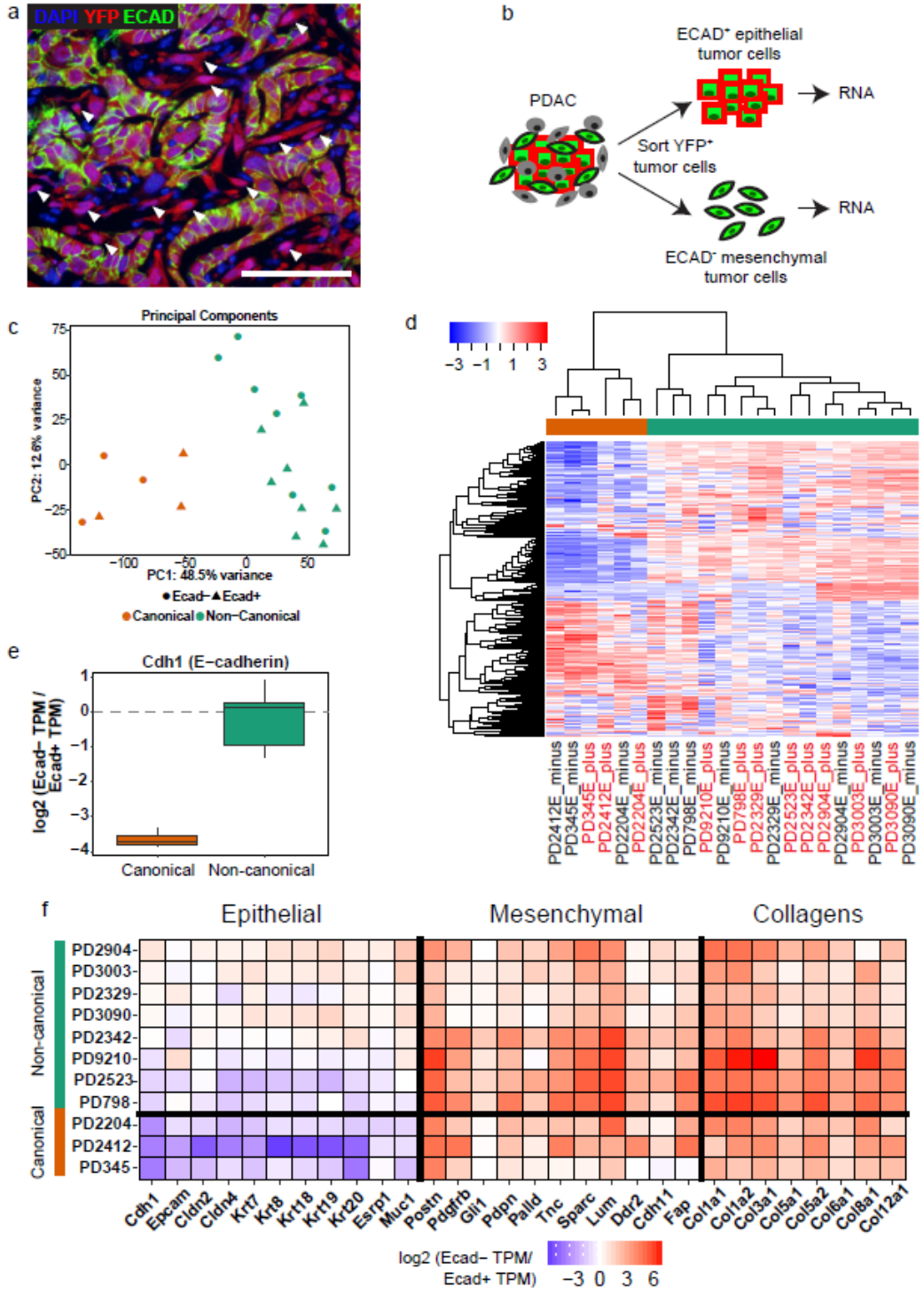

Figure 3.1: Two distinct EMT programs exist *in vivo.* (a) Representative image of KPCY tumor stained for DAPI (blue), Yfp (red) and Ecad (green). Arrowheads denote cells that lack E-cadherin expression and have undergone EMT. Scale bar, 50 μm. (b) Experimental design. Primary KPCY tumors were dissociated, stained and sorted for Ecad. Epithelial ($Yfp^+/Ecad^+$) and mesenchymal ($Yfp^+/Ecad^-$) tumor cell populations were collected for transcriptome analysis. (c) Principal component analysis. (d) Hierarchical clustering. (e) Change in Ecad expression in canonical and non-canonical tumor pairs (log2 fold change $Ecad^-$ TPM/$Ecad^+$ TPM). (f) Heat map of epithelial and mesenchymal transcripts in canonical and non-canonical tumor pairs (log2 fold change $Ecad^-$ TPM/$Ecad^+$ TPM). TPM, transcripts per million.

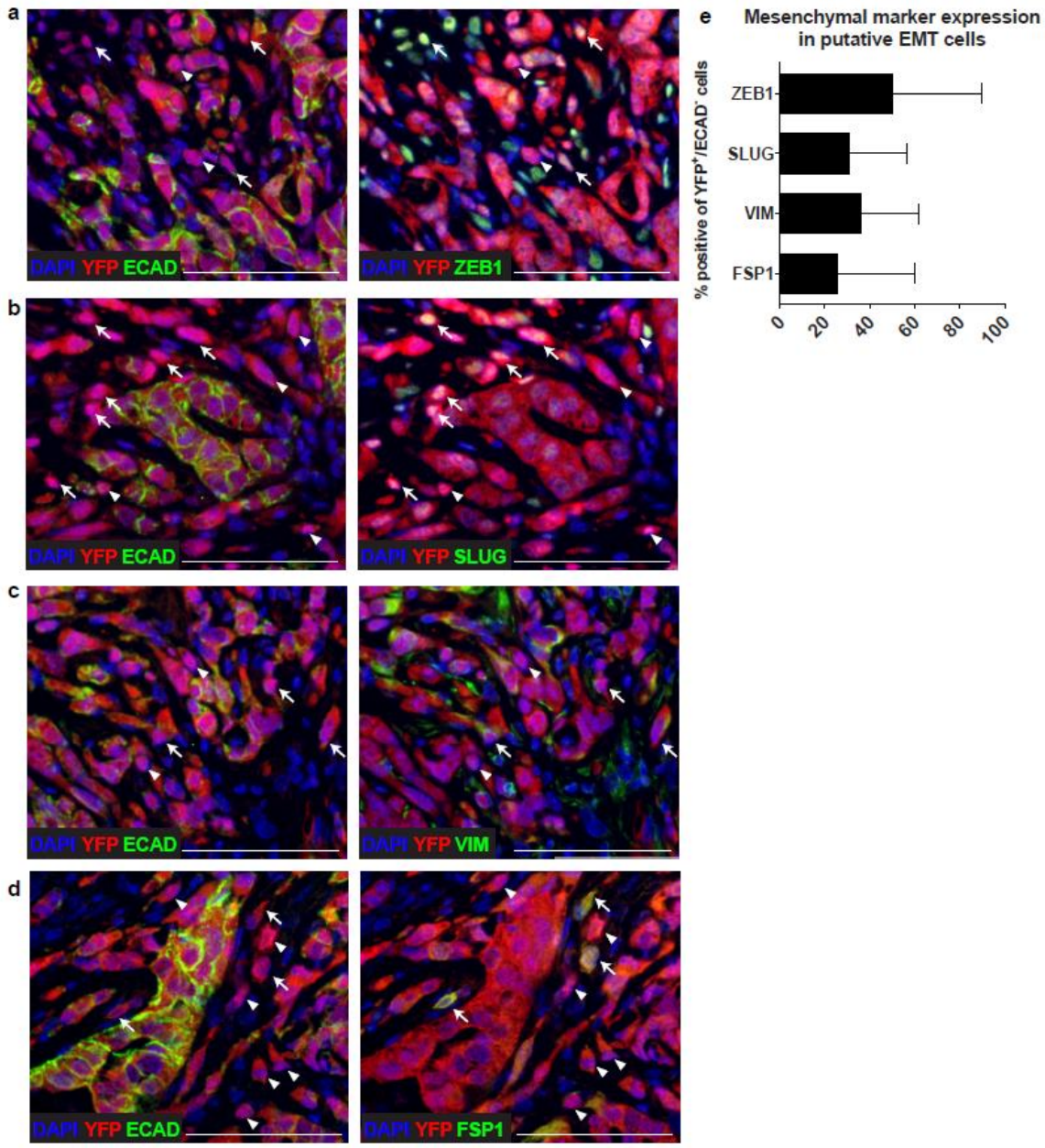

Figure 3.2: Mesenchymal protein expression varies widely during EMT *in vivo*. (a-d) Representative images of Ecad (left) and Zeb1 (a), Slug (b), Vim (c) and Fsp1 (d) expression (right); DAPI (blue), Yfp (red) and Ecad or mesenchymal marker (green). Scale bar, 50 μm. (e) Quantification of the percentage of mesenchymal marker-positive cells within the $Yfp^{+}/Ecad^{-}$ putative EMT population. Bars represent mean ± SD.

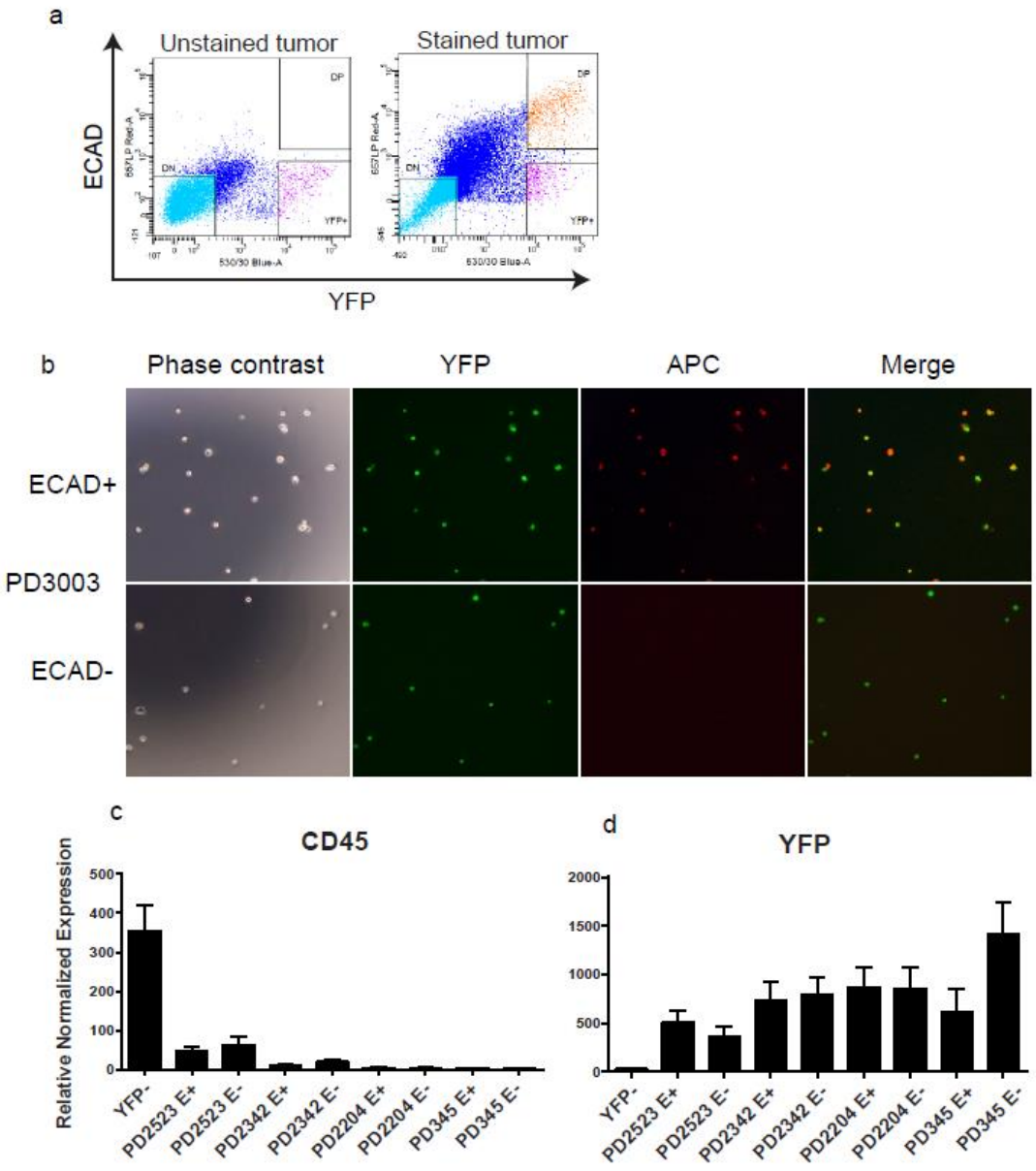

Figure 3.3: RNAseq sorting quality controls. (a) Representative FACS plot of a KPCY tumor stained for Ecad. DP, double positive. (b) Representative images of tumor cells directly after sorting to check for purity. APC, allophycocyanin (fluorophore used for Ecad). (c-d) qPCR on sorted samples for CD45 (c), a leukocyte marker, and YFP (d) to rule out contamination of non-tumor cell populations. Bars represent mean ± SEM.

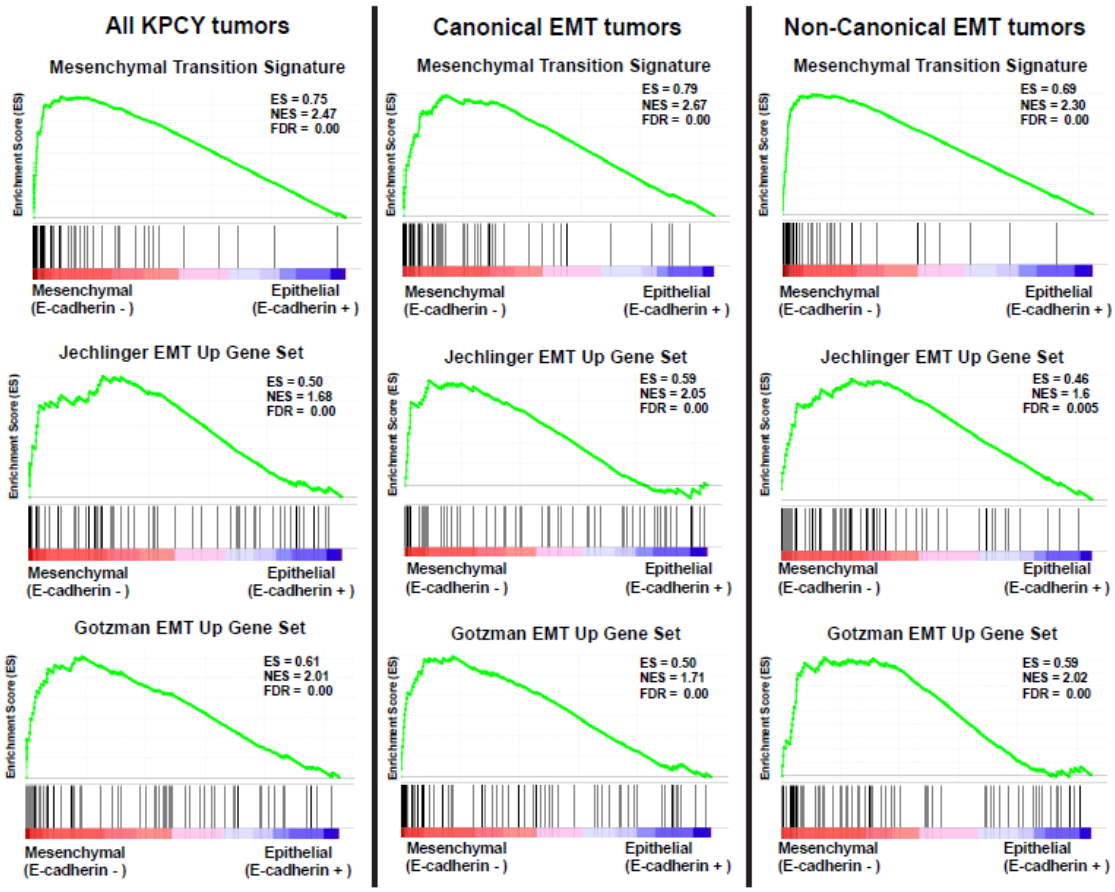

Figure 3.4: Gene set enrichment analysis (GSEA) reveals enrichment for EMT signatures in Ecad^{-} samples.

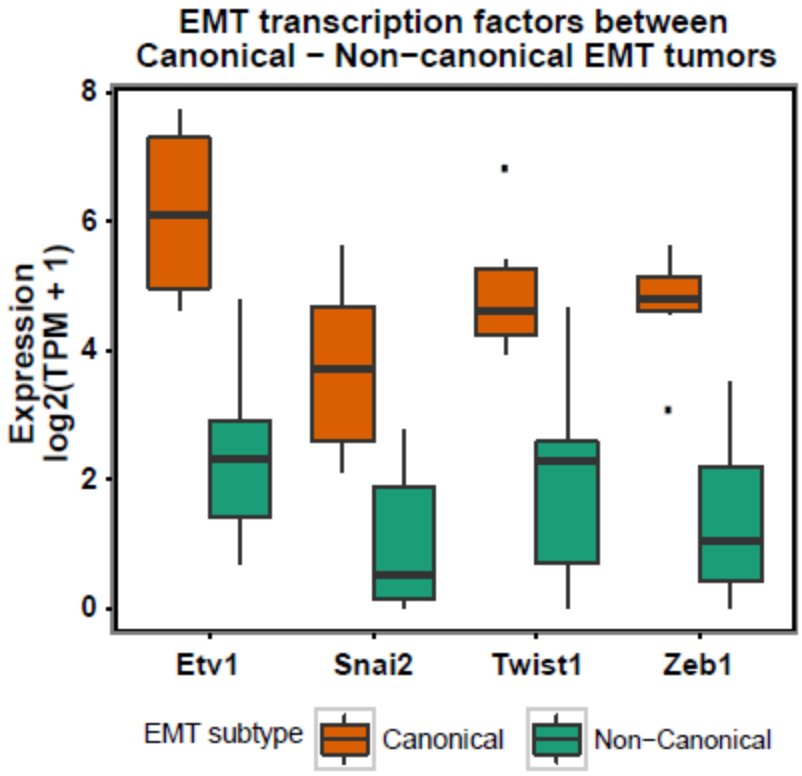

Figure 3.5: EMT-TF expression differs between canonical and non-canonical EMT.

Log2 fold change of $Ecad^-$ TPM/$Ecad^+$ TPM in canonical and non-canonical tumors.

TPM, transcripts per million.

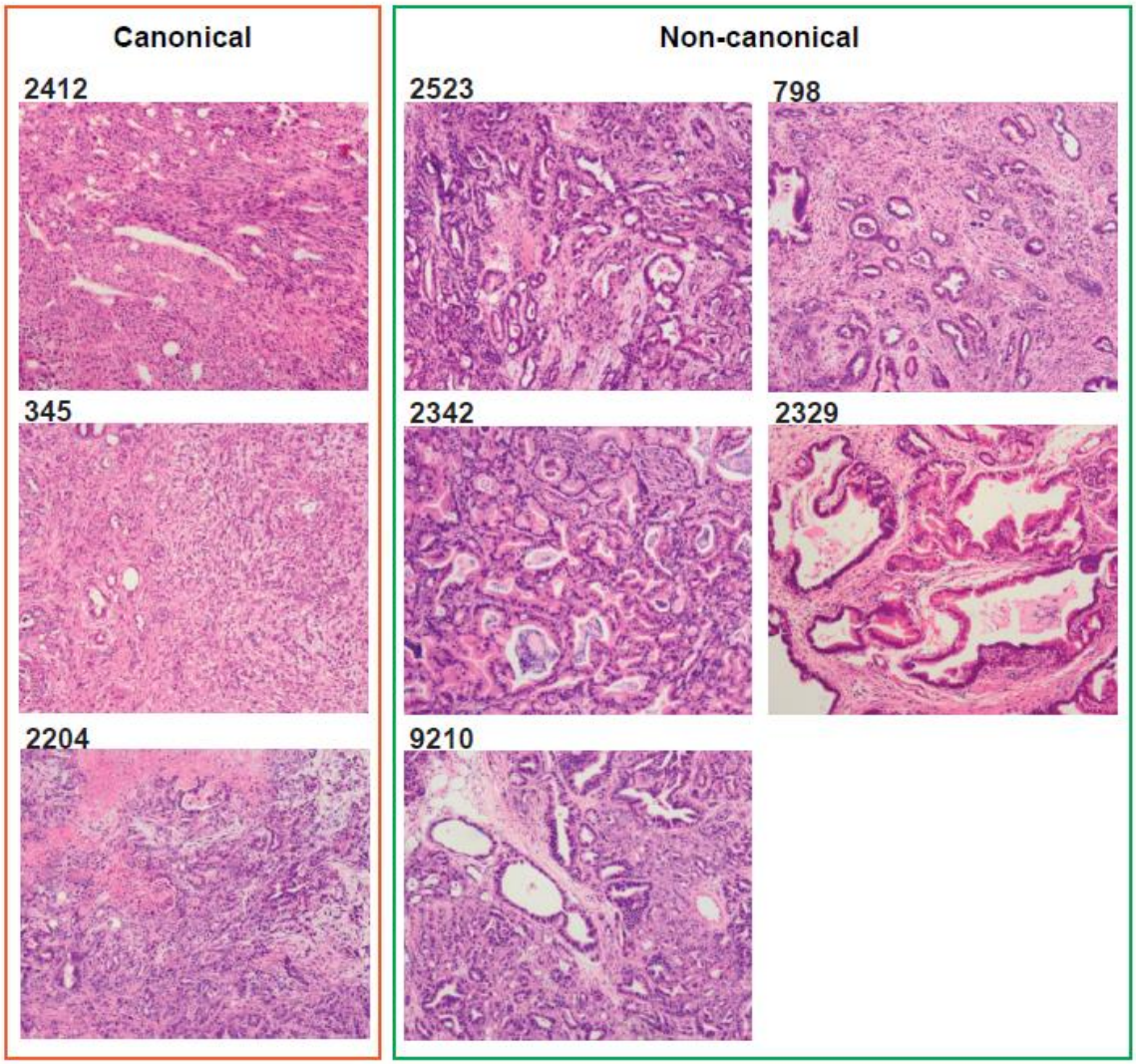

Figure 3.6: EMT subtype correlates with histology. Hematoxylin and eosin (H&E) stained KPCY tumor sections.

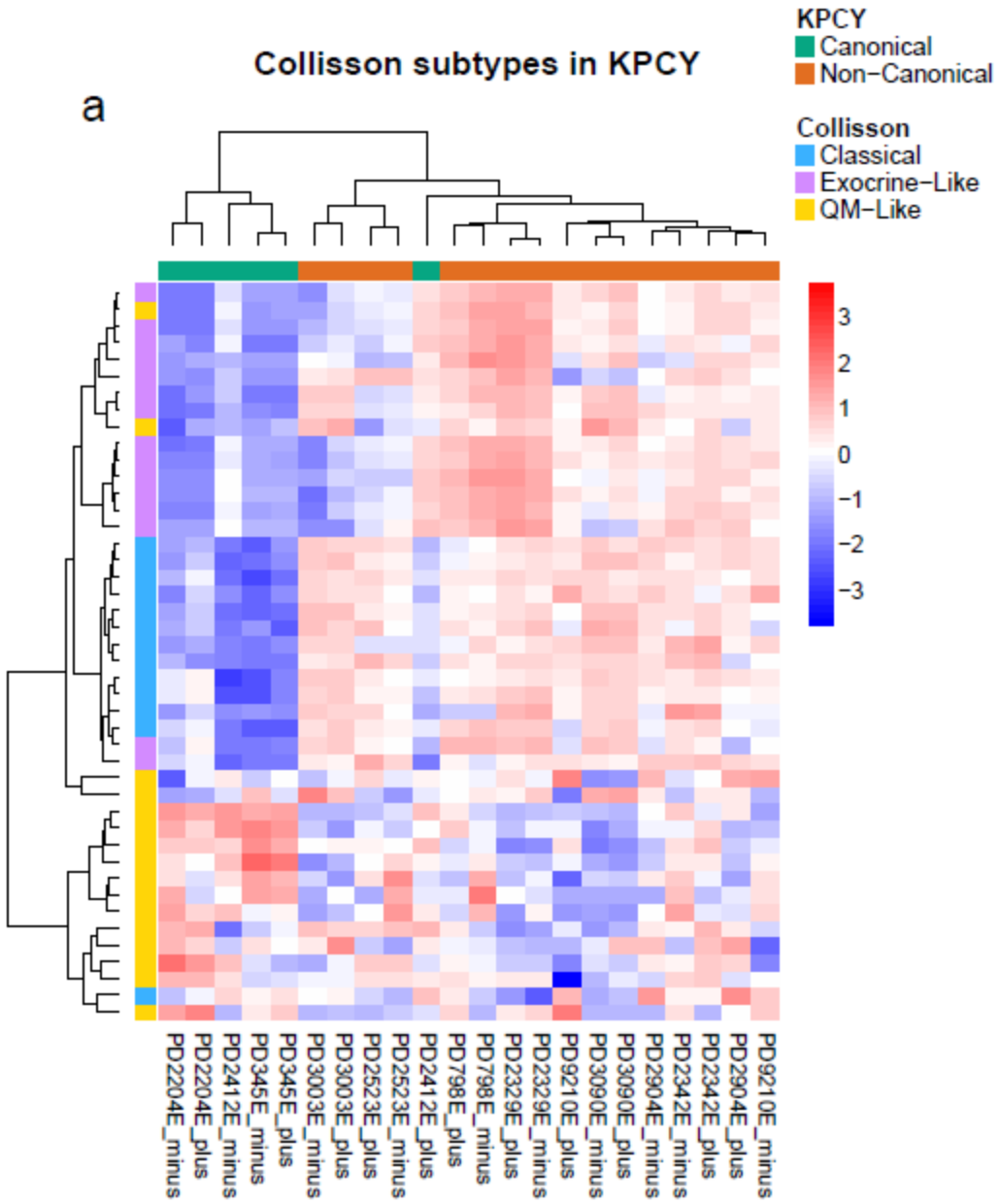
a
Collisson subtypes in KPCY
KPCY
Canonical
Non−Canonical
Collisson
Classical
Exocrine−Like
QM−Like
3
2
1
0
−1
−2
−3
PD2204E_minus
PD2204E_plus
PD2412E_minus
PD345E_minus
PD345E_plus
PD3003E_minus
PD3003E_plus
PD2523E_plus
PD2523E_minus
PD2412E_plus
PD798E_plus
PD798E_minus
PD2329E_plus
PD2329E_minus
PD9210E_plus
PD3090E_minus
PD3090E_plus
PD2904E_minus
PD2342E_minus
PD2342E_plus
PD2904E_plus
PD9210E_minus

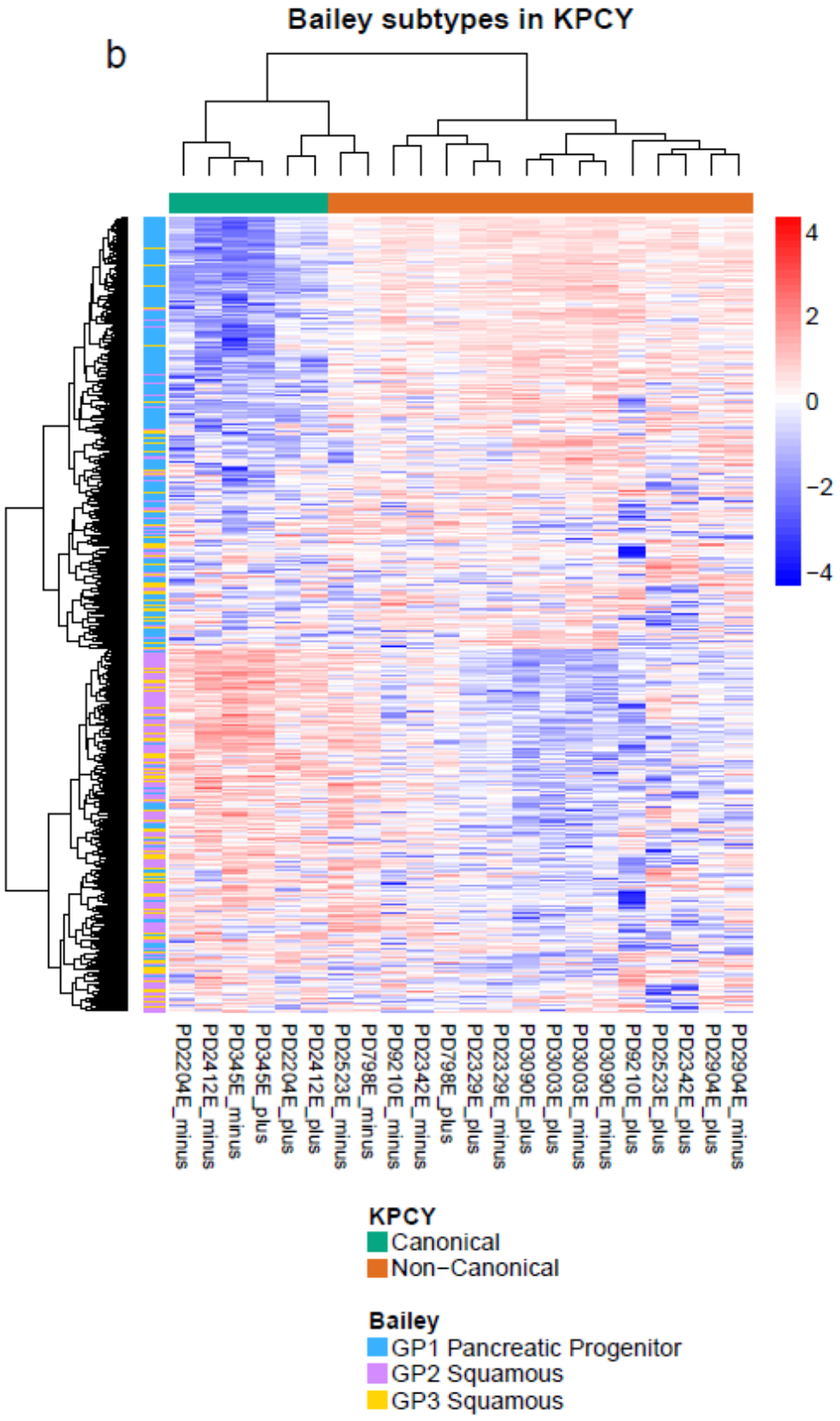
Bailey subtypes in KPCY
b
4
2
0
−2
−4
PD2204E_minus
PD2412E_minus
PD345E_minus
PD345E_plus
PD2204E_plus
PD2412E_plus
PD2523E_minus
PD798E_minus
PD9210E_minus
PD2342E_minus
PD798E_plus
PD2329E_plus
PD2329E_minus
PD3090E_plus
PD3003E_plus
PD3003E_minus
PD3090E_minus
PD9210E_plus
PD2523E_plus
PD2342E_plus
PD2904E_plus
PD2904E_minus
KPCY
Canonical
Non−Canonical
Bailey
GP1 Pancreatic Progenitor
GP2 Squamous
GP3 Squamous

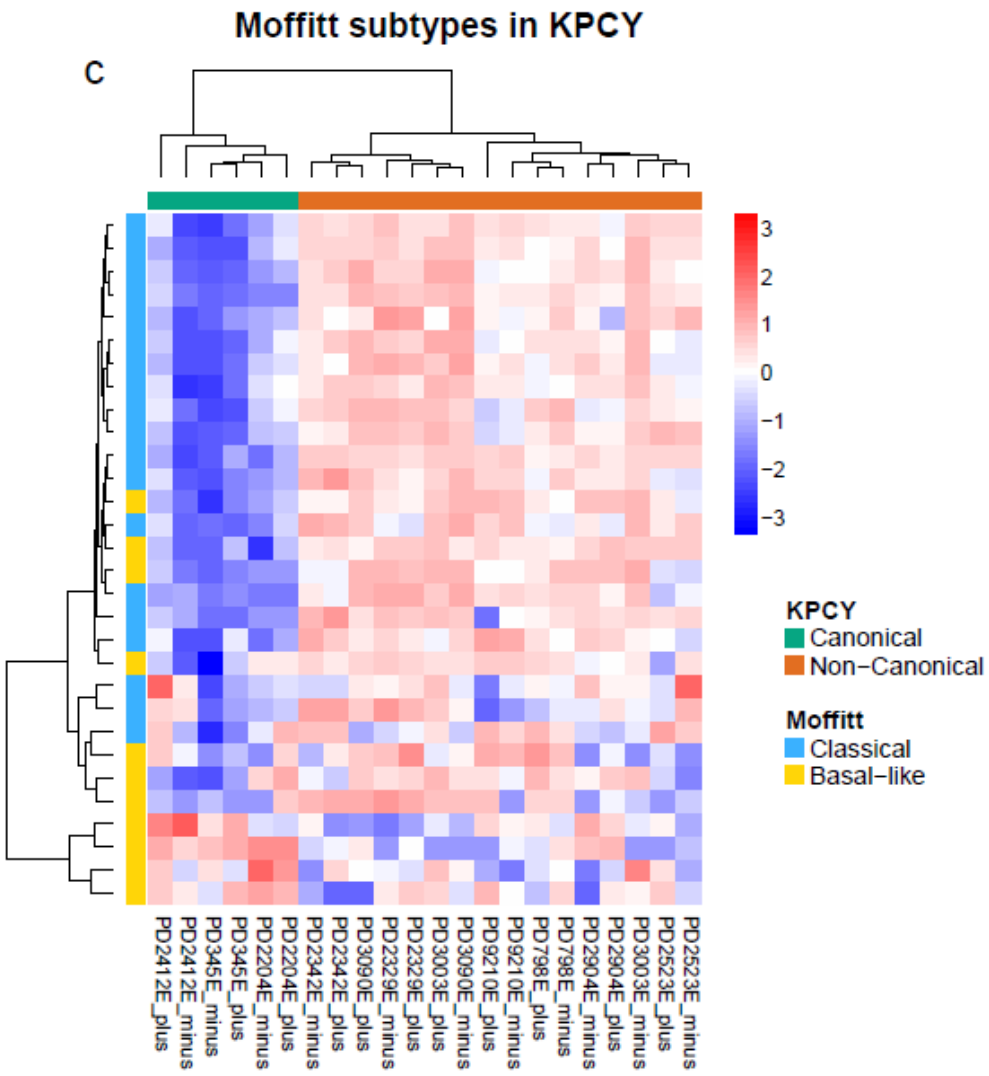

Figure 3.7: EMT subtype correlates with PDAC subtype. Hierarchical clustering of KPCY transcriptomes based on the Collisson (a), Bailey (b) and Moffitt (c) gene signatures for PDAC subtypes.

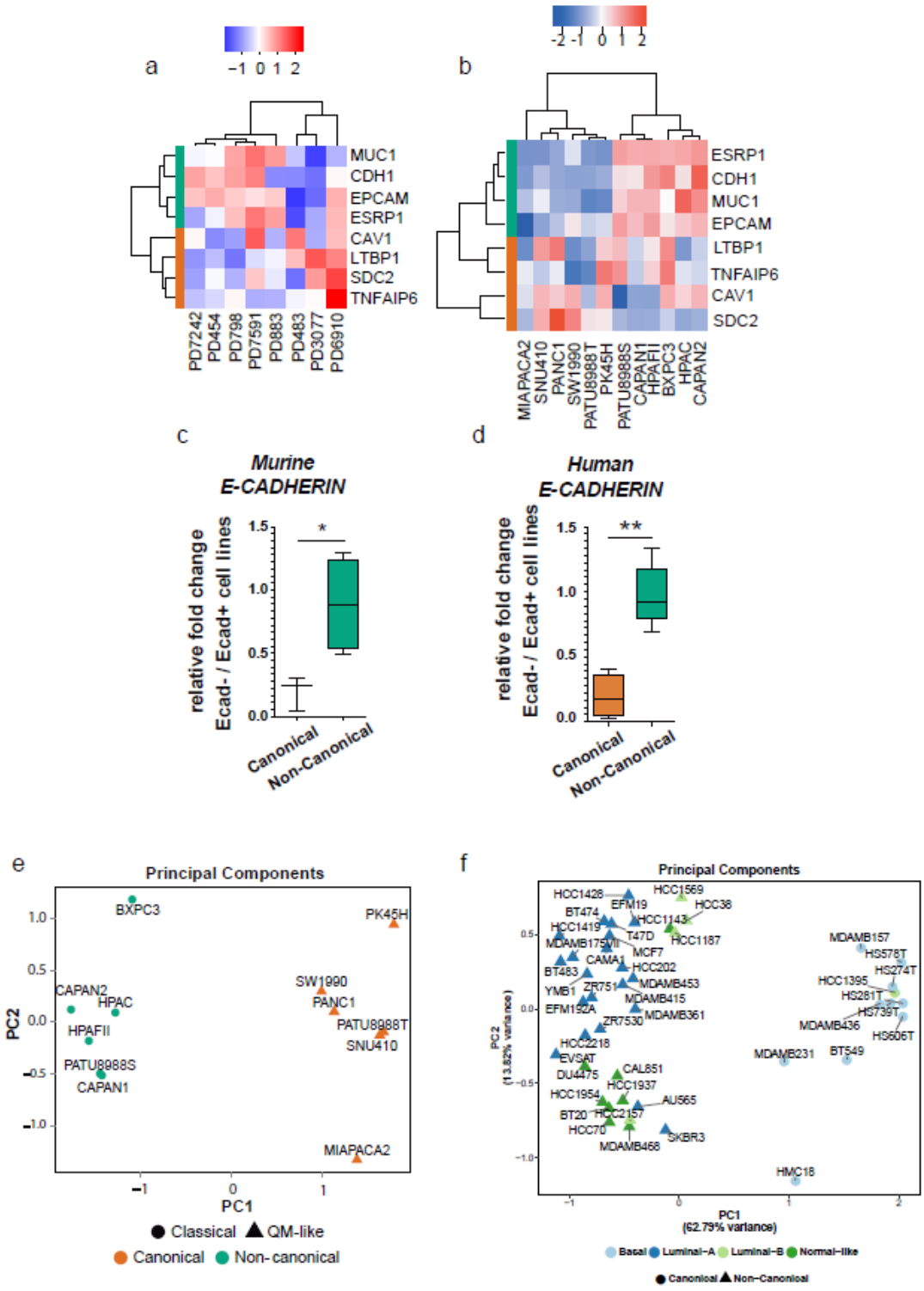

Figure 3.8: Cell lines segregate into canonical and non-canonical EMT. (a) 8-gene signature heatmap for KPCY tumor cell lines based on qPCR. (b) 8-gene signature

heatmap for established human PDAC cell lines based on expression data from the Cancer Cell Line Encyclopedia (CCLE). (c) Ecad expression (log2 fold change $Ecad^-$ /$Ecad^+$) of KPCY tumor cell lines sorted on Ecad. (d) Ecad expression (log2 fold change $Ecad^-$/$Ecad^+$) of human PDAC cell lines sorted on Ecad. (e) Principal component analysis of human PDAC cell lines based on whole transcriptome expression data from CCLE. (f) Principal component analysis of human breast cancer cell lines based on whole transcriptome expression data from CCLE.

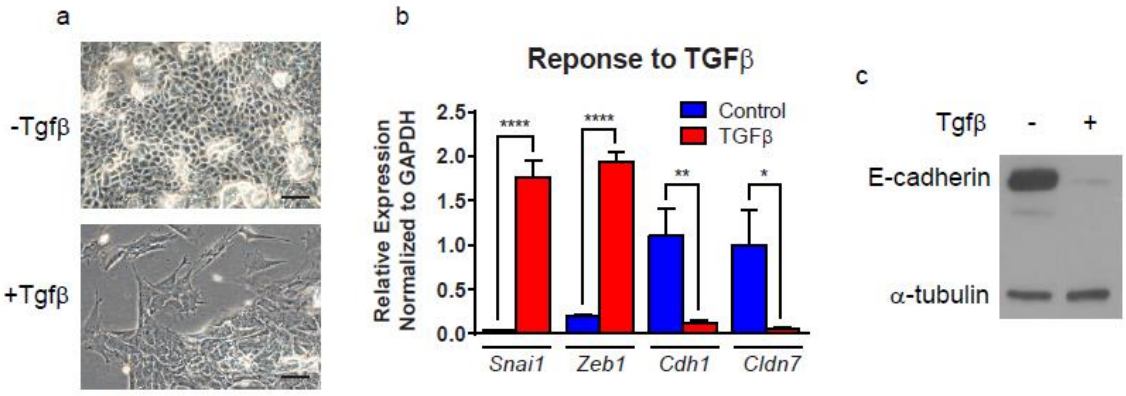

Figure 3.9: Non-canonical cell lines are competent to undergo canonical EMT. (a) Representative phase contrast images of non-canonical cell line PD7591 ± Tgfβ treatment (5 ng/mL for 7d). Scale bars 100µm. (b) Expression of Tgfβ responsive genes ± Tgfβ treatment normalized to GAPDH. (c) Western blot for E-cadherin ± Tgfβ treatment.

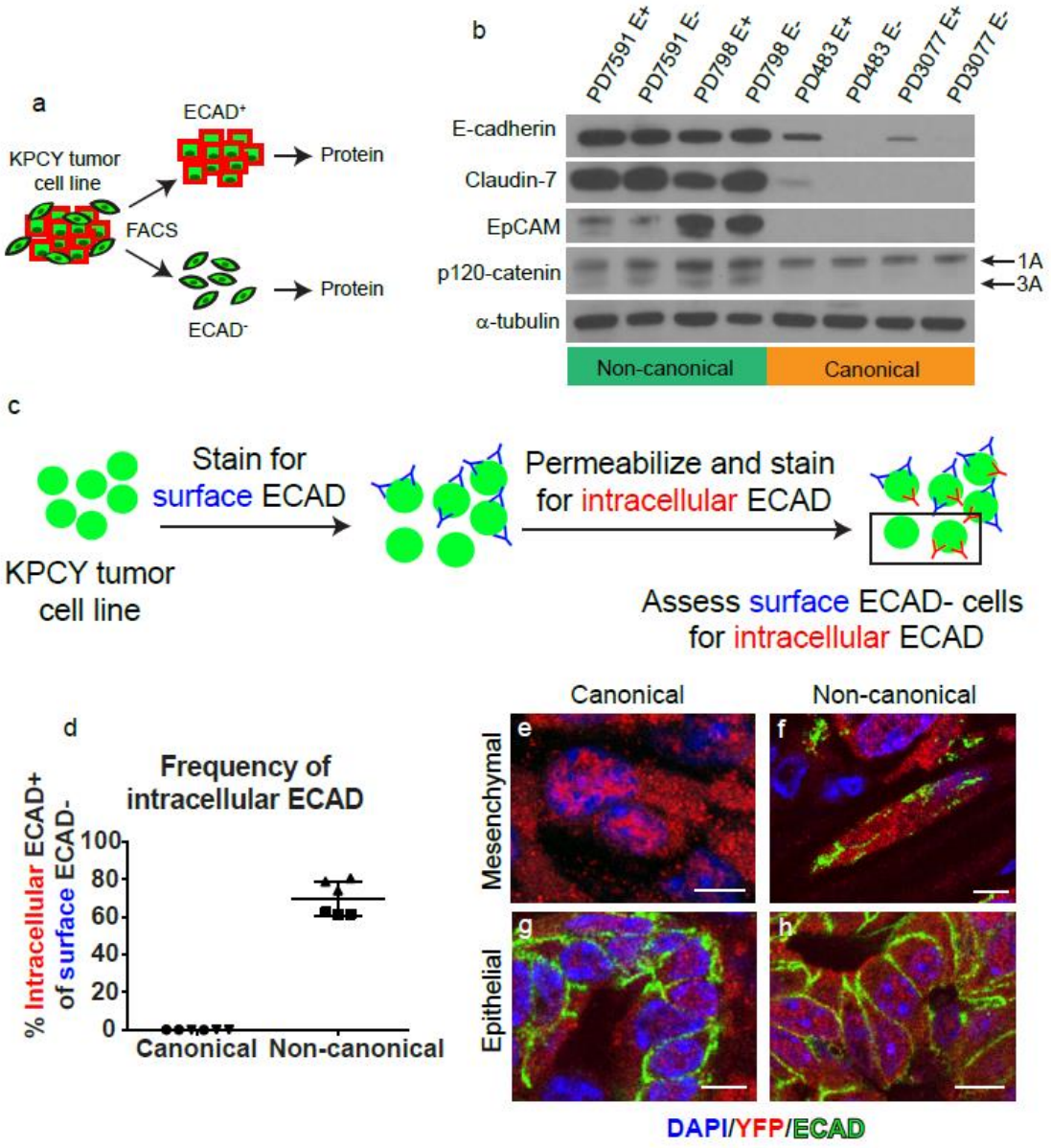

Figure 3.10: Non-canonical EMT is characterized by Ecad internalization. (a) Experimental design for acquiring protein from Ecad-sorted KPCY tumor cell lines. (b) Western blot for epithelial proteins on Ecad-sorted samples. (c) Experimental design for double Ecad labeling flow cytometry. (d) Quantification of the percentage of surface Ecad$^-$ cells with intracellular Ecad expression. (e-h) Confocal images of RNAseq tumor sections stained for DAPI (blue), Yfp (red) and Ecad (green). Scale bars 10μm.

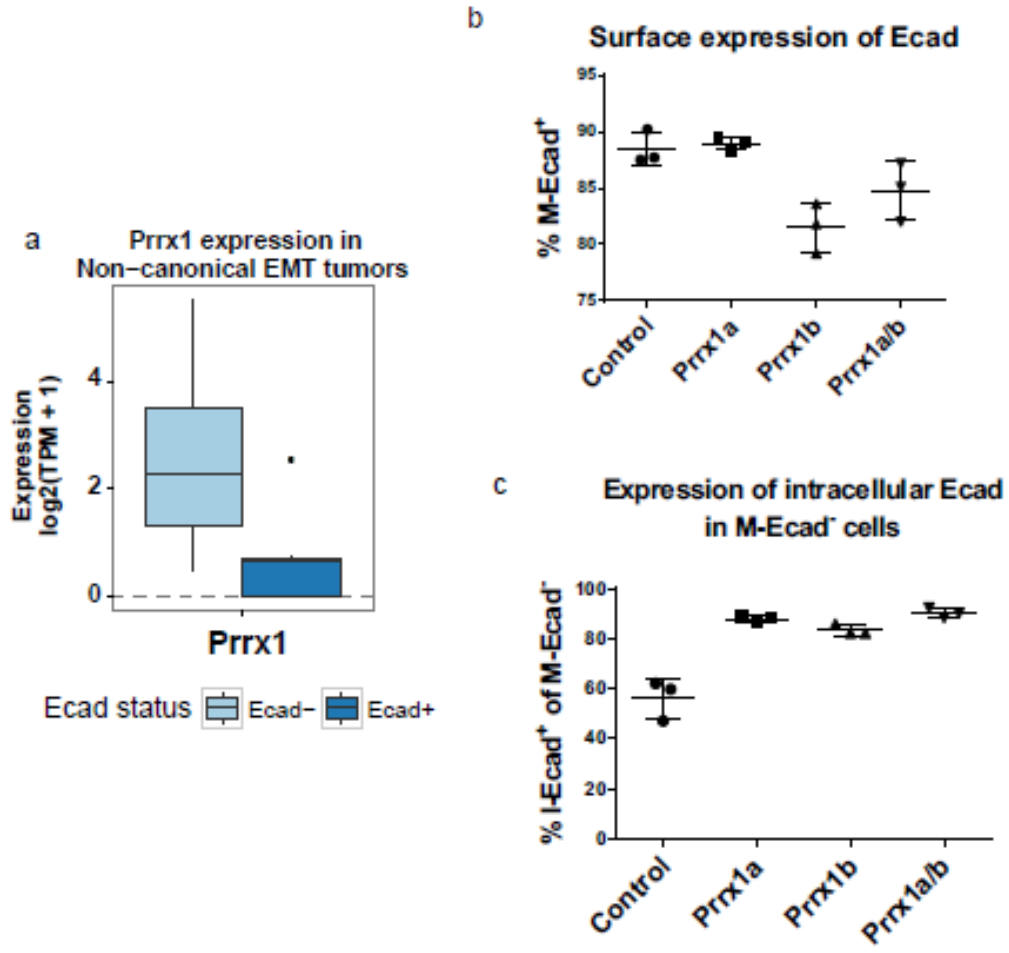

Figure 3.11: Prrx1 regulates Ecad trafficking. (a) Prrx1 expression in non-canonical RNAseq samples. (b) Surface expression of Ecad in non-canonical cell line PD7591 expressing control vector, Prrx1a, Prrx1b or Prrx1a/b (M-Ecad, Membranous Ecad). (c) Expression of intracellular Ecad (I-Ecad) in M-Ecad$^-$ cells in non-canonical cell line PD7591 expressing control vector, Prrx1a, Prrx1b or Prrx1a/b.

a

	10K	1K	100	10
NC-E	14/18	9/18	4/16	1/18
NC-M	18/18	11/18	4/16	1/18
C-E	10/12	8/14	3/14	0/14
C-M	9/12	7/14	1/14	1/14

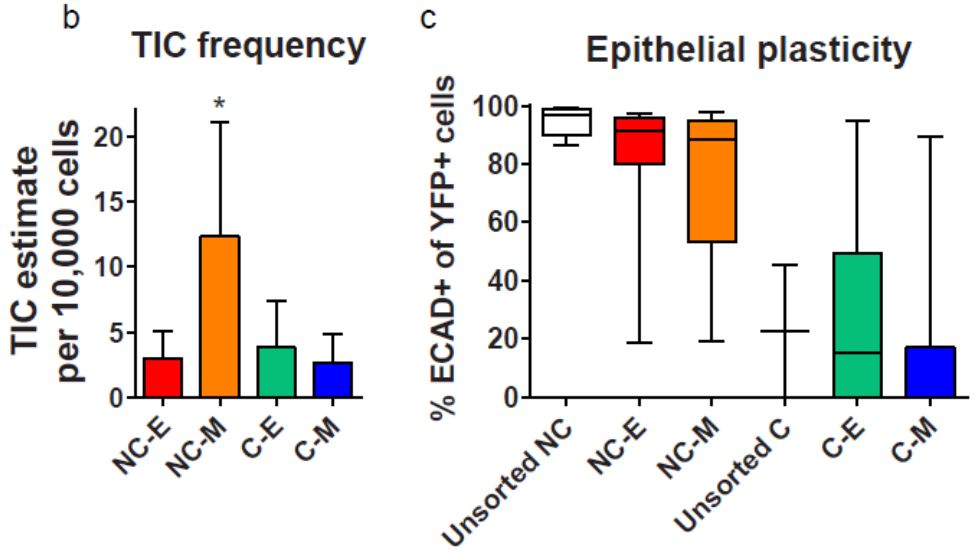

Figure 3.12: Non-canonical EMT confers enhanced tumor initiation potential and epithelial plasticity. (a) Limiting dilution assay results. Canonical and non-canonical KPCY tumor cell lines were sorted on Ecad and injected subcutaneously in NOD/SCID mice at 10,000; 1,000; 100; and 10 cells. (b) Tumor initiating cell (TIC) frequency, calculated using Extreme Limiting Dilution Analysis (ELDA) software[182]. (c) E-cadherin expression based on flow cytometry within unsorted and Ecad-sorted tumors from the limiting dilution experiment. Bars represent mean ± SD. P-values were calculated using Student's T-test. *, $p<0.05$.

Antibody	Dilution	Vendor
Rat α-Ecad	1:200-1:1000	Thermofisher & Takara Bio
Rabbit α-Cldn7	1:100	Abcam
Mouse α-p120 catenin	1:200	BD Biosciences
Rabbit α-Slug	1:100	Gift of the Habener Lab
Rabbit α-Zeb1	1:100 + TSA	Santa Cruz Biotechnology
Rabbit α-Vimentin	1:100	Cell Signaling Technology
Rabbit α-Fsp1	1:500	Dako
Mouse α-tubulin	1:5000	Sigma Aldrich

Table 3.1: Antibodies used in Chapter 3.

CHAPTER 4: Conclusions and Future Directions

Parallel evolution of a metastatic lesion and its attendant microenvironment

Throughout the study in Chapter 2, we focus on the development of the metastatic microenvironment in an autochthonous mouse model of pancreatic cancer. I found that single disseminated cells and small tumor cell clusters exhibit EMT features and lack an obvious tumor microenvironment, while larger lesions regain epithelial morphology and accumulate desmoplasia that closely resembles that of primary PDAC. I also observed that large metastases are hypovascular and poorly perfused while single cells and small lesions are well vascularized. Leukocyte populations did not show a strong association with metastatic lesions of any size but were increased overall in metastatic livers, especially macrophages and myeloid-derived suppressor cells (MDSCs). Adaptive immune cells such as T-lymphocytes were essentially absent from the metastatic microenvironment, consistent with the exclusion of this cell type from primary PDAC tumors. My results illustrate a gradual accretion of stroma and epithelial features during metastatic growth, and to my knowledge this is the first study describing the stepwise progression of spontaneous metastatic colonization.

The correlative nature of this work opens up many new potential avenues into the biology of metastasis. I focused entirely on dissemination to the liver because it is the most common site of PDAC metastasis, raising the question of whether metastases arise similarly at other locations. There is evidence that the clonality of metastasis differs within the liver and lung compared to the diaphragm and peritoneum, perhaps reflecting disparate selection pressures at different metastatic sites. In a similar mouse model of PDAC utilizing the Confetti allele as a lineage label, our lab demonstrated that gross liver and lung metastases exhibit reduced clonality with metastatic growth, while diaphragm

and peritoneal metastases remain polyclonal even at the macro-metastasis stage[178]. This suggests that metastatic development in the lung might have a similar progression to the liver, while diaphragm and peritoneal metastases likely develop along a different route.

Another question raised by this study is how stromal cells are recruited to sites of metastasis and what role they play in colonization. Myofibroblasts are essentially absent from the microenvironment of single cells and nano-metastases, but after the 10-cell stage they robustly accumulate at metastatic lesions suggesting that tumor cells secrete a recruitment factor that must reach a local threshold to function. Tumor-derived Sonic hedgehog (Shh) is a strong fibroblast mobilization signal in primary PDAC and likely plays a role in re-establishing the metastatic microenvironment[76]. Leukocytes such as macrophages and MDSCs do not accumulate at metastatic lesions specifically but are increased throughout metastatic livers, suggesting a systemic mechanism driving leukocyte trafficking to metastatic tissues. In melanoma, tumor-derived exosomes deliver long-range signals, specifically the Met receptor, to bone marrow progenitor cells, causing them to home to the liver and establish a pre-metastatic niche[183]. Similarly, PDAC-derived exosomes are taken up by resident macrophages of the liver (Kupffer cells), which in turn signal to local stellate cells to produce fibronectin which acts as a pre-metastatic niche[31]. So perhaps the increased numbers of macrophages and MDSCs are due to exosome-based recruitment to the liver, where they help to establish a generally permissive microenvironment for incoming metastatic cells.

Our observation that metastases become more epithelial with growth is consistent with the EMT/MET hypothesis, which postulates that EMT is required for early steps of metastasis (i.e. invasion and entry into the circulation) while MET is necessary for later steps (i.e. colonization). However, in our model it is impossible to discern

whether early mesenchymal lesions differentiate into epithelial ones or if early epithelial lesions are selected for within the liver microenvironment. Two recent studies of the role of EMT in metastasis would suggest that the latter possibility is true. Using two different mesenchymal Cre lines (Fsp1- and Vim-Cre) to lineage trace tumor cells that have undergone EMT in the Polyoma Middle T (PyMT) model of breast cancer, Fischer *et al.* found that lung metastases were uniformly negative for the EMT lineage label[156]. In other words, these metastatic cells had always been epithelial and never activated Fsp1 or Vim in their lifetime, suggesting that EMT is not required for metastasis. However, these two mesenchymal genes are almost certainly not universal EMT markers (none have been identified thus far), so it is possible that PyMT tumor cells undergo EMT through a different mechanism and therefore would be missed by this system. Furthermore, this study does not rule out the possibility that mesenchymal tumor cells are required for metastasis but only as chaperones for epithelial tumor cells in a phenomenon known as cell cooperation. During cell cooperation, tumor cell clones with different but complementary abilities work together to escape the primary tumor and metastasize[184]. In another study testing the role of EMT in metastasis, Zheng *et al*. knocked out Snail and Twist in the KPC model of PDAC and found no change in metastatic burden, again suggesting that EMT is not required for metastasis[144]. However, the authors failed to demonstrate that EMT is fully abrogated in these mice, and I found that Snail is expressed at high levels in both $Ecad^{+}$ and $Ecad^{-}$ KPCY tumor cells *in vitro* and *in vivo* (Fig. 4.1), suggesting that it does not play a significant role in EMT in PDAC. Thus, it remains unclear whether EMT/MET or selection for epithelial cells occurs at metastatic sites.

EMT and response to chemotherapy

The most surprising result from Chapter 2 is the observation that chemotherapy selects for epithelial tumor cells *in vivo*. I found that tumors subjected to long-term chemotherapy had a significantly lower frequency of EMT compared to untreated controls, and after a single dose of chemotherapy mesenchymal tumor cells exhibited higher rates of apoptosis than epithelial tumor cells. This is inconsistent with numerous reports that have linked EMT to chemoresistance[144-146,156,185-187]. However, these studies often possess one of two caveats (sometimes both): A. They were performed *in vitro* and thus lack the context of the tumor microenvironment or B. They rely on a single mesenchymal gene that might not be representative of the *in vivo* EMT program. Our data is consistent with at least one study which found that mesenchymal PDAC cell lines are sensitive to gemcitabine while epithelial PDAC cell lines are sensitive to erlotinib, an EGFR inhibitor[17]. It is likely that chemoresistance is dependent on the context. Cancer type, drug(s) used, and the microenvironment can all affect the delivery, metabolism and response to a given therapy. Further studies parsing these different contexts will be necessary to fully understand mechanisms of drug resistance *in vivo*.

Discovery of an alternative mechanism of EMT *in vivo*

In Chapter 3, we focus on the mechanisms driving EMT in living tumors. I found that PDAC tumors can undergo EMT in one of two ways: through a canonical pathway involving transcriptional repression of epithelial genes, or through a non-canonical pathways involving post-translational repression of the epithelial program. PDAC subtype influences which mode of EMT tumor cells use, and there is evidence to suggest a similar correlation in breast cancer. Non-canonical EMT is characterized by

the internalization and cytoplasmic retention of epithelial proteins, which may contribute to their increased plasticity and tumor initiation potential. To my knowledge this is the first study to examine spontaneous cancer EMT in a physiologically relevant setting and the first to implicate post-translational regulation of the epithelial program as the predominant mechanism driving EMT in vivo.

There is some precedent for EMT regulation at the protein level during embryogenesis and in vitro. Snail is required during mouse gastrulation to transcriptionally repress *Ecad*, but is not sufficient to induce a full EMT: it must coordinate with p38, a mitogen-activated protein kinase (MAPK) that down-regulates Ecad protein without affecting transcription[188]. Epb41l5 is also required to down-regulate Ecad at the protein but not mRNA level during mouse gastrulation. It accomplishes this by disrupting the interaction between p120-catenin and Ecad, presumably exposing Ecad to ubiquitination by the E3 ubiquitin ligase Hakai, which facilitates Ecad internalization in association with $Rab5^{+}$ early endosomes[189]. In Madine-Darby Canine Kidney (MDCK) cells, Gata6 promotes Ecad internalization and the formation of cytoplasmic $Ecad^{+}$ punctae without effecting *Ecad* transcription, driving increased invasion[190]. It remains to be seen whether p38, Epb41l5 and Gata6 are involved in the same or parallel pathways and whether they play a role in cancer-associated EMT.

In Chapter 3, we identified Prrx1 as a potential regulator of the non-canonical EMT phenotype, in particular with regard to Ecad trafficking. Both epithelial and mesenchymal isoforms of Prrx1 were significantly increased in non-canonical Ecad- tumor samples, leading us to pursue it as a candidate driver of NC-EMT. And while both isoforms promote the accumulation of cytoplasmic Ecad, they are not sufficient to down-regulate membranous Ecad, a hallmark of EMT, suggesting that Prrx1 is a mediator but not a master regulator of NC-EMT. To identify a master regulator, we will most likely

have to focus on broad transcriptional changes rather than on individual differentially expressed genes within our dataset. One way to do this is to perform gene set enrichment analysis (GSEA) for transcription factor targets enriched within NC-EMT tumor samples[191]. At the top of the list in my preliminary analysis (Table 4.1) is Nuclear Factor of Activated T Cells (Nfat), which belongs to a calcium (Ca^{2+})-responsive family of transcription factors first discovered in the context of T-cell activation. Nfat proteins are regulated by calcineurin, which under Ca^{2+} replete conditions, dephosphorylates Nfat, allowing it to shuttle to the nucleus to modulate transcription[192]. Nfats have been implicated in PDAC progression and have been shown to promote tumor growth in PDAC through *C-myc* activation[193,194] and *p15*^{INK4b} repression[195]. Moreover, Nfat expression is associated with higher metastatic potential in colorectal cancer[196]. Therefore, based on GSEA and previous reports, Nfat would be a good candidate as a master regulator of NC-EMT in PDAC for future studies.

The discovery of an alternative, post-translationally regulated EMT paradigm begs the question of whether epithelial-mesenchymal plasticity exists as a continuum rather than two discrete phenotypic states. In a recent comprehensive review article, Nieto *et al.* propose the idea of an intermediate EMT phenotypes of varying stability characterized by dampened epithelial characteristics with or without mesenchymal features[86], reminiscent of the non-canonical EMT phenomenon described in Chapter 3. Furthermore, the authors acknowledge the inconsistency of mesenchymal qualities acquired during EMT and suggest the extent to which cells travel along the EMT continuum is highly context dependent[86]. We see evidence of this in Fig. 3.2, which demonstrates that traditional mesenchymal markers exhibit high inter- and intra-tumoral heterogeneity in the KPCY model. It is becoming increasingly clear that EMT is much more complex than previously thought: with so many EMT-inducing extracellular cues,

numerous signaling pathways, multiple layers of regulation and diverse molecular outputs, EMT can no longer be considered a simple binary switch between epithelium and mesenchyme.

Concluding remarks

My thesis work was built upon the observation that pre-malignant pancreatic cells exhibit EMT features and are capable of seeding distant organs before frank malignancy. From there, it was a natural progression to study the cellular and molecular mechanisms of EMT and metastasis. This was made possible by the combination of a cancer model with lineage labeling, a technique borrowed from developmental biology. It is essentially impossible to identify tumor cells in situ that have undergone EMT without the aid of a lineage label, since they seamlessly blend in with true mesenchymal cells in the surrounding stroma. Furthermore, single disseminated cells and small metastatic lesions would be exceedingly difficult to locate within the vast parenchyma of the liver sans reporter. Without such a model, we would never know the events that take place during spontaneous metastatic colonization, nor would we learn that classical EMT mechanisms do not apply to the majority of PDAC tumors. This speaks to the power of animal modeling and the value of looking for innovative solutions in other fields.

Despite recent advances, many questions remain about the biology of EMT and metastasis. This work describes the stepwise progression of metastatic colonization but it stops short of uncovering the molecular requirements. Future studies will be necessary to address the mechanisms of stromal recruitment, metastasis-stroma crosstalk, the role of stroma in supporting colonization, and drug resistance of single disseminated cells. This work also revealed an alternative but predominant mode of EMT in living PDAC

tumors that challenges the paradigm of transcriptional regulation by EMT-TFs. However, it remains unclear what signals drive non-canonical EMT *in vivo*, what master regulators orchestrate it and what its molecular requirements are. It would also be interesting to find out whether the non-canonical EMT phenomenon is a general mechanism utilized by other cancer types. In Chapter 3, I presented evidence that well differentiated breast cancer cell lines fit the non-canonical EMT profile while poorly differentiated cell lines aligned with a canonical EMT expression pattern, however the true test will be to sort those cell lines on Ecad and perform qPCR to see how *Ecad* transcript behaves during EMT. Finally, a comparison of the metastatic potential of NC-EMT and C-EMT cells remains untested: perhaps NC-EMT cells are better equipped to metastasize because they retain both epithelial and mesenchymal properties and are thus more plastic. The answers to these questions will shed light on the metastatic process and expose its potential weaknesses, hopefully leading to a new generation of anti-metastatic therapies.

Chapter 4 Figures and Figure Legends

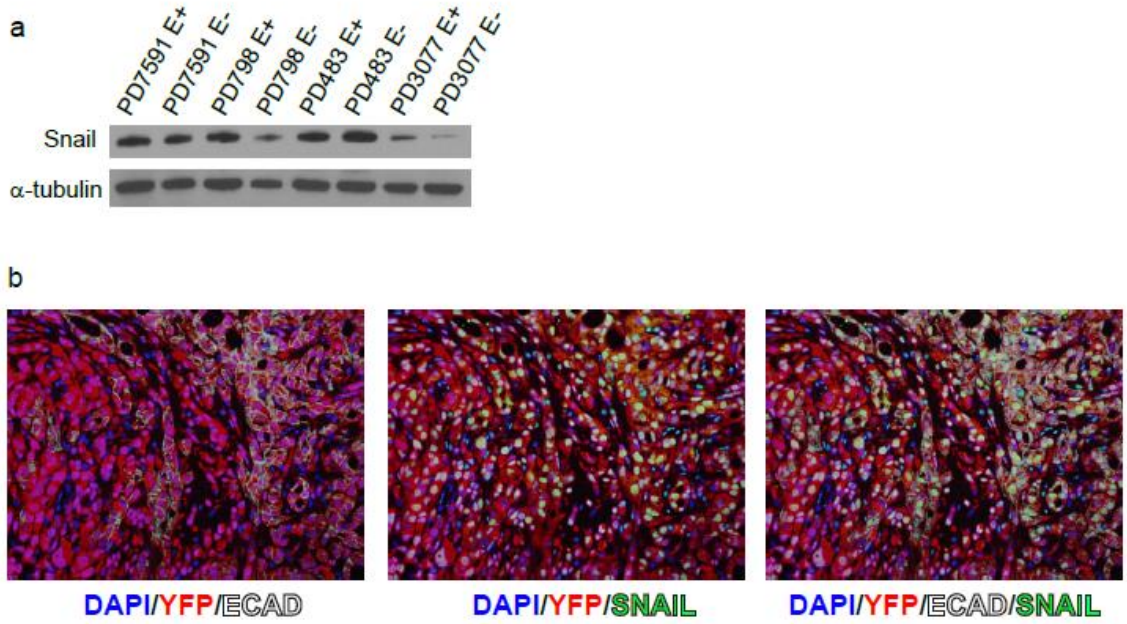

Figure 4.1: Snail expression does not correlate with EMT in KPCY tumors. (a) KPCY tumor cell lines were sorted on Ecad and probed by Western blot for Snail. (b) KPCY tumor sections were stained for DAPI (blue), YFP (red), ECAD (white) and Snail (green).

Gene Set Name	# Genes in overlap	p-value	FDR q-value
TGGAAA_V$NFAT_Q4_01	48	3.18E-20	1.95E-17
GGGAGGRR_V$MAZ_Q6	50	1.65E-18	5.07E-16
CTTTGT_V$LEF1_Q2	45	2.88E-17	5.9E-15
AACTTT_UNKNOWN	38	5.77E-12	8.51E-11
GGGCGGR_V$SP1_Q6	48	6.92E-13	8.51E-11
TTGTTT_V$FOXO4_01	39	1.77E-12	1.81E-10
CAGGTG_V$E12_Q6	43	2.08E-12	1.83E-10
CAGCTG_V$AP4_Q5	32	1.58E-11	1.21E-9
TGANTCA_V$AP1_C	27	3.42E-11	2.33E-9
RYTTCCTG_V$ETS2_B	26	9.03E-11	5.55E-9

Table 4.1: Enriched transcription factor targets in non-canonical Ecad$^-$ samples.

BIBLIOGRAPHY

1 Howlader, N. *et al.* (SEER, Bethesda, MD, 2014).

2 Ryan, D. P., Hong, T. S. & Bardeesy, N. Pancreatic Adenocarcinoma. *New England Journal of Medicine* **371**, 1039-1049, doi:10.1056/NEJMra1404198 (2014).

3 Shaib, Y., Davila, J., Naumann, C. & El-Serag, H. The impact of curative intent surgery on the survival of pancreatic cancer patients: A US Population-based study. *American Journal of Gastroenterology* **102**, 1377-1382, doi:10.1111/j.1572-0241.2007.01202.x (2007).

4 Oettle, H. *et al.* Adjuvant chemotherapy with gemcitabine vs observation in patients undergoing curative-intent resection of pancreatic cancer - A Randomized controlled trial. *Jama-Journal of the American Medical Association* **297**, 267-277, doi:10.1001/jama.297.3.267 (2007).

5 Iacobuzio-Donahue, C. A. *et al.* DPC4 Gene Status of the Primary Carcinoma Correlates With Patterns of Failure in Patients With Pancreatic Cancer. *Journal of Clinical Oncology* **27**, 1806-1813, doi:10.1200/jco.2008.17.7188 (2009).

6 Scarlett, C. J., Salisbury, E. L., Biankin, A. V. & Kench, J. Precursor lesions in pancreatic cancer: morphological and molecular pathology. *Pathology* **43**, 183-200, doi:10.1097/PAT.0b013e3283445e3a (2011).

7 Brosens, L. A. A., Hackeng, W. M., Offerhaus, G. J., Hruban, R. H. & Wood, L. D. Pancreatic adenocarcinoma pathology: changing "landscape". *Journal of Gastrointestinal Oncology* **6**, 358-374, doi:10.3978/j.issn.2078-6891.2015.032 (2015).

8 Rasheed, Z., Matsui, W. & Maitra, A. in *Pancreatic cancer and tumor microenvironment* (eds PJ Grippo & HG Munshi) (Transworld Research Network, 2012).

9 Provenzano, P. P. *et al.* Enzymatic Targeting of the Stroma Ablates Physical Barriers to Treatment of Pancreatic Ductal Adenocarcinoma. *Cancer Cell* **21**, 418-429, doi:10.1016/j.ccr.2012.01.007 (2012).

10 Olive, K. P. *et al.* Inhibition of Hedgehog Signaling Enhances Delivery of Chemotherapy in a Mouse Model of Pancreatic Cancer. *Science* **324**, 1457-1461, doi:10.1126/science.1171362 (2009).

11 Jacobetz, M. A. *et al.* Hyaluronan impairs vascular function and drug delivery in a mouse model of pancreatic cancer. *Gut* **62**, 112-U153, doi:10.1136/gutjnl-2012-302529 (2013).

12 Kanda, M. *et al.* Presence of Somatic Mutations in Most Early-Stage Pancreatic Intraepithelial Neoplasia. *Gastroenterology* **142**, 730-U129, doi:10.1053/j.gastro.2011.12.042 (2012).

13 Jones, S. *et al.* Core signaling pathways in human pancreatic cancers revealed by global genomic analyses. *Science* **321**, 1801-1806, doi:10.1126/science.1164368 (2008).

14 Waddell, N. *et al.* Whole genomes redefine the mutational landscape of pancreatic cancer. *Nature* **518**, 495-501, doi:10.1038/nature14169 (2015).

15 Aguirre, A. J. *et al.* Activated Kras and Ink4a/Arf deficiency cooperate to produce metastatic pancreatic ductal adenocarcinoma. *Genes & Development* **17**, 3112-3126, doi:10.1101/gad.1158703 (2003).

16 Hustinx, S. R. *et al.* Concordant loss of MTAP and p16/CDKN2A expression in pancreatic intraepithelial neoplasia: evidence of homozygous deletion in a noninvasive precursor lesion. *Modern Pathology* **18**, 959-963, doi:10.1038/modpathol.3800377 (2005).

17 Collisson, E. A. *et al.* Subtypes of pancreatic ductal adenocarcinoma and their differing responses to therapy. *Nature Medicine* **17**, 500-U140, doi:10.1038/nm.2344 (2011).

18 Bailey, P. *et al.* Genomic analyses identify molecular subtypes of pancreatic cancer. *Nature* **531**, 47-+, doi:10.1038/nature16965 (2016).

19 Moffitt, R. A. *et al.* Virtual microdissection identifies distinct tumor- and stroma-specific subtypes of pancreatic ductal adenocarcinoma. *Nature Genetics* **47**, 1168-+, doi:10.1038/ng.3398 (2015).

20 Cavalcante, L. D. & Monteiro, G. Gemcitabine: Metabolism and molecular mechanisms of action, sensitivity and chemoresistance in pancreatic cancer. *European Journal of Pharmacology* **741**, 8-16, doi:10.1010/j.ejphar.2014.07.041 (2014).
21 Heinemann, V., Boeck, S., Hinke, A., Labianca, R. & Louvet, C. Meta-analysis of randomized trials: Evaluation of benefit from gemcitabine-based combination chemotherapy applied in advanced pancreatic cancer. *Bmc Cancer* **8**, 11, doi:10.1186/1471-2407-8-82 (2008).
22 Von Hoff, D. D. *et al.* Increased Survival in Pancreatic Cancer with nab-Paclitaxel plus Gemcitabine. *New England Journal of Medicine* **369**, 1691-1703, doi:10.1056/NEJMoa1304369 (2013).
23 Conroy, T. *et al.* FOLFIRINOX versus Gemcitabine for Metastatic Pancreatic Cancer. *New England Journal of Medicine* **364**, 1817-1825 (2011).
24 Sperti, C., Pasquali, C., Piccoli, A. & Pedrazzoli, S. Recurrence after resection for ductal adenocarcinoma of the pancreas. *World Journal of Surgery* **21**, 195-200 (1997).
25 Smeenk, H. G., Tran, T. C. K., Erdmann, J., van Eijck, C. H. J. & Jeekel, J. Survival after surgical management of pancreatic adenocarcinoma: does curative and radical surgery truly exist? *Langenbecks Archives of Surgery* **390**, 94-103, doi:10.1007/s00423-004-0476-9 (2005).
26 Kleeff, J. *et al.* Surgery for recurrent pancreatic ductal adenocarcinoma. *Annals of Surgery* **245**, 566-572, doi:10.1097/01.sla.0000245845.06772.7d (2007).
27 Steeg, P. S. Targeting metastasis. *Nature Reviews Cancer* **16**, 201-218, doi:10.1038/nrc.2016.25 (2016).
28 Cannistra, M. *et al.* Metastases of pancreatic adenocarcinoma: A systematic review of literature and a new functional concept. *International Journal of Surgery* **21**, S15-S21, doi:10.1016/j.ijsu.2015.04.093 (2015).
29 Paget, S. S. The distribution of secondary growths in cancer of the breast. 1889. *Cancer and metastasis reviews* **8**, 98-101.
30 Lee, E. *et al.* Breast cancer cells condition lymphatic endothelial cells within pre-metastatic niches to promote metastasis. *Nature Communications* **5**, doi:10.1038/ncomms5715 (2014).
31 Costa-Silva, B. *et al.* Pancreatic cancer exosomes initiate pre-metastatic niche formation in the liver. *Nature Cell Biology* **17**, 816-+, doi:10.1038/ncb3169 (2015).
32 Hoshino, A. *et al.* Tumour exosome integrins determine organotropic metastasis. *Nature* **527**, 329-+, doi:10.1038/nature15756 (2015).
33 Wculek, S. K. & Malanchi, I. Neutrophils support lung colonization of metastasis-initiating breast cancer cells. *Nature* **528**, 413-+, doi:10.1038/nature16140 (2015).
34 Cox, T. R. *et al.* The hypoxic cancer secretome induces pre-metastatic bone lesions through lysyl oxidase. *Nature* **522**, 106-U279, doi:10.1038/nature14492 (2015).
35 Imai, T. *et al.* Elevated expression of E-cadherin and alpha-, and gamma-catenins in metastatic lesions compared with primary epithelial ovarian carcinomas. *Human Pathology* **35**, 1469-1476, doi:10.1016/j.humpath.2004.09.014 (2004).
36 Gunji, N. *et al.* Pancreatic carcinoma - Correlation between E-cadherin and alpha-catenin expression status and liver metastasis. *Cancer* **82**, 1649-1656 (1998).
37 Oka, H. *et al.* EXPRESSION OF E-CADHERIN CELL-ADHESION MOLECULES IN HUMAN BREAST-CANCER TISSUES AND ITS RELATIONSHIP TO METASTASIS. *Cancer Research* **53**, 1696-1701 (1993).
38 Nieto, M. A. Epithelial Plasticity: A Common Theme in Embryonic and Cancer Cells. *Science* **342**, 708-+, doi:10.1126/science.1234850 (2013).
39 Chaffer, C. L. *et al.* Mesenchymal-to-epithelial transition facilitates bladder cancer metastasis: Role of fibroblast growth factor receptor-2. *Cancer Research* **66**, 11271-11278, doi:10.1158/0008-5472.can-06-2044 (2006).
40 Tsai, J. H., Donaher, J. L., Murphy, D. A., Chau, S. & Yang, J. Spatiotemporal Regulation of Epithelial-Mesenchymal Transition Is Essential for Squamous Cell Carcinoma Metastasis. *Cancer Cell* **22**, 725-736, doi:10.1016/j.ccr.2012.09.022 (2012).

41 Ocana, O. H. *et al.* Metastatic Colonization Requires the Repression of the Epithelial-Mesenchymal Transition Inducer Prrx1. *Cancer Cell* **22**, 709-724, doi:10.1016/j.ccr.2012.10.012 (2012).
42 Loebel, D. A. F., Watson, C. M., De Young, A. & Tam, P. P. L. Lineage choice and differentiation in mouse embryos and embryonic stem cells. *Developmental Biology* **264**, 1-14, doi:10.1016/s0012-1606(03)00390-7 (2003).
43 Dorsky, R. I., Yang-Snyder, J., Moon, R. T. & Raible, D. W. Control of neural crest cell fate by the Wnt signaling pathway. *Developmental Biology* **198**, 179-179 (1998).
44 Anastas, J. N. & Moon, R. T. WNT signalling pathways as therapeutic targets in cancer. *Nature Reviews Cancer* **13**, 11-26, doi:10.1038/nrc3419 (2013).
45 Petersen, C. P. & Reddien, P. W. Wnt Signaling and the Polarity of the Primary Body Axis. *Cell* **139**, 1056-1068, doi:10.1016/j.cell.2009.11.035 (2009).
46 Sokol, S. Y. Maintaining embryonic stem cell pluripotency with Wnt signaling. *Development* **138**, 4341-4350, doi:10.1242/dev.066209 (2011).
47 De Calisto, J., Araya, C., Marchant, L., Riaz, C. F. & Mayor, R. Essential role of non-canonical Wnt signalling in neural crest migration. *Development* **132**, 2587-2597, doi:10.1242/dev.01857 (2005).
48 Giles, R. H., van Es, J. H. & Clevers, H. Caught up in a Wnt storm: Wnt signaling in cancer. *Biochimica Et Biophysica Acta-Reviews on Cancer* **1653**, 1-24, doi:10.1016/s0304-419x(03)00005-2 (2003).
49 Bell, D. A. Origins and molecular pathology of ovarian cancer. *Modern Pathology* **18**, S19-S32, doi:10.1038/modpathol.3800306 (2005).
50 Polakis, P. The many ways of Wnt in cancer. *Current Opinion in Genetics & Development* **17**, 45-51, doi:10.1016/j.gde.2006.12.007 (2007).
51 Zeller, R., Lopez-Rios, J. & Zuniga, A. Vertebrate limb bud development: moving towards integrative analysis of organogenesis. *Nature Reviews Genetics* **10**, 845-858, doi:10.1038/nrg2681 (2009).
52 Thesleff, I. & Sharpe, P. Signalling networks regulating dental development. *Mechanisms of Development* **67**, 111-123, doi:10.1016/s0925-4773(97)00115-9 (1997).
53 Ulloa, F. & Briscoe, J. Morphogens and the control of cell proliferation and patterning in the spinal cord. *Cell Cycle* **6**, 2640-2649 (2007).
54 Ingham, P. W. & McMahon, A. P. Hedgehog signaling in animal development: paradigms and principles. *Genes & Development* **15**, 3059-3087, doi:10.1101/gad.938601 (2001).
55 Briscoe, J. & Therond, P. P. The mechanisms of Hedgehog signalling and its roles in development and disease. *Nature Reviews Molecular Cell Biology* **14**, 416-429, doi:10.1038/nrm3598 (2013).
56 Athar, M., Tang, X. W., Lee, J. L., Kopelovich, L. & Kim, A. L. Hedgehog signalling in skin development and cancer. *Experimental Dermatology* **15**, 667-677, doi:10.1111/j.0906-6705.2006.00473.x (2006).
57 Tian, H. *et al.* Hedgehog signaling is restricted to the stromal compartment during pancreatic carcinogenesis. *Proceedings of the National Academy of Sciences of the United States of America* **106**, 4254-4259, doi:10.1073/pnas.0813203106 (2009).
58 Rhim, A. D. *et al.* Stromal Elements Act to Restrain, Rather Than Support, Pancreatic Ductal Adenocarcinoma. *Cancer Cell* **25**, 735-747, doi:10.1016/j.ccr.2014.04.021 (2014).
59 Andersson, E. R., Sandberg, R. & Lendahl, U. Notch signaling: simplicity in design, versatility in function. *Development* **138**, 3593-3612, doi:10.1242/dev.063610 (2011).
60 Bray, S. J. Notch signalling: a simple pathway becomes complex. *Nature Reviews Molecular Cell Biology* **7**, 678-689, doi:10.1038/nrm2009 (2006).
61 Bolos, V., Grego-Bessa, J. & de la Pompa, J. L. Notch signaling in development and cancer. *Endocrine Reviews* **28**, 339-363, doi:10.1210/er.2006-0046 (2007).
62 Avila, J. L. & Kissil, J. L. Notch signaling in pancreatic cancer: oncogene or tumor suppressor? *Trends in Molecular Medicine* **19**, 320-327, doi:10.1016/j.molmed.2013.03.003 (2013).

63 Radtke, F. & Raj, K. The role of Notch in tumorigenesis: Oncogene or tumour suppressor? *Nature Reviews Cancer* **3**, 756-767, doi:10.1038/nrc1186 (2003).
64 Demehri, S. & Kopan, R. Notch signaling in bulge stem cells is not required for selection of hair follicle fate. *Development* **136**, 891-896, doi:10.1242/dev.030700 (2009).
65 Heisenberg, C. P. & Solnica-Krezel, L. Back and forth between cell fate specification and movement during vertebrate gastrulation. *Current Opinion in Genetics & Development* **18**, 311-316, doi:10.1016/j.gde.2008.07.011 (2008).
66 Strutz, F. *et al.* Role of basic fibroblast growth factor-2 in epithelial-mesenchymal transformation. *Kidney International* **61**, 1714-1728, doi:10.1046/j.1523-1755.2002.00333.x (2002).
67 Moustakas, A. & Heldin, C. H. Signaling networks guiding epithelial-mesenchymal transitions during embryogenesis and cancer progression. *Cancer Science* **98**, 1512-1520, doi:10.1111/j.1349-7006.2007.00550.x (2007).
68 Pan, D. J. The Hippo Signaling Pathway in Development and Cancer. *Developmental Cell* **19**, 491-505, doi:10.1016/j.devcel.2010.09.011 (2010).
69 Fu, J. & Hsu, W. Epidermal Wnt Controls Hair Follicle Induction by Orchestrating Dynamic Signaling Crosstalk between the Epidermis and Dermis. *Journal of Investigative Dermatology* **133**, 890-898, doi:10.1038/jid.2012.407 (2013).
70 Li, J. Y. *et al.* BMP-SHH Signaling Network Controls Epithelial Stem Cell Fate via Regulation of Its Niche in the Developing Tooth. *Developmental Cell* **33**, 125-135, doi:10.1016/j.devcel.2015.02.021 (2015).
71 Hrycaj, S. M. *et al.* Hox5 Genes Regulate the Wnt2/2b-Bmp4-Signaling Axis during Lung Development. *Cell Reports* **12**, 903-912, doi:10.1016/j.celrep.2015.07.020 (2015).
72 Landsman, L. *et al.* Pancreatic Mesenchyme Regulates Epithelial Organogenesis throughout Development. *Plos Biology* **9**, doi:10.1371/journal.pbio.1001143 (2011).
73 Levinson, R. & Mendelsohn, C. Stromal progenitors are important for patterning epithelial and mesenchymal cell types in the embryonic kidney. *Seminars in Cell & Developmental Biology* **14**, 225-231, doi:10.1016/s1084-9521(03)00025-9 (2003).
74 Wells, K. L. *et al.* Dynamic relationship of the epithelium and mesenchyme during salivary gland initiation: the role of Fgf10. *Biology Open* **2**, 981-989, doi:10.1242/bio.20135306 (2013).
75 Butterfield, N. C., McGlinn, E. & Wicking, C. THE MOLECULAR REGULATION OF VERTEBRATE LIMB PATTERNING. *Organogenesis in Development* **90**, 319-341, doi:10.1016/s0070-2153(10)90009-4 (2010).
76 Bailey, J. M. *et al.* Sonic Hedgehog Promotes Desmoplasia in Pancreatic Cancer. *Clinical Cancer Research* **14**, 5995-6004, doi:10.1158/1078-0432.ccr-08-0291 (2008).
77 Bailey, J. M., Mohr, A. M. & Hollingsworth, M. A. Sonic hedgehog paracrine signaling regulates metastasis and lymphangiogenesis in pancreatic cancer. *Oncogene* **28**, 3513-3525, doi:10.1038/onc.2009.220 (2009).
78 Ozdemir, B. C. *et al.* Depletion of Carcinoma-Associated Fibroblasts and Fibrosis Induces Immunosuppression and Accelerates Pancreas Cancer with Reduced Survival. *Cancer Cell* **25**, 719-734, doi:10.1016/j.ccr.2014.04.005 (2014).
79 Ciruna, B. & Rossant, J. FGF signaling regulates mesoderm cell fate specification and morphogenetic movement at the primitive streak. *Developmental Cell* **1**, 37-49, doi:10.1016/s1534-5807(01)00017-x (2001).
80 Peinado, H., Olmeda, D. & Cano, A. Snail, ZEB and bHLH factors in tumour progression: an alliance against the epithelial phenotype? *Nature Reviews Cancer* **7**, 415-428, doi:10.1038/nrc2131 (2007).
81 Yang, J. *et al.* Twist, a master regulator of morphogenesis, plays an essential role in tumor metastasis. *Cell* **117**, 927-939, doi:10.1016/j.cell.2004.06.006 (2004).
82 De Craene, B. *et al.* The transcription factor snail induces tumor cell invasion through modulation of the epithelial cell differentiation program. *Cancer Research* **65**, 6237-6244, doi:10.1158/0008-5472.can-04-3545 (2005).

83 Cheung, M. *et al.* The transcriptional control of trunk neural crest induction, survival, and delamination. *Developmental Cell* **8**, 179-192, doi:10.1016/j.devcel.2004.12.010 (2005).
84 Hajra, K. M., Chen, D. Y. S. & Fearon, E. R. The SLUG zinc-finger protein represses E-cadherin in breast cancer. *Cancer Research* **62**, 1613-1618 (2002).
85 Comijn, J. *et al.* The two-handed E box binding zinc finger protein SIP1 downregulates E-cadherin and induces invasion. *Molecular Cell* **7**, 1267-1278, doi:10.1016/s1097-2765(01)00260-x (2001).
86 Nieto, M. A., Huang, R. Y. J., Jackson, R. A. & Thiery, J. P. EMT: 2016. *Cell* **166**, 21-45, doi:10.1016/j.cell.2016.06.028 (2016).
87 van Roy, F. & Berx, G. The cell-cell adhesion molecule E-cadherin. *Cellular and Molecular Life Sciences* **65**, 3756-3788, doi:10.1007/s00018-008-8281-1 (2008).
88 Onder, T. T. *et al.* Loss of E-cadherin promotes metastasis via multiple downstream transcriptional pathways. *Cancer Research* **68**, 3645-3654, doi:10.1158/0008-5472.can-07-2938 (2008).
89 Ikenouchi, J., Matsuda, M., Furuse, M. & Tsukita, S. Regulation of tight junctions during the epithelium-mesenchyme transition: direct repression of the gene expression of claudins/occludin by Snail. *Journal of Cell Science* **116**, 1959-1967, doi:10.1242/jcs.00389 (2003).
90 Aigner, K. *et al.* The transcription factor ZEB1 (delta EF1) promotes tumour cell dedifferentiation by repressing master regulators of epithelial polarity. *Oncogene* **26**, 6979-6988, doi:10.1038/sj.onc.1210508 (2007).
91 Vandewalle, C. *et al.* SIP1/ZEB2 induces EMT by repressing genes of different epithelial cell-cell junctions. *Nucleic Acids Research* **33**, 6566-6578, doi:10.1093/nar/gki965 (2005).
92 Lim, J. & Thiery, J. P. Epithelial-mesenchymal transitions: insights from development. *Development* **139**, 3471-3486, doi:10.1242/dev.071209 (2012).
93 Kim, N. H. *et al.* A p53/miRNA-34 axis regulates Snail1-dependent cancer cell epithelial-mesenchymal transition. *Journal of Cell Biology* **195**, 417-433, doi:10.1083/jcb.201103097 (2011).
94 Siemens, H. *et al.* miR-34 and SNAIL form a double-negative feedback loop to regulate epithelial-mesenchymal transitions. *Cell Cycle* **10**, 4256-4271, doi:10.4161/cc.10.24.18552 (2011).
95 Bracken, C. P. *et al.* A double-negative feedback loop between ZEB1-SIP1 and the microRNA-200 family regulates epithelial-mesenchymal transition. *Cancer Research* **68**, 7846-7854, doi:10.1158/0008-5472.can-08-1942 (2008).
96 Burk, U. *et al.* A reciprocal repression between ZEB1 and members of the miR-200 family promotes EMT and invasion in cancer cells. *Embo Reports* **9**, 582-589, doi:10.1038/embor.2008.74 (2008).
97 Gregory, P. A. *et al.* The mir-200 family and mir-205 regulate epithelial to mesenchymal transition by targeting ZEB1 and SIP1. *Nature Cell Biology* **10**, 593-601, doi:10.1038/ncb1722 (2008).
98 Korpal, M., Lee, E. S., Hu, G. H. & Kang, Y. B. The miR-200 family inhibits epithelial-mesenchymal transition and cancer cell migration by direct targeting of E-cadherin transcriptional repressors ZEB1 and ZEB2. *Journal of Biological Chemistry* **283**, 14910-14914, doi:10.1074/jbc.C800074200 (2008).
99 Park, S. M., Gaur, A. B., Lengyel, E. & Peter, M. E. The miR-200 family determines the epithelial phenotype of cancer cells by targeting the E-cadherin repressors ZEB1 and ZEB2. *Genes & Development* **22**, 894-907, doi:10.1101/gad.1640608 (2008).
100 Matsushita, S. Fate mapping study of the endoderm of the 1.5-day-old chick embryo. *Rouxs Archives of Developmental Biology* **205**, 225-231, doi:10.1007/bf00365800 (1996).
101 Dale, L. & Slack, J. M. W. FATE MAP FOR THE 32-CELL STAGE OF XENOPUS-LAEVIS. *Development* **99**, 527-551 (1987).
102 Kimmel, C. B., Warga, R. M. & Schilling, T. F. ORIGIN AND ORGANIZATION OF THE ZEBRAFISH FATE MAP. *Development* **108**, 581-594 (1990).

103 Voziyanov, Y., Pathania, S. & Jayaram, M. A general model for site-specific recombination by the integrase family recombinases. *Nucleic Acids Research* **27**, 930-941, doi:10.1093/nar/27.4.930 (1999).
104 Sternberg, N., Hamilton, D. & Hoess, R. BACTERIOPHAGE-P1 SITE-SPECIFIC RECOMBINATION .2. RECOMBINATION BETWEEN LOXP AND THE BACTERIAL CHROMOSOME. *Journal of Molecular Biology* **150**, 487-507, doi:10.1016/0022-2836(81)90376-4 (1981).
105 Sauer, B. & Henderson, N. SITE-SPECIFIC DNA RECOMBINATION IN MAMMALIAN-CELLS BY THE CRE RECOMBINASE OF BACTERIOPHAGE-P1. *Proceedings of the National Academy of Sciences of the United States of America* **85**, 5166-5170, doi:10.1073/pnas.85.14.5166 (1988).
106 Araki, K., Imaizumi, T., Okuyama, K., Oike, Y. & Yamamura, K. Efficiency of recombination by Cre transient expression in embryonic stem cells: Comparison of various promoters. *Journal of Biochemistry* **122**, 977-982 (1997).
107 Barker, N. *et al.* Identification of stem cells in small intestine and colon by marker gene Lgr5. *Nature* **449**, 1003-U1001, doi:10.1038/nature06196 (2007).
108 Schepers, A. G. *et al.* Lineage Tracing Reveals Lgr5(+) Stem Cell Activity in Mouse Intestinal Adenomas. *Science* **337**, 730-735, doi:10.1126/science.1224676 (2012).
109 Barker, N. *et al.* Crypt stem cells as the cells-of-origin of intestinal cancer. *Nature* **457**, 608-U119, doi:10.1038/nature07602 (2009).
110 Driessens, G., Beck, B., Caauwe, A., Simons, B. D. & Blanpain, C. Defining the mode of tumour growth by clonal analysis. *Nature* **488**, 527-+, doi:10.1038/nature11344 (2012).
111 Wang, G. Y., Wang, J., Mancianti, M. L. & Epstein, E. H. Basal Cell Carcinomas Arise from Hair Follicle Stem Cells in Ptch1(+/-) Mice. *Cancer Cell* **19**, 114-124, doi:10.1016/j.ccr.2010.11.007 (2011).
112 Guest, R. V. *et al.* Cell Lineage Tracing Reveals a Biliary Origin of Intrahepatic Cholangiocarcinoma. *Cancer Research* **74**, 1005-1010, doi:10.1158/0008-5472.can-13-1911 (2014).
113 Choi, N., Zhang, B. Y., Zhang, L., Ittmann, M. & Xin, L. Adult Murine Prostate Basal and Luminal Cells Are Self-Sustained Lineages that Can Both Serve as Targets for Prostate Cancer Initiation. *Cancer Cell* **21**, 253-265, doi:10.1016/j.ccr.2012.01.005 (2012).
114 Li, S. L. *et al.* A Keratin 15 Containing Stem Cell Population From the Hair Follicle Contributes to Squamous Papilloma Development in the Mouse. *Molecular Carcinogenesis* **52**, 751-759, doi:10.1002/mc.21896 (2013).
115 Liu, C. *et al.* Mosaic Analysis with Double Markers Reveals Tumor Cell of Origin in Glioma. *Cell* **146**, 209-221, doi:10.1016/j.cell.2011.06.014 (2011).
116 Greaves, M. Evolutionary Determinants of Cancer. *Cancer Discovery* **5**, 806-820, doi:10.1158/2159-8290.cd-15-0439 (2015).
117 Tabassum, D. P. & Polyak, K. Tumorigenesis: it takes a village. *Nature Reviews Cancer* **15**, 473-483, doi:10.1038/nrc3971 (2015).
118 Marusyk, A. *et al.* Non-cell-autonomous driving of tumour growth supports sub-clonal heterogeneity. *Nature* **514**, 54-+, doi:10.1038/nature13556 (2014).
119 Snippert, H. J. *et al.* Intestinal Crypt Homeostasis Results from Neutral Competition between Symmetrically Dividing Lgr5 Stem Cells. *Cell* **143**, 134-144, doi:10.1016/j.cell.2010.09.016 (2010).
120 Nagy, A. Cre recombinase: The universal reagent for genome tailoring. *Genesis* **26**, 99-109, doi:10.1002/(sici)1526-968x(200002)26:2<99::aid-gene1>3.0.co;2-b (2000).
121 Maddipati, R. & Stanger, B. Pancreatic Cancer Metastases Harbor Evidence of Polyclonality. (2015).
122 Chen, J. *et al.* A restricted cell population propagates glioblastoma growth after chemotherapy. *Nature* **488**, 522-+, doi:10.1038/nature11287 (2012).
123 Vanner, R. J. *et al.* Quiescent Sox(2+) Cells Drive Hierarchical Growth and Relapse in Sonic Hedgehog Subgroup Medulloblastoma. *Cancer Cell* **26**, 33-47, doi:10.1016/j.ccr.2014.05.005 (2014).

124 Rhim, A. D. *et al.* EMT and Dissemination Precede Pancreatic Tumor Formation. *Cell* **148**, 349-361, doi:10.1016/j.cell.2011.11.025 (2012).
125 Aytes, A. *et al.* ETV4 promotes metastasis in response to activation of PI3-kinase and Ras signaling in a mouse model of advanced prostate cancer. *Proceedings of the National Academy of Sciences of the United States of America* **110**, E3506-E3515, doi:10.1073/pnas.1303558110 (2013).
126 Guerra, C. & Barbacid, M. Genetically engineered mouse models of pancreatic adenocarcinoma. *Molecular Oncology* **7**, 232-247, doi:10.1016/j.molonc.2013.02.002 (2013).
127 Stanger, B. Z. & Hebrok, M. Control of Cell Identity in Pancreas Development and Regeneration. *Gastroenterology* **144**, 1170-1179, doi:10.1053/j.gastro.2013.01.074 (2013).
128 Magnuson, M. A. & Osipovich, A. B. Pancreas-Specific Cre Driver Lines and Considerations for Their Prudent Use. *Cell Metabolism* **18**, 9-20, doi:10.1016/j.cmet.2013.06.011 (2013).
129 Herreros-Villanueva, M., Hijona, E., Cosme, A. & Bujanda, L. Mouse models of pancreatic cancer. *World Journal of Gastroenterology* **18**, 1286-1294, doi:10.3748/wjg.v18.i12.1286 (2012).
130 Siegal, R., Ma, J., Zou, Z. & Jemal, A. Cancer statistics, 2014. *CA* **64**, 9-29 (2014).
131 Valastyan, S. & Weinberg, R. A. Tumor Metastasis: Molecular Insights and Evolving Paradigms. *Cell* **147**, 275-292, doi:10.1016/j.cell.2011.09.024 (2011).
132 Kowalski, P. J., Rubin, M. A. & Kleer, C. G. E-cadherin expression in primary carcinomas of the breast and its distant metastases. *Breast Cancer Research* **5**, R217-R222, doi:10.1186/bcr651 (2003).
133 Brabletz, T. To differentiate or not - routes towards metastasis. *Nature Reviews Cancer* **12**, 425-436, doi:10.1038/nrc3265 (2012).
134 Hingorani, S. R. *et al.* Preinvasive and invasive ductal pancreatic cancer and its early detection in the mouse. *Cancer Cell* **4**, 437-450, doi:10.1016/s1535-6108(03)00309-x (2003).
135 Hingorani, S. R. *et al.* Trp53(R172H) and KraS(G12D) cooperate to promote chromosomal instability and widely metastatic pancreatic ductal adenocarcinoma in mice. *Cancer Cell* **7**, 469-483, doi:10.1016/j.ccr.2005.04.023 (2005).
136 Huber, M. A., Kraut, N. & Beug, H. Molecular requirements for epithelial-mesenchymal transition during tumor progression. *Current Opinion in Cell Biology* **17**, 548-558, doi:10.1016/j.ceb.2005.08.001 (2005).
137 Okada, H., Danoff, T. M., Kalluri, R. & Neilson, E. G. Early role of Fsp1 in epithelial-mesenchymal transformation. *American Journal of Physiology-Renal Physiology* **273**, F563-F574 (1997).
138 Waghray, M., Yalamanchili, M., di Magliano, M. P. & Simeone, D. M. Deciphering the role of stroma in pancreatic cancer. *Current Opinion in Gastroenterology* **29**, 537-543, doi:10.1097/MOG.0b013e328363affe (2013).
139 Zheng, X. *et al.* Epithelial-to-mesenchymal transition is dispensable for metastasis but induces chemoresistance in pancreatic cancer. *Nature Medicine* **527**, 525-530 (2015).
140 Pandol, S., Edderkaoui, M., Gukovsky, I., Lugea, A. & Gukovskaya, A. Desmoplasia of Pancreatic Ductal Adenocarcinoma. *Clinical Gastroenterology and Hepatology* **7**, S44-S47, doi:10.1016/j.cgh.2009.07.039 (2009).
141 Frantz, C., Stewart, K. M. & Weaver, V. M. The extracellular matrix at a glance. *Journal of Cell Science* **123**, 4195-4200, doi:10.1242/jcs.023820 (2010).
142 Bayne, L. J. *et al.* Tumor-Derived Granulocyte-Macrophage Colony-Stimulating Factor Regulates Myeloid Inflammation and T Cell Immunity in Pancreatic Cancer. *Cancer Cell* **21**, 822-835, doi:10.1016/j.ccr.2012.04.025 (2012).
143 Clark, C. E. *et al.* Dynamics of the immune reaction to pancreatic cancer from inception to invasion. *Cancer Research* **67**, 9518-9527, doi:10.1158/0008-5472.can-07-0175 (2007).

144 Zheng, X. F. *et al.* Epithelial-to-mesenchymal transition is dispensable for metastasis but induces chemoresistance in pancreatic cancer. *Nature* **527**, 525-+, doi:10.1038/nature16064 (2015).
145 Yin, T. *et al.* Expression of snail in pancreatic cancer promotes metastasis and chemoresistance. *Journal of Surgical Research* **141**, 196-203, doi:10.1016/j.jss.2006.09.027 (2007).
146 Shah, A. N. *et al.* Development and characterization of gemcitabine-resistant pancreatic tumor cells. *Annals of Surgical Oncology* **14**, 3629-3637, doi:10.1245/s10434-007-9583-5 (2007).
147 Whatcott, C. J., Watanabe, A., LoBello, J., Von Hoff, D. & Han, H. Y. Desmoplasia in primary tumors and metastatic lesions of pancreatic cancer. *Cancer Research* **74**, doi:10.1158/1538-7445.am2014-191 (2014).
148 Heeg, S. *et al.* The Ets-Transcription Factor Etv1 Regulates Stromal Expansion and Metastasis in Pancreatic Cancer. *Gastroenterology* **148**, S47-S47 (2015).
149 Von Hoff, D. D. *et al.* SPARC correlation with response to gemcitabine (G) plus nab-paclitaxel (nab-P) in patients with advanced metastatic pancreatic cancer: A phase I/II study. *Journal of Clinical Oncology* **27** (2009).
150 Hidalgo, M. *et al.* SPARC Expression Did Not Predict Efficacy of nab-Paclitaxel Plus Gemcitabine or Gemcitabine Alone for Metastatic Pancreatic Cancer in an Exploratory Analysis of the Phase III MPACT Trial. *Clinical Cancer Research* (2015).
151 Neesse, A. *et al.* SPARC independent drug delivery and antitumour effects of nab-paclitaxel in genetically engineered mice. *Gut* **63**, 974-983, doi:10.1136/gutjnl-2013-305559 (2014).
152 Von Hoff, D. D. *et al.* Gemcitabine Plus nab-Paclitaxel Is an Active Regimen in Patients With Advanced Pancreatic Cancer: A Phase I/II Trial. *Journal of Clinical Oncology* **29**, 4548-4554, doi:10.1200/jco.2011.36.5742 (2011).
153 Cornish, T. C. & Halushka, M. K. Color Deconvolution for the Analysis of Tissue Microarrays. *Analytical and Quantitative Cytology and Histology* **31**, 304-312 (2009).
154 Ye, X. & Weinberg, R. A. Epithelial-Mesenchymal Plasticity: A Central Regulator of Cancer Progression. *Trends in Cell Biology* **25**, 675-686, doi:10.1016/j.tcb.2015.07.012 (2015).
155 Xue, C. S., Plieth, D., Venkov, C., Xu, C. & Neilson, E. G. The gatekeeper effect of epithelial-mesenchymal transition regulates the frequency of breast cancer metastasis. *Cancer Research* **63**, 3386-3394 (2003).
156 Fischer, K. R. *et al.* Epithelial-to-mesenchymal transition is not required for lung metastasis but contributes to chemoresistance. *Nature* **527**, 472-+, doi:10.1038/nature15748 (2015).
157 Spaderna, S. *et al.* The transcriptional repressor ZEB1 promotes metastasis and loss of cell polarity in cancer. *Cancer Research* **68**, 537-544, doi:10.1158/0008-5472.can-07-5682 (2008).
158 Zheng, H. & Kang, Y. Multilayer control of the EMT master regulators. *Oncogene* **33**, 1755-1763, doi:10.1038/onc.2013.128 (2014).
159 Lamouille, S., Xu, J. & Derynck, R. Molecular mechanisms of epithelial-mesenchymal transition. *Nature Reviews Molecular Cell Biology* **15**, 178-196, doi:10.1038/nrm3758 (2014).
160 Thiery, J. P., Acloque, H., Huang, R. Y. J. & Nieto, M. A. Epithelial-Mesenchymal Transitions in Development and Disease. *Cell* **139**, 871-890, doi:10.1016/j.cell.2009.11.007 (2009).
161 Trimboli, A. J. *et al.* Direct evidence for epithelial-mesenchymal transitions in breast cancer. *Cancer Research* **68**, 937-945, doi:10.1158/0008-5472.can-07-2148 (2008).
162 Beerling, E. *et al.* Plasticity between Epithelial and Mesenchymal States Unlinks EMT from Metastasis-Enhancing Stem Cell Capacity. *Cell Reports* **14**, 2281-2288, doi:10.1016/j.celrep.2016.02.034 (2016).

163 Husemann, Y. *et al.* Systemic spread is an early step in breast cancer. *Cancer Cell* **13**, 58-68, doi:10.1016/j.ccr.2007.12.003 (2008).
164 Zavadil, J. & Bottinger, E. P. TGF-beta and epithelial-to-mesenchymal transitions. *Oncogene* **24**, 5764-5774, doi:10.1038/sj.onc.1208927 (2005).
165 Weidner, K. M., Sachs, M. & Birchmeier, W. THE MET RECEPTOR TYROSINE KINASE TRANSDUCES MOTILITY, PROLIFERATION, AND MORPHOGENIC SIGNALS OF SCATTER FACTOR HEPATOCYTE GROWTH-FACTOR IN EPITHELIAL-CELLS. *Journal of Cell Biology* **121**, 145-154, doi:10.1083/jcb.121.1.145 (1993).
166 Yook, J. I., Li, X. Y., Ota, I., Fearon, E. R. & Weiss, S. J. Wnt-dependent regulation of the E-cadherin repressor snail. *Journal of Biological Chemistry* **280**, 11740-11748, doi:10.1074/jbc.M413878200 (2005).
167 Lo, H. W. *et al.* Epidermal growth factor receptor cooperates with signal transducer and activator of transcription 3 to induce epithelial-mesenchymal transition in cancer cells via up-regulation of TWIST gene expression. *Cancer Research* **67**, 9066-9076, doi:10.1158/0008-5472.can-07-0575 (2007).
168 Howe, E. N., Cochrane, D. R. & Richer, J. K. Targets of miR-200c mediate suppression of cell motility and anoikis resistance. *Breast Cancer Research* **13**, doi:R45 10.1186/bcr2867 (2011).
169 Pieters, T., van Roy, F. & van Hengel, J. Functions of p120ctn isoforms in cell-cell adhesion and intracellular signaling. *Frontiers in Bioscience-Landmark* **17**, 1669-1694, doi:10.2741/4012 (2012).
170 Reichert, M. *et al.* The Prrx1 homeodomain transcription factor plays a central role in pancreatic regeneration and carcinogenesis. *Genes & Development* **27**, 288-300, doi:10.1101/gad.204453.112 (2013).
171 Takano, S. *et al.* Prrx1 isoform switching regulates pancreatic cancer invasion and metastatic colonization. *Genes & Development* **30**, 233-247, doi:10.1101/gad.263327 (2016).
172 Le, T. L., Yap, A. S. & Stow, J. L. Recycling of E-cadherin: A potential mechanism for regulating cadherin dynamics. *Journal of Cell Biology* **146**, 219-232, doi:10.1083/jcb.146.1.219 (1999).
173 Erami, Z. *et al.* Intravital FRAP Imaging using an E-cadherin-GFP Mouse Reveals Disease- and Drug-Dependent Dynamic Regulation of Cell-Cell Junctions in Live Tissue. *Cell Reports* **14**, 152-167, doi:10.1016/j.celrep.2015.12.020 (2016).
174 Cavey, M., Rauzi, M., Lenne, P. F. & Lecuit, T. A two-tiered mechanism for stabilization and immobilization of E-cadherin. *Nature* **453**, 751-U752, doi:10.1038/nature06953 (2008).
175 de Beco, S., Perney, J. B., Coscoy, S. & Amblard, F. Mechanosensitive Adaptation of E-Cadherin Turnover across adherens Junctions. *Plos One* **10**, 14, doi:10.1371/journal.pone.0128281 (2015).
176 Hong, S. M. *et al.* Loss of E-cadherin expression and outcome among patients with resectable pancreatic adenocarcinomas. *Modern Pathology* **24**, 1237-1247, doi:10.1038/modpathol.2011.74 (2011).
177 Aceto, N. *et al.* Circulating Tumor Cell Clusters Are Oligoclonal Precursors of Breast Cancer Metastasis. *Cell* **158**, 1110-1122, doi:10.1016/j.cell.2014.07.013 (2014).
178 Maddipati, R. & Stanger, B. Z. Pancreatic Cancer Metastases Harbor Evidence of Polyclonality. *Cancer Discovery* **5**, 1086-1097, doi:10.1158/2159-8290.cd-15-0120 (2015).
179 Au, S. H. *et al.* Clusters of circulating tumor cells traverse capillary-sized vessels. *Proceedings of the National Academy of Sciences of the United States of America* **113**, 4947-4952, doi:10.1073/pnas.1524448113 (2016).
180 Savagner, P. in *Cellular Adhesion in Development and Disease* Vol. 112 *Current Topics in Developmental Biology* (ed A. S. Yap) 273-300 (Elsevier Academic Press Inc, 2015).
181 Barretina, J. *et al.* The Cancer Cell Line Encyclopedia enables predictive modelling of anticancer drug sensitivity. *Nature* **483**, 603-607, doi:10.1038/nature11003 (2012).

182 Hu, Y. F. & Smyth, G. K. ELDA: Extreme limiting dilution analysis for comparing depleted and enriched populations in stem cell and other assays. *Journal of Immunological Methods* **347**, 70-78, doi:10.1016/j.jim.2009.06.008 (2009).
183 Peinado, H. *et al.* Melanoma exosomes educate bone marrow progenitor cells toward a pro-metastatic phenotype through MET. *Nature Medicine* **18**, 883-+, doi:10.1038/nm.2753 (2012).
184 Tsuji, T., Ibaragi, S. & Hu, G. F. Epithelial-Mesenchymal Transition and Cell Cooperativity in Metastasis. *Cancer Research* **69**, 7135-7139, doi:10.1158/0008-5472.can-09-1618 (2009).
185 Ahmed, N., Abubaker, K., Findlay, J. & Quinn, M. Epithelial Mesenchymal Transition and Cancer Stem Cell-Like Phenotypes Facilitate Chemoresistance in Recurrent Ovarian Cancer. *Current Cancer Drug Targets* **10**, 268-278 (2010).
186 Izumiya, M. *et al.* Chemoresistance Is Associated with Cancer Stem Cell-like Properties and Epithelial-to-Mesenchymal Transition in Pancreatic Cancer Cells. *Anticancer Research* **32**, 3847-3853 (2012).
187 Ren, J., Chen, Y. T., Song, H. Z., Chen, L. B. & Wang, R. Inhibition of ZEB1 reverses EMT and chemoresistance in docetaxel-resistant human lung adenocarcinoma cell line. *Journal of Cellular Biochemistry* **114**, 1395-1403, doi:10.1002/jcb.24481 (2013).
188 Zohn, I. E. *et al.* p38 and a p38-interacting protein are critical for downregulation of E-cadherin during mouse gastrulation. *Cell* **125**, 957-969, doi:10.1016/j.cell.2006.03.048 (2006).
189 Hirano, M., Hashimoto, S., Yonemura, S., Sabe, H. & Aizawa, S. EPB41L5 functions to post-transcriptionally regulate cadherin and integrin during epithelial-mesenchymal transition. *Journal of Cell Biology* **182**, 1217-1230, doi:10.1083/jcb.200712086 (2008).
190 Campbell, K., Whissell, G., Franch-Marro, X., Batlle, E. & Casanova, J. Specific GATA Factors Act as Conserved Inducers of an Endodermal-EMT. *Developmental Cell* **21**, 1051-1061, doi:10.1016/j.devcel.2011.10.005 (2011).
191 Subramanian, A. *et al.* Gene set enrichment analysis: A knowledge-based approach for interpreting genome-wide expression profiles. *Proceedings of the National Academy of Sciences of the United States of America* **102**, 15545-15550, doi:10.1073/pnas.0506580102 (2005).
192 Arlt, A., Schafer, H. & Kalthoff, H. The 'N-factors' in pancreatic cancer: functional relevance of NF-kappa B, NFAT and Nrf2 in pancreatic cancer. *Oncogenesis* **1**, doi:10.1038/oncsis.2012.35 (2012).
193 Buchholz, M. *et al.* Overexpression of c-myc in pancreatic cancer caused by ectopic activation of NFATc1 and the Ca2+/calcineurin signaling pathway. *Embo Journal* **25**, 3714-3724, doi:10.1038/sj.emboj.7601246 (2006).
194 Koenig, A. *et al.* NFAT-Induced Histone Acetylation Relay Switch Promotes c-Myc-Dependent Growth in Pancreatic Cancer Cells. *Gastroenterology* **138**, 1189-U1487, doi:10.1053/j.gastro.2009.10.045 (2010).
195 Baumgart, S. *et al.* Restricted Heterochromatin Formation Links NFATc2 Repressor Activity With Growth Promotion in Pancreatic Cancer. *Gastroenterology* **142**, 388-U314, doi:10.1053/j.gastro.2011.11.001 (2012).
196 Tripathi, M. K. *et al.* Nuclear Factor of Activated T-cell Activity Is Associated with Metastatic Capacity in Colon Cancer. *Cancer Research* **74**, 6947-6957, doi:10.1158/0008-5472.can-14-1592 (2014).